

NPS ARCHIVE
2000
BOLANIS, I.

DUDLEY FOX LIBRARY
NAVY GRADUATE SCHOOL
MONTAGUE, CA 93945-101

NAVAL POSTGRADUATE SCHOOL Monterey, California



THESIS

PREDICTION OF WIRELESS COMMUNICATION
SYSTEMS PERFORMANCE IN INDOOR APPLICATIONS

by

Ilias Bolanis

December 2000

Thesis Advisor:
Co-Advisor:

Jovan Lebaric
James Luscombe

Approved for public release; distribution is unlimited.

REPORT DOCUMENTATION PAGE

Form Approved
OMB No. 0704-0188

Public reporting burden for this collection of information is estimated to average 1 hour per response, including the time for reviewing instruction, searching existing data sources, gathering and maintaining the data needed, and completing and reviewing the collection of information. Send comments regarding this burden estimate or any other aspect of this collection of information, including suggestions for reducing this burden, to Washington headquarters Services, Directorate for Information Operations and Reports, 1215 Jefferson Davis Highway, Suite 1204, Arlington, VA 22202-4302, and to the Office of Management and Budget, Paperwork Reduction Project (0704-0188) Washington DC 20503.

1. AGENCY USE ONLY (Leave blank)		2. REPORT DATE December 2000	3. REPORT TYPE AND DATES COVERED Master's Thesis	
4. TITLE AND SUBTITLE Prediction of Wireless Communication Systems Performance in Indoor Applications			5. FUNDING NUMBERS	
6. AUTHOR(S) Bolanis, Ilias				
7. PERFORMING ORGANIZATION NAME(S) AND ADDRESS(ES) Naval Postgraduate School Monterey, CA 93943-5000			8. PERFORMING ORGANIZATION REPORT NUMBER	
9. SPONSORING / MONITORING AGENCY NAME(S) AND ADDRESS(ES)			10. SPONSORING / MONITORING AGENCY REPORT NUMBER	
11. SUPPLEMENTARY NOTES The views expressed in this thesis are those of the author and do not reflect the official policy or position of the Department of Defence or the U.S. Government.				
12a. DISTRIBUTION / AVAILABILITY STATEMENT Approved for public release; distribution is unlimited.			12b. DISTRIBUTION CODE	
13. ABSTRACT (maximum 200 words) Due to a shift in the interest in wireless applications, from outdoor to indoor environments, new modelling solutions had to be designed to account for the immense complexity of the latter. Essentially, two categories of indoor propagation models prevailed until the mid-90's: the Empirical and the Physical models. They both predicted important characteristics of a given confined environment like the coverage area, transmitted power requirements, number and location of base stations or access points. The implementation of wireless communications systems onboard naval assets is expected to offer numerous advantages and enhance the existing shipboard communications systems. That, in turn, calls for a reliable and cost-effective means of estimating the expected link budget in such environments, especially when the infrastructure in question is yet to be built, as is the case in a ship class under development. This thesis treats the problem of indoor propagation modeling using the Numerical Electromagnetic Code-Basic Scattering Code (NEC-BSC) and compares the predicted results obtained by this code with actual measurements performed inside a building at the Naval Postgraduate School. A number of important conclusions regarding the validity of NEC-BSC for indoor applications are being reached and some intriguing statistical results are being presented.				
14. SUBJECT TERMS Simulation of signal propagation, indoor radio propagation, NEC-BSC			15. NUMBER OF PAGES 207	
			16. PRICE CODE	
17. SECURITY CLASSIFICATION OF REPORT Unclassified	18. SECURITY CLASSIFICATION OF THIS PAGE Unclassified	19. SECURITY CLASSIFICATION OF ABSTRACT Unclassified	20. LIMITATION OF ABSTRACT UL	

THIS PAGE INTENTIONALLY LEFT BLANK

Approved for public release; distribution is unlimited.

**PREDICTION OF WIRELESS COMMUNICATION SYSTEMS
PERFORMANCE IN INDOOR APPLICATIONS**

Ilias Bolanis
Lieutenant, Hellenic Navy
B.S., Hellenic Naval Academy, 1990

Submitted in partial fulfilment of the
requirements for the degree of

MASTER OF SCIENCE IN ELECTRICAL ENGINEERING

from the

**NAVAL POSTGRADUATE SCHOOL
December 2000**

NPS ARCHIVE
2000
BOLANIS, I.

~~18315~~
~~064535~~
C.1

THIS PAGE INTENTIONALLY LEFT BLANK

ABSTRACT

Due to a shift in the interest in wireless applications, from outdoor to indoor environments, new modelling solutions had to be designed to account for the immense complexity of the latter. Essentially, two categories of indoor propagation models prevailed until the mid-90's: the Empirical and the Physical models. They both predicted important characteristics of a given confined environment like the coverage area, transmitted power requirements, number and location of base stations or access points. The implementation of wireless communications systems onboard naval assets is expected to offer numerous advantages and enhance the existing shipboard communications systems. That, in turn, calls for a reliable and cost-effective means of estimating the expected link budget in such environments, especially when the infrastructure in question is yet to be built, as is the case in a ship class under development.

This thesis treats the problem of indoor propagation modeling using the Numerical Electromagnetic Code-Basic Scattering Code (NEC-BSC) and compares the predicted results obtained by this code with actual measurements performed inside a building at the Naval Postgraduate School. A number of important conclusions regarding the validity of NEC-BSC for indoor applications are being reached and some intriguing statistical results are being presented.

THIS PAGE INTENTIONALLY LEFT BLANK

TABLE OF CONTENTS

I. INTRODUCTION.....	1
A. MOVING TOWARDS WIRELESS.....	1
B. INTEREST FOR WIRELESS INDOOR USE	2
C. DEVELOPING A SHIPBOARD W.C.S.....	4
D. GOAL FOR THIS THESIS.....	6
E. THESIS OUTLINE.....	6
II. BACKGROUND	9
A. THE INDOOR RADIO CHANNEL	9
1. Complex Environment	9
2. Multipath Fading.....	11
a. Reflection.....	12
b. Scattering	12
c. Refraction.....	13
b. Diffraction.....	13
3. Path Loss.....	13
B. MODELLING THE INDOOR RADIO CHANNEL.....	17
1. Categories of Models	17
a. Empirical.....	17
b. Physical.....	18
c. Other Models.....	19
2. Language and Input Data Tools	19
3. Extracted Data.....	20
4. Succinct Comparison of Empirical & Physical Models	21
a. Advantages.....	22
b. Disadvantages	22
5. In Which Group Does NEC-BSC Fall?.....	24
III. NEC-BSC	25
A. SHORT DESCRIPTION AND BACKGROUND.....	25
B. OTHER WORKS BASED ON NEC-BSC	25
C. NEC-BSC CAPABILITIES AND INHERENT ADVANTAGES	27
D. LIMITATIONS OF THE CODE.....	29
IV. NEC-BSC EXAMPLES	33
A. A RECTANGULAR PEC ROOM WITH A CYLINDER	33
1. Circular Near-Field Pattern	34
2. Line Near-Field Pattern.....	36
B. A TYPICAL ROOM.....	37
C. COMPARISON WITH THE SHOOTING-AND-BOUNCING RAY METHOD (SBR).....	44
V. THE MODEL	51
A. GEOMETRY DEFINITION	51
1. Metallic Mesh.....	55
2. "Equivalent" Composite Wall.....	57
B. MEASUREMENTS.....	58

C. SIMPLIFICATIONS	59
1. ZD Commands	60
2. Plates	60
3. Presence of People	61
4. Radiation Scattered by Neighbouring Buildings	61
5. Clear Space Boundaries	61
VI. SIMULATION ANALYSIS	63
A. PLATFORM CONFIGURATION AND TIME PERFORMANCE	63
B. COMPARISON WITH MEASUREMENTS	64
C. SIMULATIONS	67
1. Testing Different Model Approaches	67
2. Comparing with Free Space	68
D. STATISTICS	69
1. Flow of Work	69
2. Results	74
3. Other Problems	78
a. Command ZD 11	79
b. Commands not Supported by Workbench	79
c. Polar Plot Command	79
VII. CONCLUSIONS AND RECOMMENDATIONS	81
A. CONCLUSIONS AND UNRESOLVED ISSUES	81
B. RECOMMENDATIONS	83
APPENDIX A. NEC-BSC INPUT FILES	87
APPENDIX B. MATHCAD DATA PROCESSING FILES	149
LIST OF REFERENCES	185
INITIAL DISTRIBUTION LIST	189

LIST OF FIGURES

Figure 1.1: Access Point Installed at the Network Lab of the NPS ECE Department	4
Figure 2.1: Example of Multipath Fading <i>line-of-sight</i> Case.....	10
Figure 2.2: Example of Multipath Fading <i>Obstructed</i> Case	11
Figure 2.3: Effect of Surface Roughness on Reflection.....	12
Figure 2.4: Fresnel Zones	16
Figure 2.5: 0.6 times First Fresnel Zone	16
Figure 2.6: Bullard’s 2 nd Floor Relative Signal Strength Coverage Map Generated by PlaceBase.....	21
Figure 4.1: Ground Plan of Room with Cylinder.....	34
Figure 4.2: Circular Pattern: Area Covered by Rays	35
Figure 4.3: E-field Components versus Angle φ Plot Created by Workbench	36
Figure 4.4: Total E-field versus Distance (vertical polarization).....	37
Figure 4.5: A Typical Room.....	40
Figure 4.6: Excess Gain (dB) (oblique view)	41
Figure 4.7: E-field Normalized Difference	42
Figure 4.8: Normalized Difference Random Variable Compared to Gaussian pdf	42
Figure 4.9: Normalized Difference Random Variable cdf versus Loss in dB	43
Figure 4.10: Room with Closet.....	44
Figure 4.11: SBR and NEC-BSC (w/o PEC) Results	47
Figure 4.12: SBR and NEC-BSC (with PEC) Results	47
Figure 4.13: Contrasting the Relative Difference of the PEC with the no-PEC Solution.....	48
Figure 4.14: NEC-BSC Path Loss Results for the Furnished and Empty Room	50
Figure 5.1: Bullard’s Second Floor Created with the NEC-BSC	52
Figure 5.2: Lucent Technologies WaveLAN Coverage.....	59
Figure 6.1: Predicted Excess Gain/Loss in Bullard 2 nd Floor (open doors).....	65
Figure 6.2: Predicted Excess Gain/Loss for Closed Doors.....	65

Figure 6.3: Comparison of Measured and Predicted Data Matrices	66
Figure 6.4: Predicted Excess Gain/Loss Using Double-Sided Coated Walls	68
Figure 6.5: Predicted Excess Gain/Loss (antenna in the middle of the floor).....	69
Figure 6.6: Antenna Locations Used in the Statistics Analysis Input Files	72
Figure 6.7: Histogram of All Distance-Groups pdfs (Ant. at Location 2)	72
Figure 6.8: Average-pdf of the Room Gain Plotted Against Gaussian pdf.....	73
Figure 6.9: Cdf of Random Variable r (antenna at location 2)	74
Figure 6.10: Average-pdf Plotted Against Gaussian Distribution	77
Figure 6.11: Room-Gain cdf Plotted Against Gaussian Distribution.....	78

LIST OF TABLES

Table 3.1: Variables Limits	31
Table 4.1: Room's Dimensions.....	38
Table 4.2: Room's Properties	39
Table 5.1: Constitutive Parameters Used in the NEC-BSC Input Files	55
Table 6.1: Room Gain Parameters	76

THIS PAGE INTENTIONALLY LEFT BLANK

ACKNOWLEDGEMENT

The following lines are devoted to all those who contributed to the completion of this arduous undertaking which lasted roughly one year.

Special thanks are extended to Mrs. Allyn McGuire, General Engineer/Planner of NPS Public Works, who was courteous enough to provide me with several copies of Bullard Hall blueprints. Although direct cooperation was never attained, I still feel honoured to have been helped by the author of NEC-BSC, Dr. Ronald Marhekfa. Dr. Xiaoping Yun clarified some essential parts of the measurements that were conducted on the second floor of Bullard, and his assistance is greatly appreciated. Furthermore, I am indebted to Dr. Richard Adler, the only person at NPS with prior exposure on NEC-BSC, who introduced me to this code's myths and realities while I was still fumbling around in a sea of questions. I also recognize Dr. James Luscombe for correcting my English while reviewing this thesis. I am much obliged to Dr. Jovan Lebaric for his unstinting support and for always producing cogent arguments as to how to cope with some awkward, NEC-BSC related predicaments. An additional thanks is extended to Lt Yannis Martinos H.N. for his excellent partnership and exemplary cooperation.

Little would I achieve, had I not been guided by my parents throughout my life in many respects and my gratitude to them will be immutable. And last, but certainly not least, I would like to thank my wife, Eleni Perdikouri, for enduring countless hours of neglect during the preparation for this project.

THIS PAGE INTENTIONALLY LEFT BLANK

EXECUTIVE SUMMARY

The ongoing effort of introducing wireless communication systems onboard naval assets provides a noticeable incentive for developing software tools capable of predicting the signal strength variations in indoor environments. To this end, this thesis focused on a tool developed by the Ohio State University Electroscience Lab (OSU-ESL) called Numerical Electromagnetic Code-Basic Scattering Code (NEC-BSC) and evaluated its applicability to confined spaces. Initially, some simple geometries were created in an effort to gain familiarity with the code and its capabilities and limitations. Even at this early stage, it was found that the code erroneously generated electromagnetic waves penetrating the surface of a perfectly electrical conducting (PEC) cylinder. However, a comparison of NEC-BSC predicted values with the results presented by a different approach called shooting-and-bouncing ray method (SBR) in a relatively simple rectangular room with furniture offered encouraging results.

The major task, in any event, was to compare the signal strength predicted values obtained by NEC-BSC to actual measurements conducted inside a building at the Naval Postgraduate School in the 2.4 GHz ISM band. The comparison was executed in two ways. First, by contrasting the NEC-BSC and physical electric field strength coverage maps and, second, by creating two data matrices based on the predicted and measured values. In the former case the two maps agreed very well, whereas in the latter the agreement was not illuminating and that could possibly be attributed to the many inherent errors associated with the second approach. In parallel, a statistical analysis of the electric field strength variation was performed in the same building using NEC-BSC. In particular, the antenna was placed in five different locations and, subsequently, five sets

of data were acquired. Then the excess electric field “room gain” over free space was calculated for all same-floor points within certain distances from the antenna called “distance-groups.” In this manner, a random variable was defined describing the variation of the so-called “room gain” inside the building under consideration and its probability density function (pdf) and cumulative distribution function (cdf) were computed. It was found that regardless of the distance between the transmitter and the receiver on the same floor the aforementioned random variable had a lognormal distribution and its pdf and cdf obeyed a Gaussian pdf and cdf, respectively, having identical mean and variance. Furthermore, the modeled floor of the building was found to exhibit gain over free space for all antenna locations. Finally, the mean value of the “room gain” random variable ranged from 4.276 to 8.322 dB while its standard deviation varied from 4.624 to 5.275 dB.

I. INTRODUCTION

This highly technological era has been called “digital revolution,” in correspondence with the 19th century’s “industrial revolution.” An important long-lasting contributor to this revolution is the wireless communications.

A. MOVING TOWARDS WIRELESS

Wired communications have offered for quite a long time a reliable and speedy means of exchanging ideas and promoting cooperation amongst businesses and individuals. However, as the demand for more capacity and flexibility grew, new solutions had to be considered. “Mobility” was the new logo and that entailed terminals and equipment moving around, installation being easy and quick, inherent resistance to natural and manmade disasters being vital. The cost of achieving all that with conventional approaches was posing an impediment to progress. Wireless communications not only satisfied the above requirements but they also introduced new ideas like roaming, creative solutions like setting a network at locations where cable could not go, and modern schemes which could support already existing technologies like the Internet. Furthermore, wireless communications helped in cutting down expenses since the exorbitant price of replacing the wiring in and around a building was no longer an issue, promoted the concept of cells (e.g. megacells, macrocells, microcells) thereby enabling communications at high rates, and made communications available to larger portions of the population.

B. INTEREST FOR WIRELESS INDOOR USE

Nevertheless, there were still persons and sites excluded and a huge increase in the number of potential users. Customers were experiencing a shift to yet another idea: service provided anywhere, anytime. Moreover, the planning for broadcasting services like Terrestrial Digital Audio Broadcasting (T-DAB) or Digital Video Broadcast Television (DVB-T) [1] conveyed a clear message: Picocells had to be invented and coverage in confined environments should be taken for granted. Additional motivation was given with the advent of Personal Communication Systems (P.C.S.), and various emerging wireless standards like IEEE STD 802.11 [2], HIPERLAN/2 (High Performance Radio Local Area Network) [3], HomeRF [4], and Bluetooth [5].

Until recently, the majority of indoor wireless systems occupied the 1.8-2.0 GHz band (e.g. Digital European Cordless Telephone-DECT, Personal Access Communication Systems-PACS, Personal Handyphone System-PHS) [6]. Yet, this trend has shifted to the license-free Industrial Scientific & Medical (ISM) bands, 902 to 908 MHz, 2400 to 2483.5 MHz, and 5725 to 5850 MHz. These bands allow fee-free operation, inasmuch as no one actually owns these frequencies. The 2.4 to 2.485 GHz band attracted some extra preference on the part of the business world. Europe and the US adopted the same 2.4 GHz band, whereas Japan allocated only the frequencies 2.471 to 2.497 GHz. In addition, apart from some exceptions like Nokia Rooftop [7] operating at 5.8 GHz, most of companies have largely invested in 2.4 GHz projects. The reason appears to be two-fold. First, the bandwidth of ISM 2.4 GHz is three times that of 900 MHz, and, second, 2.4

GHz is subjected to less “radio-traffic” and its resulting interference. There is also move into the 5.2 GHz ISM band because of an even wider bandwidth.

Remarkable and tempting as all the aforementioned arguments may be, they fail to reveal the difficulties of indoor propagation. Simply put, radio transmission and reception within buildings or other enclosed environments suffers from various phenomena. Primarily, *Multipath fading* is caused by the simultaneous arrival of electromagnetic (EM) waves from different directions via reflection, refraction, diffraction, and scattering, which add either constructively or destructively. Consequently, the received signal varies dramatically, even if we move the mobile antenna as little as a half-wavelength distance in any direction. In this context, the signal strength may degrade severely the communications range.

Despite the problems associated with the indoor radio channel, the necessity for meeting the demand for microcellular and picocellular communications remained. Research on this field was launched as early as 1982 by British Telecom [6]. Measurements at various frequencies inside diverse buildings were performed. Soon, a new requirement for the determination of the link budget was realized. Should a robust Wireless System be designed, the modeling of the indoor radio channel had to be done successfully.

Essentially, until the mid-90’s two kinds of indoor propagation models were being utilized: *Empirical* and *Physical*. The former is based on actual measurements run in the locations of interest with the intention of coming up with an analytical formula, which could later be applied to a similar environment. The latter depends on the laws of physics,

the UTD/GTD (Uniform and Geometrical Theory of Diffraction) in particular, and uses site specific (SISP) information. Both models strive to determine the coverage area, transmitted power requirements, number of base stations or access points (AP) (Figure 1.1), optimum locations for antenna mounting, and all other major concerns of communication engineers dealing with indoor wireless communications system (W.C.S.). Further discussion on indoor radio propagation and the models pertaining to it will be made in the following chapter.

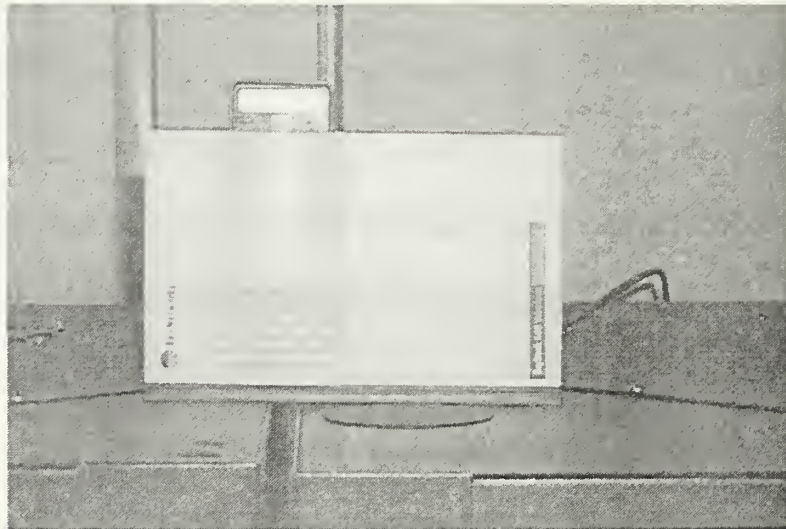


Figure 1.1: Access Point Installed at the Network Lab of the NPS ECE Department (From [29])

C. DEVELOPING A SHIPBOARD W.C.S.

Considering the numerous advantages of W.C.S., the U.S. Navy recently launched a thorough study on this field [8,9,10,11]. In 1999, test, evaluation, and installation of personal communication system (P.C.S.) onboard various U.S. ships took place [12].

Although research is still in progress and the market has not arrived at a mature stage, the benefits of implementing a shipboard W.C.S. are pronounced and well established:

- **Availability:** Current commercial solutions for wireless local area network (WLAN) may already satisfy the Navy's requirements [11]. Selection could be made over a broad variety of packages so long as they are compatible with the IEEE STD 802.11.
- **Affordability:** Not only the acquisition cost will be low but, by virtue of cabling elimination, the support and maintenance expenses will be reduced as well. The W.C.S. could be built with ruggedized commercial off-the-shelf (COTS) digital equipment rather than Navy-proprietary solutions.
- **Flexibility and Mobility:** The W.C.S. could be easily installed in previously unreachable locations on the ship. Furthermore, crew members could have access to a centralized system from virtually any ship compartment and, in turn, their whereabouts could be monitored providing vital information, should any dangerous situation arise.
- **Survivability:** Wireless systems mitigate the effects caused by cable plant damage, fire or other minor or major disturbance. A fault-tolerant operating system should be the ultimate goal.
- **Back-up:** When mostly needed, in case of emergency, WLAN could either be used for damage control communications or simply substitute the existing wired LAN. For this purpose, an anti-fading system with a directional antenna could be implemented to account for fire and the fire extinguishing effects [13].

- **Improved data handling:** Information collection will be done expeditiously and report assessment will be carried out on the spot, enabling instant digital processing.
- **Expandability and variability:** Having already been tested for interoperability in the commercial sector with encouraging results, WLAN's are expected to be incorporated in various arrangements and offer an architecture which will support a plethora of configurations without sacrificing the end-to-end performance.

D. GOAL FOR THIS THESIS

Driven by the ongoing effort of introducing W.C.S. onboard Naval assets, this thesis addressed the problem of indoor propagation modeling using a tool developed by the Ohio State University Electroscience Lab (OSU-ESL); specifically, the Numerical Electromagnetic Code- Basic Scattering Code (NEC-BSC). The approach initially consisted of creating simple geometries in order to gain familiarity with the code and its capabilities. The next was the simulation of the second floor of Bullard Hall, at the Naval Postgraduate School (NPS), in Monterey, California. Finally, a comparison was made between the NEC-BSC predicted results and those measured M.M. Matthews [11].

E. THESIS OUTLINE

This thesis is divided into seven chapters. The second chapter discusses the theoretical background for an indoor radio channel and gives insight into previous work on prediction of radio propagation in confined environments. Chapter III introduces the NEC-BSC and summarizes its limitations and capabilities. Next, various simple

simulations involving uncomplicated geometries are run and explained in Chapter IV. Chapter V describes the modeling of the simulated floor and the simplifications adopted in our model. All results and the statistics extracted from the simulations are shown in Chapter VI. Finally, in Chapter VII, the conclusions are presented and some recommendations for further work are made.

THIS PAGE INTENTIONALLY LEFT BLANK

II. BACKGROUND

A. THE INDOOR RADIO CHANNEL

1. Complex Environment

The indoor radio channel is a complex propagation environment and there is good evidence through years of research that it is more complicated than an outdoor radio channel. This is due to the vast diversity of the potential surroundings.

Broadening the service area to reach more end users at higher data rates and virtually everywhere was not an easy task to undertake. Eventually, picocells had to be designed and put into practice. In doing so, businesses extended wireless networks coverage to include office buildings, industrial plants, railway stations, tunnels, and airports. Users could be either static (e.g. by establishing a WLAN between PC's) or mobile (e.g. by expanding cellular telephony services).

Prior experience obtained in various outdoor schemes does not guarantee applicability in enclosed sites. Unlike city and rural topologies, the indoor environment consists solely of man-made structures and obstacles like walls, partitions, windows, furnishings etc. In addition, in indoor cells there is no material uniformity, and many more flat surfaces compared to outdoor cells. Given that the frequencies of interest reside in the ISM band, the dimensions of obstacles are typically much larger than the radio wavelength (λ). Moreover, the observed channel depends on the type of building, whether there are doors opened or closed, location of antennas, presence of people, etc. Shadowing regions are also an issue because by placing the transmitter and receiver

inside the same building, many obstructed paths are created and diffraction tends to be a significant contributor to the received signal strength. Even the existence of corridors plays a role since it exhibits a waveguide behavior [14,15]. All these parameters have a noticeable effect on the resulting propagation. They produce a multipath environment in the sense that many potential transmission and arrival paths can exist.

As opposed to macrocells, picocells, sometimes called indoorcells, have been found to be more deterministic than statistical and are not stationary in space and time [16].

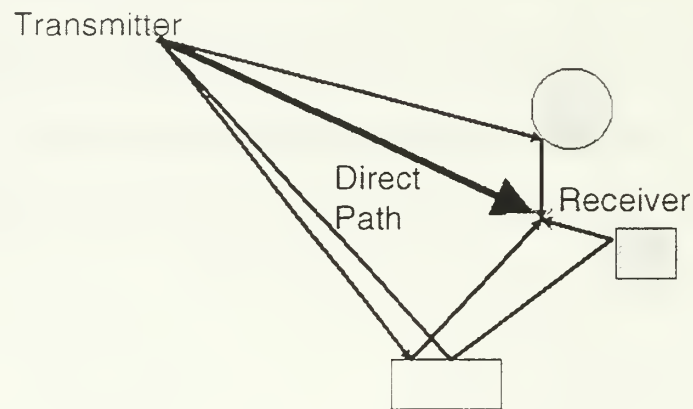


Figure 2.1: Example of Multipath Fading *line-of-sight* Case (From Ref [17])

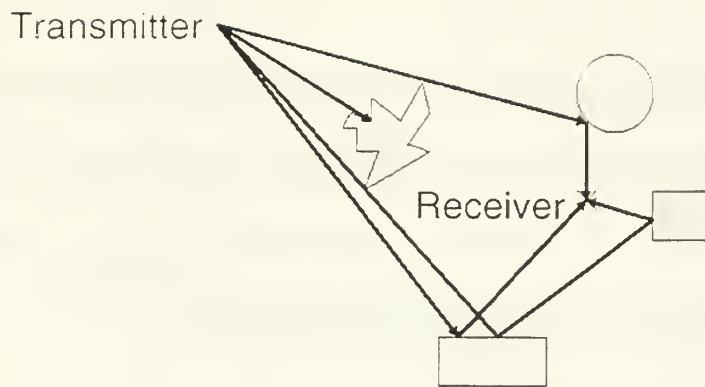


Figure 2.2: Example of Multipath Fading *Obstructed Case* (From Ref [17])

2. Multipath Fading

In this complex environment, the EM waves generated from the transmitter reach the receiver via numerous paths with unequal contribution. A line-of-sight (LOS) may not exist (figure 2.1), in which case only obstructed (OBS) paths are present (figure 2.2). The signal traveling via these paths can be gravely attenuated because of wall penetration and/or reflection/diffraction from various absorbing materials on the premises. However, even if a LOS is present there are still other propagation paths whose contribution might be of lesser significance yet not at all negligible. Consequently, the signal arriving at the receiver will be distorted with the sum of all signals received tending to have random phases. The received signal power usually varies as much as 30-40 dB (small-scale fading) when the receiver is moved for only a fraction of wavelength. Statistical analysis has shown that the magnitude of the sum of arriving signals may be described as Rician random variable (when a LOS path exists) or as Rayleigh random variable (if only OBS propagation paths are present) [17]. In particular, the phenomena leading to multipath fading are the following:

a) *Reflection*

Reflection comes about when an EM wave strikes an obstacle with dimensions much larger than the wavelength. In this case, the surface is said to be “smooth” and the wave specularly reflected. The criterion used in deciding whether this behavior should be anticipated is the *Rayleigh Criterion*:

$$\Delta h < \frac{\lambda}{8 \cos \theta_i} \quad (2.1)$$

where Δh is the height difference between two points on the surface under consideration, λ the wavelength, θ the incidence angle. If the inequality (2.1) holds, then the Rayleigh criterion is met and the surface is assumed to be “smooth.”

b) *Scattering*

Scattering happens when the object hindering the EM wave’s path has dimensions either comparable to or smaller than the wavelength. The EM energy is reradiated in all directions as shown in Figure 2.3.

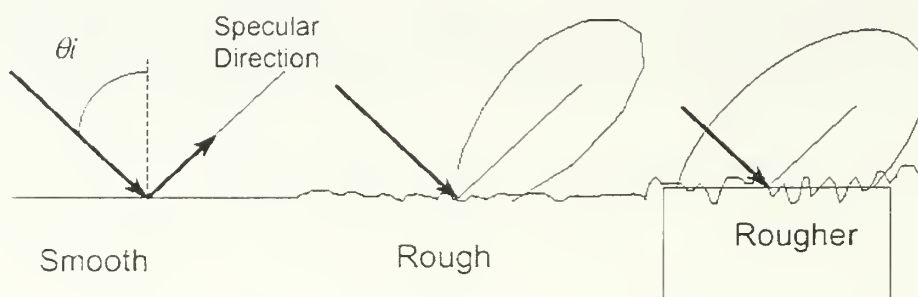


Figure 2.3: Effect of Surface Roughness on Reflection (From Ref [17])

c) *Refraction*

Refraction represents the change in the direction of propagation of an EM wave as it crosses the interface of two media with different velocities of propagation.

d) *Diffraction*

Diffraction occurs when an obstruction made of material impervious to EM energy stands in the path of propagation. The area behind this obstruction is defined as the *Shadowing Region*. Huygen's principle in this case dictates that secondary EM waves will be generated from the edges of the obstacle and EM energy will eventually "creep around" and propagate in the shadowing region, albeit with reduced magnitude. Thus, diffraction contributes substantially to signal reception in non-line-of-sight (NLOS) situations.

3. Path Loss

In an effort to design and establish a W.C.S. in an indoor environment, the communications engineer will need prior accurate knowledge of certain factors like the potential coverage area, best locations for antenna placement, transmitting power requirements, etc. In short, the *link budget*, in which all gains and attenuations of the channel are considered with the ultimate goal of estimating the performance of the communication system in the given surroundings, needs to be determined. An essential tool indicative of the expected communications link quality is the *path loss* (PL), which is the difference, expressed in dB, between received and transmitted power. An example of what can be expected in an indoor office environment is given in [18], where

measurements at 2.4 GHz were performed and it was found that the maximum acceptable PL was 123 dB with the SNR (signal-to-noise ratio) always more than 20 dB.

Early works in this area revealed an inclination to a simplified approach in describing the indoor channel. It was thought that the PL models used in the mobile channel could just as easily be conveyed to indoor applications by adding an *attenuation factor* (AF) to account for walls, floors, etc. The attenuation factor model was a paradigm in this regard:

$$PL(d)[dB] = PL(d_0)[dB] + 10n_{sf} \log\left(\frac{d}{d_0}\right) + FAF[dB] \quad (2.2) \text{ from [6]}$$

where d and d_0 represent the distance in meters from the transmitter to the receiver and to a reference point, respectively, n_{sf} denotes the attenuation exponent for the “same floor” measurements, and the FAF is simply a factor whose values usually depend on the radio frequency and the number of penetrated floors.

In the same fashion, the Keenan model takes into account the number of floors and walls between transmitter and receiver, n_f and n_w , respectively, and the corresponding attenuation factors, i.e. a_f and a_w :

$$L = L_1 + 20 \log r + n_f a_f + n_w a_w \quad (2.3) \text{ from [17]}$$

where L_1 denotes the loss at distance $r = 1\text{m}$.

However, this concept is not justified in [14] where it is argued that the resulting error margins reach unacceptable levels in some indoor environments.

Indeed [19] and [20] clearly point out that the PL within buildings does not depend on the distance alone, but also on the floor area, the number of walls, partitions and obstacles between the transmitter and receiver, and on the signals leaving and returning to the building (in case of proximity to neighboring buildings). In addition, the survey in [14] concluded that the frequency of the radio wave is also significant inasmuch as the higher it is the lower the penetration, and thus the path loss. Through a different perspective, in [21] it is suggested that another concern is the path the EM wave follows to reach the receiver: specular paths result in cumulative transmission PL whereas the diffracted ones (whenever not passing through many walls) display a lower PL.

It should be stressed, nonetheless, that there is considerable difference in the observed statistics of PL between the “same room” and “many rooms” propagation case. In the former case the PL exhibits a slow-fading fluctuation profile, but at the same time the attenuation factor approaches the free-space $n = 2$ [22]. In the latter case, on the other hand, the further away the transmitter’s room is, the attenuation factor may take very different values. For instance, in [23] and [24] it was estimated that $n = 6.0$ at 2.3 GHz and in [14] it was estimated that $n = 3.0$ for an office building.

A typical example of the immense diversity characterizing the results reported in the literature is given in [14] where the measured PL through concrete ranged from 7 dB to 27 dB depending on the approach chosen. By contrast, in [15] it was estimated at 3.5 dB.

Although it is true that PL depends on the number of obstructions (which are many in the indoor environment) between transmitter and receiver, it is also true that not

all of them are deemed significant. An interesting theoretical rule of thumb is whether the obstruction in question occupies 0.6 times the first *Fresnel zone*. In this case, the impact on the received signal strength is low. The radius r_n of the n^{th} Fresnel zone is given by (assuming $r_n \ll d_1, d_2$):

$$r_n \approx \sqrt{\frac{n\lambda d_1 d_2}{d_1 + d_2}} \quad (2.4) \text{ from [17]}$$

All the pertinent distances are shown in Figures 2.4 and 2.5.

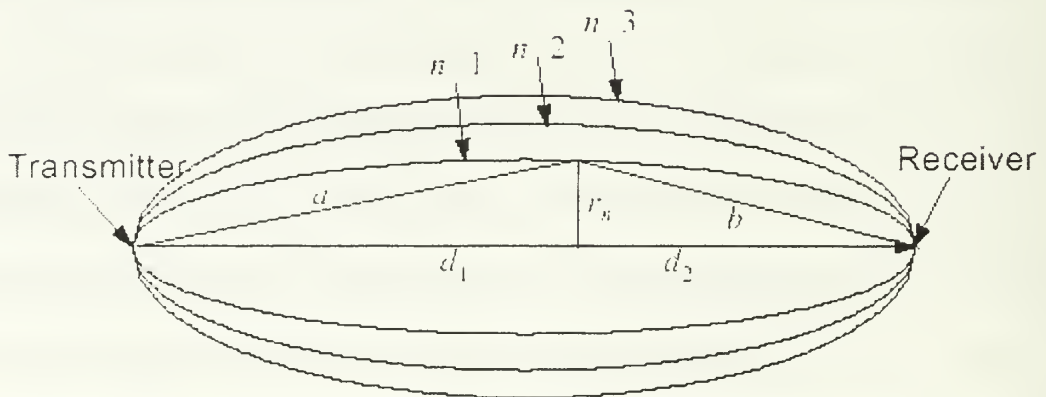
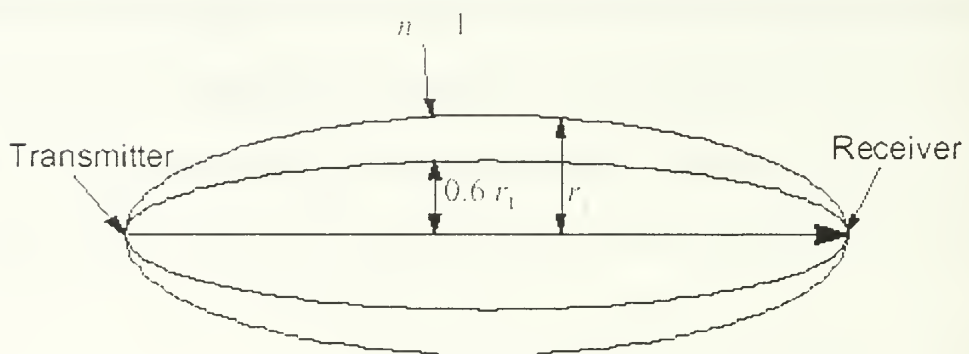


Figure 2.4: Fresnel Zones (From [17])



- 'Forbidden' region
- First Fresnel zone

Figure 2.5: 0.6 times First Fresnel Zone (From [17])

B. MODELLING THE INDOOR RADIO CHANNEL

Given the increasing demand for indoor W.C.S., installation in diverse confined environments and the driving force of business competition dictates a prompt and reliable mechanism of predicting the performance of any system under such harsh operating conditions. Measuring the signal strength in one building and subsequently estimating the best antenna locations appears to be a tempting and simplified approach. However, this method would have applicability only in identical buildings since it is well known that only slight differences in the geometry of the building or in the properties of the materials constituting the surroundings, or even a small alteration in the transmitted frequency, would create a very dissimilar situation. Furthermore, performing measurements in all existing buildings or other constructions (factories, train stations etc) is an unrealistic method, inasmuch as it would necessitate vast human and equipment resources. The answer was given by the indoor radio channel models.

1. Categories of models

Extensive research in the literature has indicated that we can distinguish three categories of models:

a) Empirical

These are also called *statistical* models and their principal feature is the extraction of an expression, which could be a function of several parameters (e.g. attenuation factors for concrete walls, windows etc), accurate enough to fit curves of a set of measured data. This expression usually has a broad field of applicability, but cannot be universally used nonetheless. Often this means that these models yield satisfactory results

for a group of buildings that display characteristics similar to the ones where the measurements were taken. Examples of empirical solutions are the Keenan factor model, the COST231 [17], the Ericsson Breakpoint model [6], and the model of [18] where attenuation due to walls was not taken into account.

b) Physical

These are also called *deterministic* or *site specific* (SISP) models. They have recently dominated the field of indoor radio prediction tools since their evolution is dependent on computer growth and improvement. They basically utilize various ray-tracing techniques and largely depend on the EM laws of physics and the data of the specific site where they are applied. Physics plays a significant role through the use of the theory of UTD/GTD and the Method of Moments (MoM) [25]. Moreover, the data frequently include the constitutive parameters of the materials found in the site under consideration, the detailed topography obtained by blueprints, and the precise location of obstacles. A different but useful approach is proposed by finite difference time domain (FDTD) models where fewer resource requirements have to be met compared to UTD/MoM models [26].

SISP models mostly take advantage of the high frequency approach, which enables the simulation of radio propagation in the form of rays. Therefore, the resulting total field strength at the receiver's position is computed as the sum of all the arriving rays generated by the transmitter. The rays follow multiple paths consisting of reflections, refractions, diffractions, scattering, and also double or triple bounce components (e.g. reflection/diffraction, or reflection/diffraction/reflection). However, not all SISP models

account for all possible combinations. More specifically, diffracted rays were not examined in [19], [21], and [27] while scattering was not considered in [28], [27], and [1]. Furthermore, the FDTD model of [26] does not include ground reflections and the effect of antenna height. On the other hand, PlaceBase tool takes into account all the above but fails to consider furniture and obstacles [29].

Examples of GTD/UTD and MoM models are described in [28], [1], [30], and [31] whereas examples of various ray-tracing techniques are analyzed in [19], [32], [33], [21], [27], and [34].

c) Other Models

There are models that do not fall into the above categories. *Hybrid* models occupy a middle ground between empirical and deterministic approaches. They combine the simplicity of the former with the flexibility of the latter producing somewhat efficient results. Two best known hybrid models are found in [1] and [35]. An entirely different solution is suggested by Artificial Neural Networks (ANN) models, which utilize the principles of Feedforward Neural Networks. An example is given in [36].

2. Language and Input Data Tools

Currently, as a survey of the literature has indicated, there are at least three languages used for code development: FORTRAN (e.g. for NEC-BSC and [30]), C++ (e.g. for [33] and [37]), and the Eclipse constraint-logic programming language [34].

With the advent of effective software tools, the time and effort for inputting data in the model is substantially minimized. Indeed, this is an important factor whenever different codes are weighed against each other since not all of them incorporate this

capability. For instance, the models of [33] and [35] make use of AutoCAD in order to convert the building data into ASCII files. By virtue of these files, the layout of the indoor environment is converted into numerical coordinates subsequently used for the simulation calculations. By contrast, the alternative to this convenience is to manually input all coordinates which, needless to say, is a relatively cumbersome task (e.g. NEC-BSC). However, we should underscore the fact that AutoCAD files are not readily available for all existing buildings. It would be rather optimistic for one to expect to find AutoCAD files for a building built in 1950's.

3. Extracted Data

The extracted results may be given in various ways. The majority of models generate ASCII raw files which include important factors such as impulse response, path loss, suggested location for AP, or all of them. In particular, PL can be expressed as a function of either frequency or distance between transmitter and receiver. Again, not all models convert automatically these raw files into graphs and the user's intervention is required in such cases. Also, some applications, like for instance WiSE, CINDOOR, WinProp, SitePlanner, PlaceBase (figure 2.6), initiate a colored graphical representation of the overall radio propagation for the building under consideration [29].

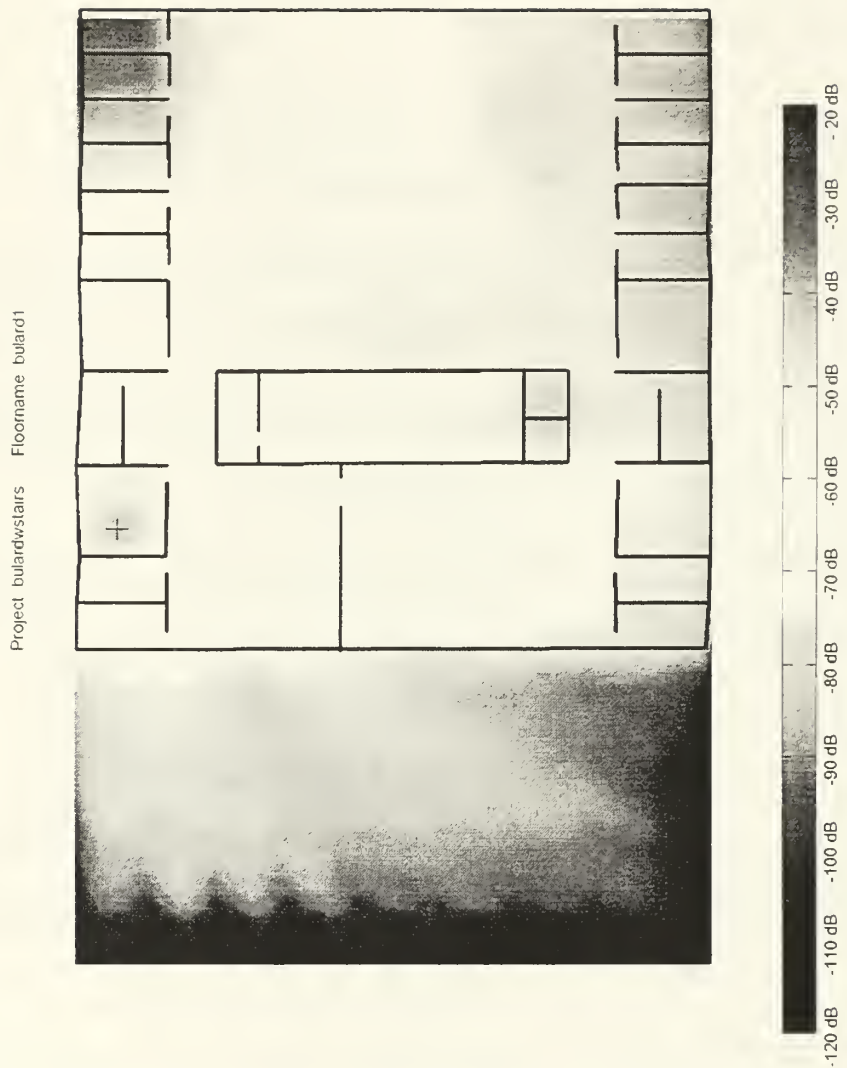


Figure 2.6: Bullard's 2nd Floor Relative Signal Strength Coverage Map Generated by PlaceBase (From [29])

4. Comparison of Empirical & Physical Models

In what follows, we attempt to contrast the two more popular models by showing their advantages and disadvantages.

a) Advantages

(1) Empirical models

- Simple and fast
- No requirement for detailed determination of the confined environment. Only basic facets are needed
- All environmental radio propagation factors are implicitly taken into account
- Computer specifications for implementing empirical models are on reasonable levels

(2) Physical models

- The more SISP data we include in the model the better the predictability for the indoor radio channel
- Reveal more physical details
- If employed properly, they are more accurate
- Predicted results are achieved without performing measurements
- Since they are based on the principles of physics, they can be used in a plethora of enclosed sites

b) Disadvantages

(1) Empirical models

- Do not take advantage of possible prior knowledge of the physical environment
- Do not provide reliable results if applied on complicated indoor situations (e.g. many obstacles, people etc)
- Do not take into account the waveguide effect that is profoundly important in corridors and tunnels
- Are inextricably dependent upon the accuracy of the measurements. All possible errors will affect the reliability of their predicted data.

(2) Physical models

- Any kind of distance or wall characteristics tolerances will have a negative impact on the results.
- In case they employ GTD/UTD methods, they inherently assume that the surfaces of the buildings and the ground are perfect flat planes, thereby neglecting scattering caused by small objects attached to those surfaces.
- In general, they are more time-consuming
- They largely depend on the accuracy of the input material properties

- They do not yield reliable results for distances far away from the transmitter due to the large number of interactions required in such cases. Hence the limitation of their coverage area.
- Since the walls and floors are inhomogeneous, some sort of trade-off becomes imperative. As a result, errors are likely.

5. In Which Group Does NEC-BSC Fall?

Clearly, since NEC-BSC obeys the UTD and accepts material properties as input data, it is regarded as a physical model. Moreover, among other calculated parameters, it implicitly extracts the PL and therefore is a path loss model. No information about the response delay is computed. NEC-BSC is described in the next chapter.

III. NEC-BSC

A. SHORT DESCRIPTION AND BACKGROUND

The Numerical Electromagnetic Code-Basic Scattering Code (NEC-BSC) is a high frequency EM analysis code, which employs the principles of UTD while interfacing concurrently with the MoM. It can simulate complicated scattering structures by utilizing relatively simple geometrical models like cylinders, plates, spheres etc. It was developed by the Ohio State University Electroscience Lab (OSU-ESL) in the early 1980's under U.S. government contract and has been upgraded many times since then.

It was originally written in FORTRAN 66 (version 1) but all subsequent versions were created with the use of improved FORTRAN 77. Very recently, (September 1999) FORTRAN 90 conversion commenced [38]. It is considered to be a user-friendly program since it requires only an elementary theoretical background in the fields of UTD, MoM, and EM diffraction. While its main features are presented later in this chapter, we should clarify at this point that this is not an antenna code in the sense that it does not calculate the current distribution or radiation resistance or any other pertinent information of antennas. Instead, given a specific current distribution, emphasis is given on the antenna pattern in various scattering environments [25].

B. OTHER WORKS BASED ON NEC-BSC

So far, the code has been used with satisfactory results for the calculation of the total electric field and the near and far field antenna pattern that arises from the following antenna-scattering structure interaction situations [39].

- From the mast or other superstructures of a ship [40].
- From a tank's body
- From the fuselage/wings of an aircraft
- From the living quarters of the International Space Station

NEC-BSC has also been used for comparison of measured and calculated patterns for different antenna placements and polarizations in these cases:

- International Space Station [41]
- Designing antennas for vehicular cellular applications (e.g. a patch-antenna studied in [42])
- Development of the Advanced Enclosed Mast/Sensor system (AEM/S) project of U.S. Navy, first introduced on USS Arthur W. Radford in September 1997 [41].
- H-60 Helicopter antenna [43]
- RCS measurements [44]

A research in the literature has revealed that this code was not thought to be attractive for predicting radio propagation in urban areas, with only one exception: a project in progress at OSU-ESL on cellular phone propagation around a building. Indeed, the code's author asserts that this is the case as there is no other work on indoor radio propagation using NEC-BSC version 4 [45]. Under this perspective the approach was challenging. Version 4 accompanied by a Graphical User Interface (GUI) named NEC-BSC Workbench was available during this thesis work. It should be stressed, however,

that during this work throughout 2000 the code was upgraded at least three times illustrating in a vivid manner its continuing revision by OSU-ESL.

C. NEC-BSC CAPABILITIES AND INHERENT ADVANTAGES

NEC-BSC can be run either on an IBM-compatible PC using Windows as operating system, or on a UNIX system. The GUI available for this code is the NEC-BSC Workbench and a Navy developed Silicon Graphics GUI for PC and UNIX, respectively. The exchange of data is performed in the form of ASCII files. The user inputs the data using either the Windows WordPad or Notepad, or the Workbench. During this process, which is based on a command word system, the user defines the geometry of structures and antennas and determines the various parameters needed to obtain a particular output antenna pattern. Initially, through the Workbench, which acts as a helpful editor, the user is informed about whether or not a syntax or another similar error exists in the input file. Then, the program's calculation engine is launched and generates warning messages, if any, and a progress bar. Finally, an output file will be created including the calculated results along with other files that the user might have asked for (e.g. an ORY file which permits the graphical representation of the EM rays used in the simulation). For instance, if the near-zone pattern of an antenna in a complex scattering environment was pursued, the resulting output will be the magnitude, phase, and dB value of the total electric and magnetic field, and the dB value of the Poynting vector at predefined observation points.

The Workbench features a visualization tool which greatly facilitates the geometry building. More specifically, the user builds the complicated environment by using simple shapes (plates, cylinders etc) and checks the arrangement with the help of Workbench.

Once the simulation run is over, the same graphical interface can be used for visualizing the reflected/scattered/diffracted paths, depicted as EM "rays", and various plots (e.g. total electric field versus distance).

The most significant capabilities of NEC-BSC are [39]:

- It can predict the Far/Near field pattern of an antenna in a complex environment
- It can provide the EMC or EM coupling between antennas in various situations
- It can determine potential radiation hazards
- It can optimize the design and placement of antennas at the early stages of development
- It can furnish the user with Radar Cross Section (RCS) calculations
- It includes the option for single frequency or multiple frequencies simulations
- UTD single, multiple, and triple plate interactions are possible.

The above discussion should enable the reader to understand the majority of the inherent advantages of NEC-BSC. However, the rest of them become clear only with experience. A good example in this respect is given in [42], though, we should note, the authors do not allude to the version they implemented. In any case, it would be instructive to consider their deductions as regards NEC-BSC:

- It is fast and time-efficient

- Various vehicle elements can be easily added or removed allowing for different EM considerations
- The position of the sources can be arbitrarily changed

D. LIMITATIONS OF THE CODE

Many of the code's limitations are directly caused by the very nature of UTD, namely [25]:

- The scattering mechanisms need to be known and included in the model. Should some be excluded or accidentally left out, the accuracy of modeling will be gravely affected.
- UTD may be employed only when the elements making up the model are large in terms of the wavelength.

Furthermore, according to NEC-BSC user's manual [39]:

- Each plate should have edges at least a wavelength long. For curved surfaces the requirement is that their major and minor radii and length should be at least a wavelength in extent.
- The source must be at least a wavelength from the surface and each antenna element should be at least a wavelength from all edges. Also, the receiving elements cannot be placed on a plate.
- The dielectric layers must be thin and support only one mode of the fields.
- At present, the solution does not contain surface waves, and hence the antenna cannot be placed close to the surface.

- The code is inadequate if a far zone backscatter or bistatic scattering result is desired.
- A diffracted field from the plate-curved surface junction is not considered in this version
- Accurate results can be expected for at most the first 30 dB of the pattern
- Graphics generation through the Workbench is restricted to some 2D (two dimensional) plots only. For 3D (three dimensional), polar, and other more complicated plots the user should resort to exporting the numerical results to other applications (e.g. MathCAD, Matlab etc).
- According to special instructions given in [38], there are certain limits as far as the total number allowed for each variable is concerned. These limits are shown in Table 3.1.

Numerous as these limitations might appear to be, they did not inhibit, at least severely, the indoor propagation simulations. All objects' dimensions in the input file were much larger than the wavelength and this fact alone satisfied most requirements. Further discussion is made in Chapter V.

Variable	Maximum number
Pattern points	1801
Defined pattern points	181
Defined frequencies	181
Plates	200
Plate edges	30
Curved entities	200
Curved sections	10
Material types	25
Material layers	20
Sources	300
Receivers	300
Antenna data points	91
Wires	200

Table 3.1: Variables limits

THIS PAGE INTENTIONALLY LEFT BLANK

IV. NEC-BSC EXAMPLES

This chapter presents three simple examples of indoor prediction using the NEC-BSC. The objective is to demonstrate some of the code's capabilities in determining the near-field pattern of an antenna surrounded by obstructions much larger than the wavelength. First, the geometry is defined and a short description of shapes and materials comprising the model is made. Then, the observation points for each run are explained. Finally, the extracted results are shown in various plots and their interpretation is discussed. MathCAD was used for these and all subsequent calculations and plots shown in this thesis. In only one case, shown later in this chapter, the NEC-BSC Workbench was used and this was done for demonstration purposes. All input files used in the following simulations are given in Appendix A.

A. A RECTANGULAR PEC ROOM WITH A CYLINDER

In this first example, we calculate the electric field (E-field) for two different near-field patterns: one forming a circle around an obstacle and one running through the middle of the room. We consider a room with dimensions 6m x 14m x 6m (width x length x height) containing a cylinder of 1 m height and 1 m radius. The cylinder is located precisely at the center of the room. All room's walls, the floor and ceiling, and the cylinder are perfect electric conductor (PEC) materials. Midway between the cylinder's central point and the 6-meter wall a vertically polarized half-wave dipole is placed. The frequency of transmission is 2.45GHz and hence the wavelength is 12.2364cm. In order to conform to all NEC-BSC requirements explained in Chapter 3, the dipole is positioned

at 3m (i.e., 24.5 times the wavelength) away from all obstacles. Furthermore, to account for correct attachment of the cylinder to both the ceiling and floor we let the cylinder intersect the floor and the ceiling at depth 0.07 times the wavelength [39], [43].

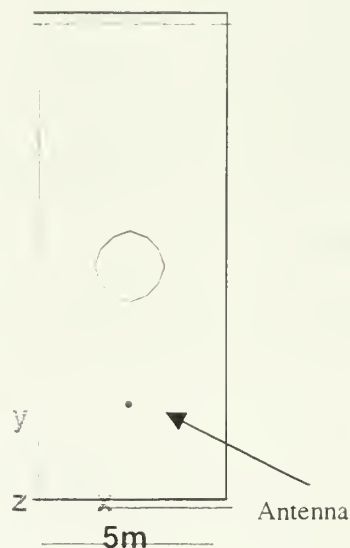


Figure 4.1: Ground Plan of Room with Cylinder

1. Circular Near-Field Pattern

The E-field in 360 points (each one corresponding to 1 degree step) around the cylinder is first calculated. The answer is given in dBV/m for all E-field components as a function of the observation points coordinates. A particularly helpful visualization tool of the Workbench allows the user to actually see the area covered by the rays launched by NEC-BSC (figure 4.2). This information is obtained by using the command LY and the program will generate an ASCII file by the extension ORY, which comprises the positions of the starting, hit, and end points of the rays along with signal strength values [39]. It should be noted that by virtue of user defined filters it is possible to exclude all

rays smaller than a certain value. Moreover, the number of interactions shown can be adjusted.

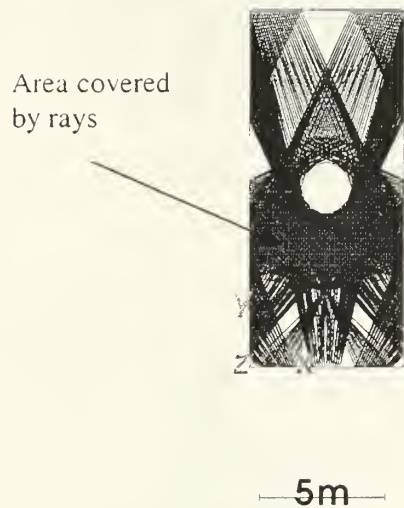


Figure 4.2: Circular Pattern: Area Covered by Rays

In figure 4.3, the plot of the results for the three E-field components as a function of angle φ is shown. As expected due to symmetry, the values at angles 0 and 180 degrees are equal. However, it is observed that the signal strength is larger at points between the cylinder and the antenna ($\varphi=270$ degrees) than behind the cylinder ($\varphi=90$ degrees). This fact can be attributed to the cylinder acting as a strong reflector in the former and as an obstacle in the latter case. The Workbench creates a plot of all three components but not of the total E-field. Hence, a separate application should be used if other than the default plot is desirable.

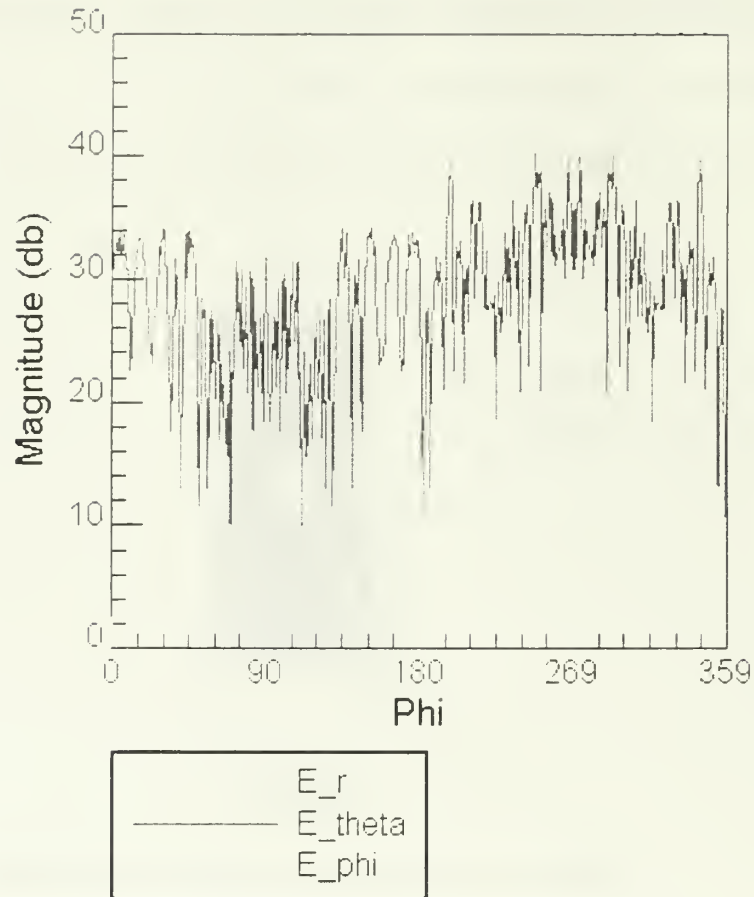


Figure 4.3: E-field Components versus Angle φ Plot Created by Workbench

2. Line near-field pattern

Let us now find the variation of the E-field along a line passing through the centers of the antenna and cylinder. The observation points are sampled at a rate of half-wavelength (i.e., 0.0612m); therefore, a line consisting of 229 points is formed. Again the field in front of the cylinder (where the antenna is located) is clearly stronger compared to the area behind the cylinder. In addition, the multipath phenomenon caused by the numerous reflections off the walls and the diffraction from the cylinder surface accounts for the deep attenuations observed in the plot shown in figure 4.4. The discontinuity at the

7-meters distance point is due to the presence of the PEC cylinder. Ideally, no penetration of rays inside the cylinder should occur. However, it can be noticed that there is erroneous prediction of E-field existence in 1m-depth inside the cylinder's interior, which manifests itself in the plot shown in figure 4.4. Every effort was taken to eradicate this anomaly. Despite the fact that the cylinder was slightly tilted and rotated in several consecutive test simulations, the problem persisted. No explanation could be found for this discrepancy apart from the suspicion that the code probably suffers from an undetected bug.

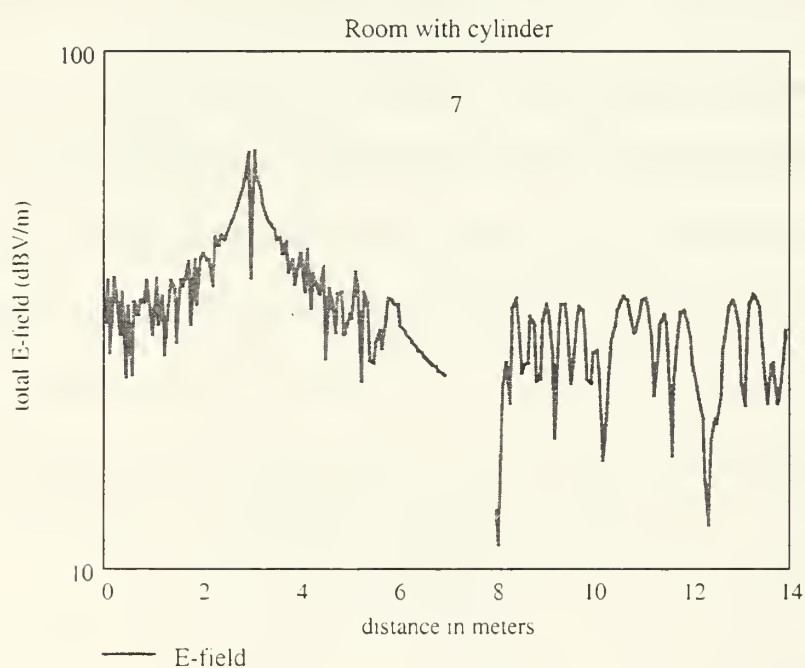


Figure 4.4: Total E-field versus Distance (vertical polarization)

B. A TYPICAL ROOM

In this example, a volumetric E-field pattern of an antenna located inside a typical room is calculated. All room's dimensions and materials' constitutive parameters were found in [47] and are shown in Tables 4.1 and 4.2. However, the observation points were

redefined to meet this example’s particular needs. The room along with the pattern used for this simulation is shown in figure 4.5.

The antenna used is a vertically polarized dipole with piecewise sinusoidal current distribution and the transmission frequency is 900MHz, hence the wavelength is equal to 0.3331m. Again no obstacle exists within the antenna’s near-field. This time we would like to know the excess gain/loss of the E-field in the entire room at a level 1.22m above the ground. For that purpose a volumetric pattern with the outer and inner loop consisting of 54 and 32 points, respectively, is defined. The sampling rate is half-wavelength which corresponds to approximately 0.1665m. Thus, the E-field is calculated at 1728 observation points. The resulting “excess gain”, i.e., the ratio of the total E-field in room over the total E-field in free space for every observation point, is shown in figure 4.6. It should be noted that for this and all subsequent excess gain/loss calculations a dynamic range of 30dB has been applied. In other words, all values more than 30dB lower than the maximum value have been set to 30 dB below the maximum. This practice was followed in order to comply with the NEC-BSC limitations [39].

All dimensions in inches	Length	Width	Height
Room	360	216	112
Smaller interior room	120	144	122
Window	32		98
Door opening	36		84

Table 4.1: Room’s Dimensions

Some different statistics were also considered in this room. First, the variation of the normalized difference between the predicted and the free space E-field as a function of distance from the antenna was investigated. Accordingly, the whole volumetric pattern was divided into several circular discs with radii ranging from 0.5 to 7 meters, thereby creating 14 “circular sectors.” Hence, all observation points fall in one of these sectors forming various “groups.” Each of them corresponds to a certain distance from the antenna. An important fact is that not every group has the same number of points owing to the unequal surface of each circular sector. Nevertheless, very significant conclusions can be reached by this approach. In figure 4.6, the resulting histogram of the aforementioned normalized differences is shown. The X-axis is the radius of each circular disc from the antenna in “steps” of 0.5 meters while the Y-axis is the number of “bins” for this computation.

Material	Thickness (in inches)	Relative permittivity	Dielectric loss tangent	Relative permeability	Magnetic loss tangent
1 st layer: 6'' bricks	0.53	3.0	0.048	1.0	0
2 nd layer: 6'' bricks	5.11	1.5	0	1.0	0
3 rd layer: 6'' bricks	0.53	3	0.048	1.0	0
Glass	0.125	5.23	0.013	1.0	0
Floor	0.125	2.38	0.048	1.0	0

Table 4.2: Room's Properties

Second, the probability density function (pdf) of the normalized difference between the E-field in the room and in free space for all distances is estimated and plotted against a Gaussian pdf for direct comparison. The Gaussian distribution, shown in figure 4.7, has zero mean and 0.6 times the variance of the normalized difference random variable.

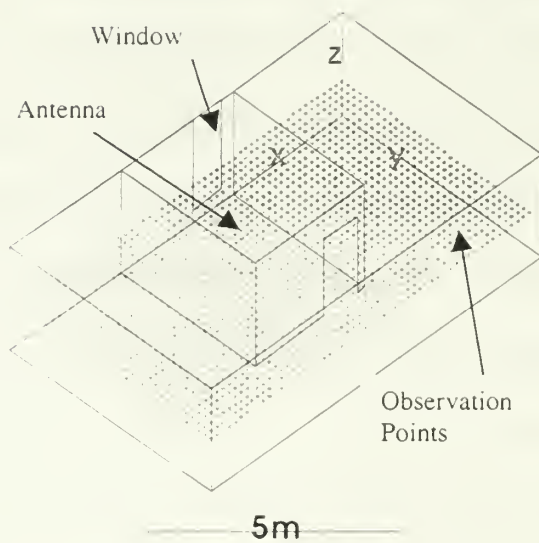
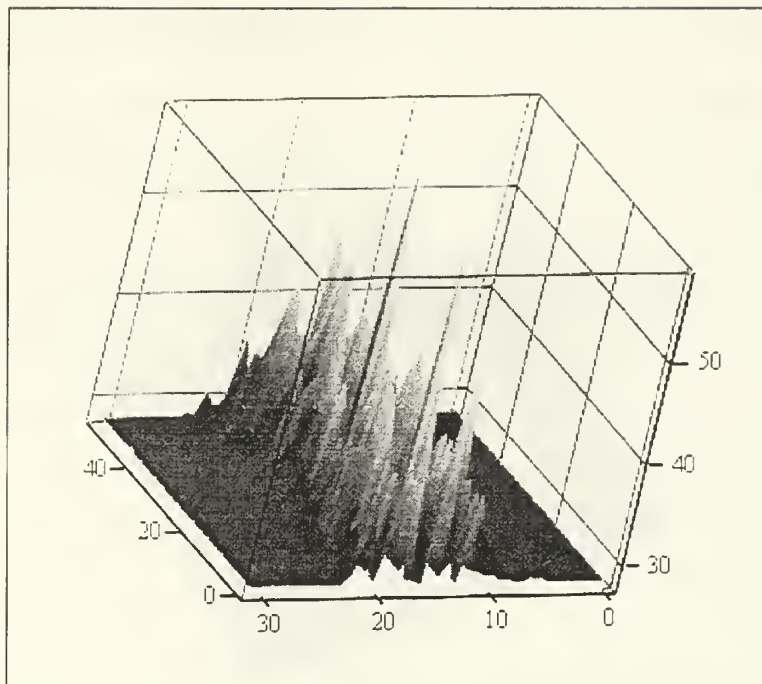
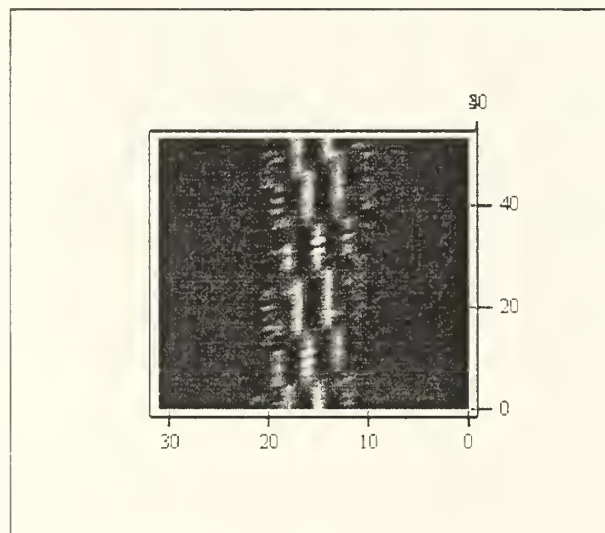


Figure 4.5: A Typical Room



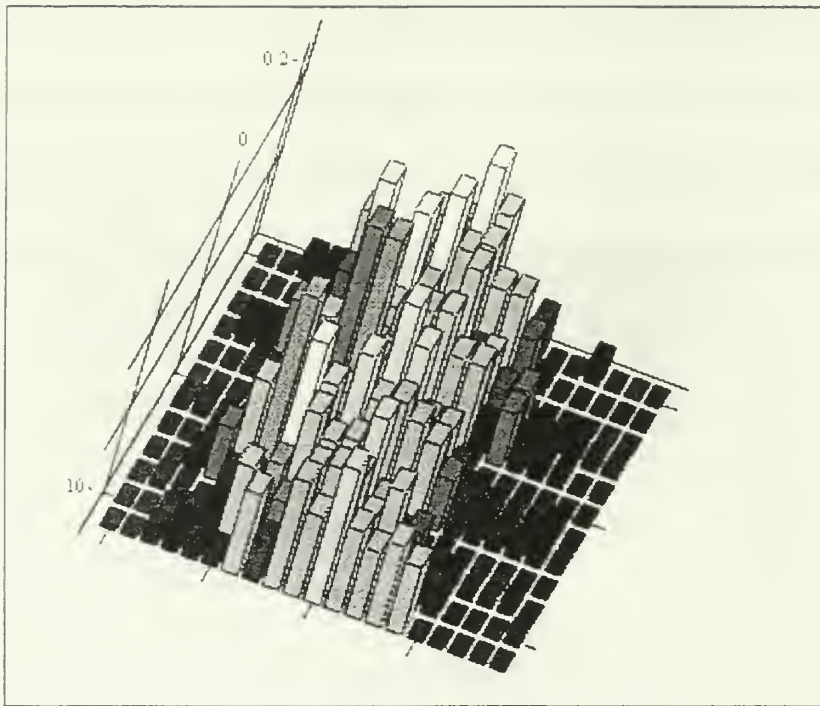
room_field

Figure 4.6: Excess Gain (dB) (oblique view)



room_field

Figure 4.6: Excess Gain (dB) (top view)



L

Figure 4.7: E-field Normalized Difference

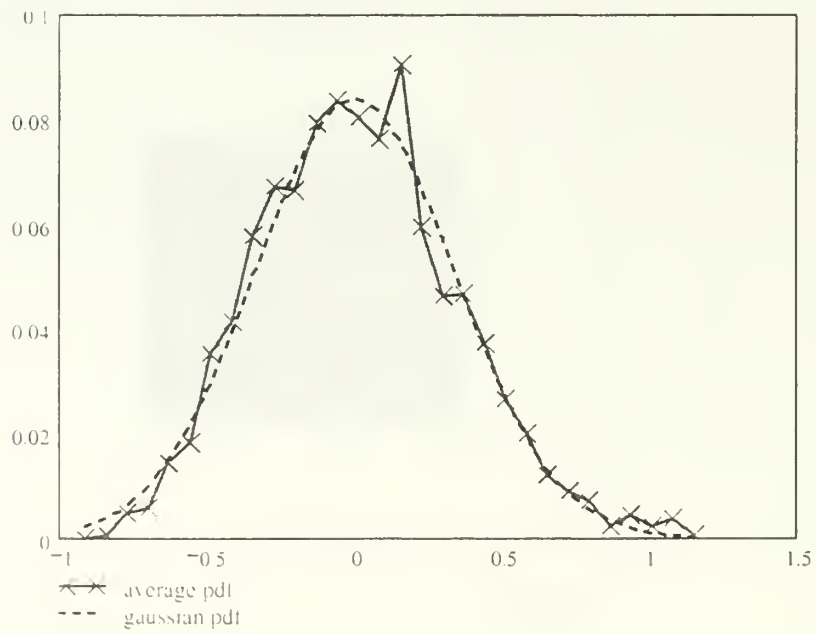


Figure 4.8: Normalized Difference Random Variable Compared to Gaussian pdf

Finally, the cumulative distribution function (cdf) for the normalized difference random variable for all ranges as a function of the loss in dB is determined. This is useful for communication engineering purposes and it is shown in figure 4.9. In the same figure it can be noticed how closely the Gaussian cdf matches the normalized difference random variable cdf. Further discussion of the importance of these statistics is made in Chapter VI.

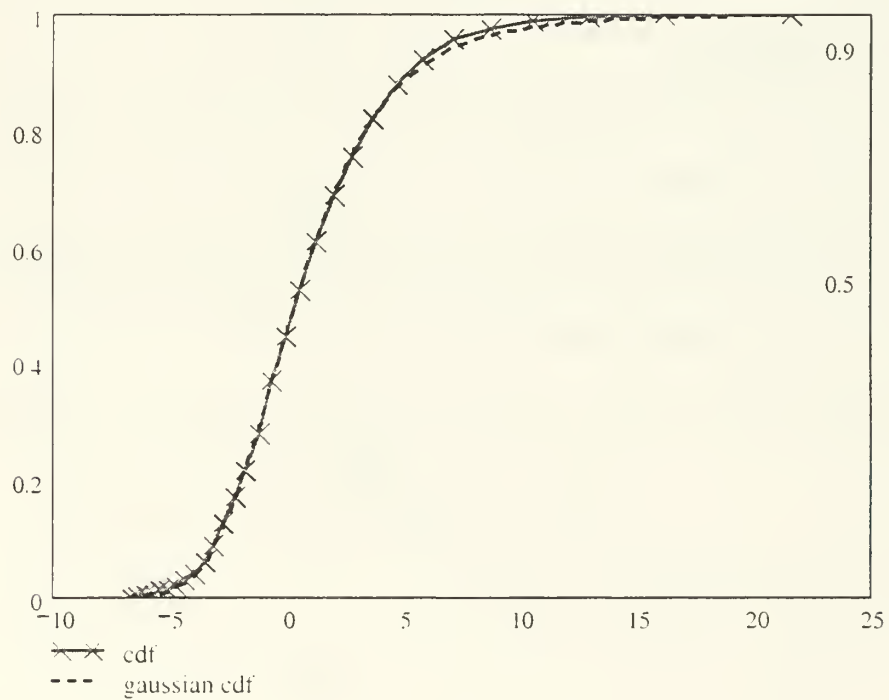


Figure 4.9: Normalized Difference Random Variable cdf versus Loss in dB

C. COMPARISON WITH THE SHOOTING-AND-BOUNCING RAY (SBR) METHOD

In this example, the path loss along a line inside a rectangular room containing a closet is found. The dimensions and material properties of this room are described in [48] where the path loss was extracted using a modified shooting-and-bouncing ray/image ray-tracing approach (SBR). The same room was also modeled in [31] and [37] and the results were compared to those of [48]. The antenna used was a vertical Hertzian dipole and the operating frequency 1GHz. A visual representation of the NEC-BSC model is shown in figure 4.10.

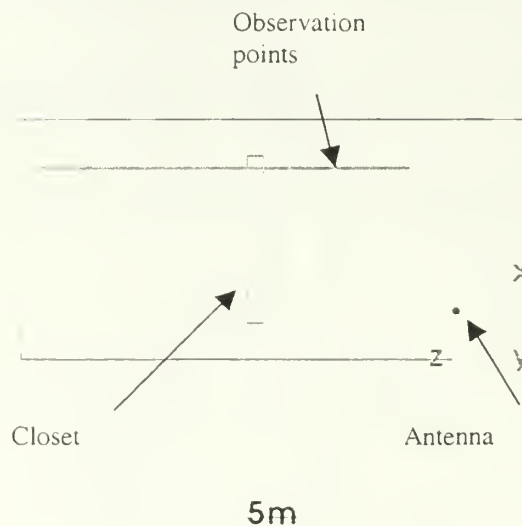


Figure 4.10: Room with Closet

As it is usually the case for most deterministic models, the task of choosing the suitable material parameters for accurately modeling composite or even uniform walls is challenging. More specifically, in NEC-BSC special consideration is required in selecting

the appropriate ZD commands as well as the correct relative permittivity (ϵ_r), loss tangent ($\tan \delta$), and relative permeability (μ_r) values for all walls and obstacles, the floor and the ceiling. This fact has been verified many times during these comparison simulations. Every effort was taken to detect that combination of commands and material properties, which would lead to the closest possible match between NEC-BSC and SBR method's predicted path loss. Clearly, since the NEC-BSC user's manual does not but scarcely lend itself into indoor environments modeling, all the burden falls on the user who will have to have a good deal of prior EM indoor propagation exposure. Furthermore, for the same reason, the correct interpretation of the results and/or the efficient intervention in the input file to make alterations, wherever applicable, are sufficient prerequisites to exclude inexperienced users from working on NEC-BSC. Prior to arriving at the results shown in this section, many discouraging predicted data were found and extensive investigation had to be performed in order to uncover the cause of the problems even for such a relatively simple room as this one.

In the second example, the floor was modeled as "half-space" material [39]. In this case, however, this choice did not work. Moreover, the information provided in [48] strongly indicated that the use of "one-sided coated" material ZD-command for modeling the ceiling and floor was necessary. Again this approach was not justified by the results. Also, converting all plates into PEC material type yielded rather optimistic results for the first several meters and inaccurate results thereafter. Therefore, contrary to what was originally perceived as the right path to follow, the employment of transparent slabs for all room's plates was chosen, resulting in satisfactory agreement with the SBR method.

Yet this approach assumes that no PEC backing behind the slabs is present, which could be viewed as a shortcoming intentionally imposed on the model. To lend credence to this unorthodox assumption, two different input files were created: one with PEC slabs at distance 0.00667 times the wavelength (0.299792 meters) behind the walls and another without these PEC slabs. The idea was to try an indirect method of accounting for the PEC backing by inserting in the original input file PEC slabs, allowing at the same time a small yet non-negligible “air-cushion” in between the wall slabs. The resulting path loss of the two approaches is plotted against the SBR results for direct comparison (figures 4.11 and 4.12). Furthermore, an even more illuminating plot is given in figure 4.13 where the relative accuracy, meaning the difference (in linear values) between the path loss values predicted by BSC and SBR, of the PEC and no-PEC results are contrasted with each other. The sharp improvement achieved by the “no-PEC solution” manifests itself by the relative proximity of the “no-PEC curve” to the x-axis (distance) as opposed to the larger variations over and below the x-axis of the “PEC solution” curve.

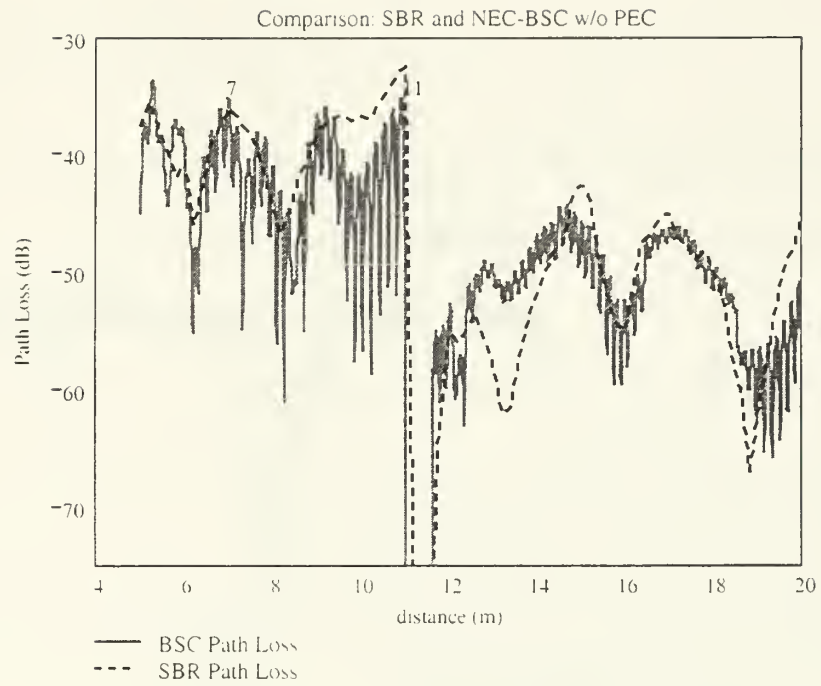


Figure 4.11: SBR and NEC-BSC (w/o PEC) Results

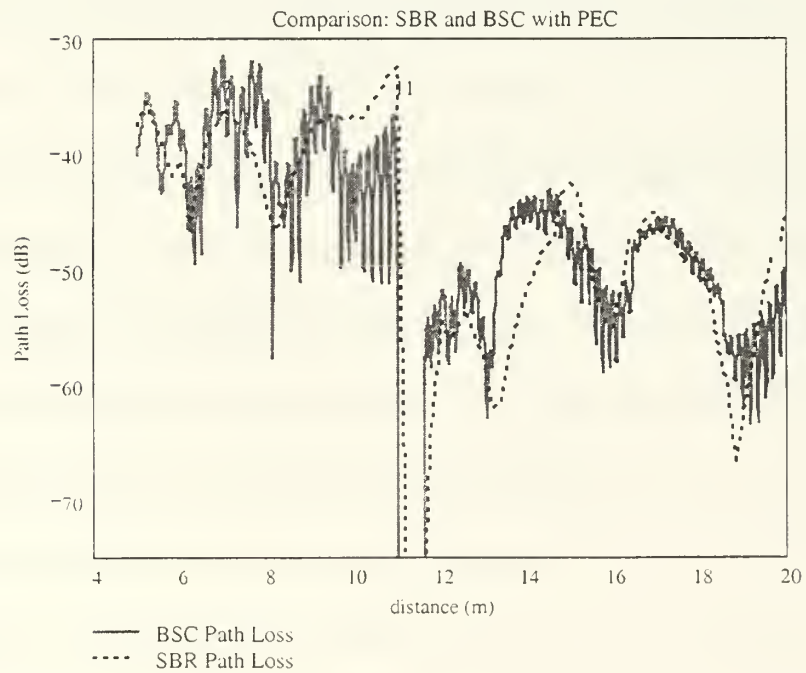


Figure 4.12: SBR and NEC-BSC (with PEC) Results

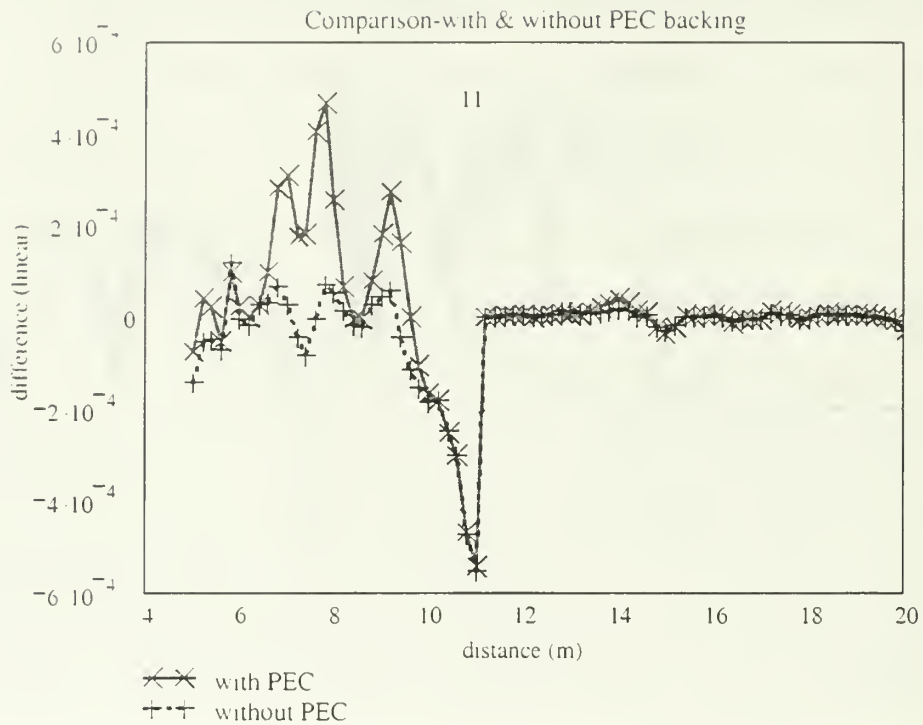


Figure 4.13: Contrasting the Relative Difference of the PEC with the no-PEC Solution

Having found a particular NEC-BSC model, which more accurately described the path loss variation along a line inside the furnished room, the next course of action was to use that model to draw some additional conclusions with regard to both NEC-BSC validity and indoor propagation in the room under consideration. In doing so, the figure 4 14 is drawn where the path loss versus distance for the empty (denoted Plempty) and the furnished (denoted PIfurnished) room are shown. The difference between the two can be explained by the existence of a typical multipath-fading environment being further affected by the presence or absence of the closet for the furnished and empty room, respectively. Furthermore, the path loss in the furnished room is slightly less than the

path loss in the empty room for all points before the closet's location (at $z = 11\text{m}$). By contrast, the former is significantly larger than the latter right after the furniture. As in the first example, this is due to the fact that the closet is a strong reflector for the part of the room closer to the antenna whereas it is a blocking obstacle for the remainder of the room.

Finally, in figure 4.11, the NEC-BSC predicted path loss is compared to the SBR method's results where a relatively good agreement is noticed. It should be noted that higher sampling rate was used in NEC-BSC compared to SBR depicted data. In particular, in NEC-BSC there was 1 observation point every 1cm while 1 data point every 20cm was used in drawing the SBR curve. In addition, the SBR data points were taken directly from the path loss graph of [48] rather than from a raw data file and, consequently, errors are certain to have been introduced in the approximations applied during that process. Therefore, some differences observed in figure 4.11 can be partly attributed to this fact. In any event, even in the comparisons presented in [31] and [37] there was not exact match between the curves of the other methods and the SBR solution. In conclusion, though not impeccable, the NEC-BSC results obtained under the afore-described assumption of no-PEC backing are reckoned to be acceptable adding some confidence to employing this code in other indoor environments.

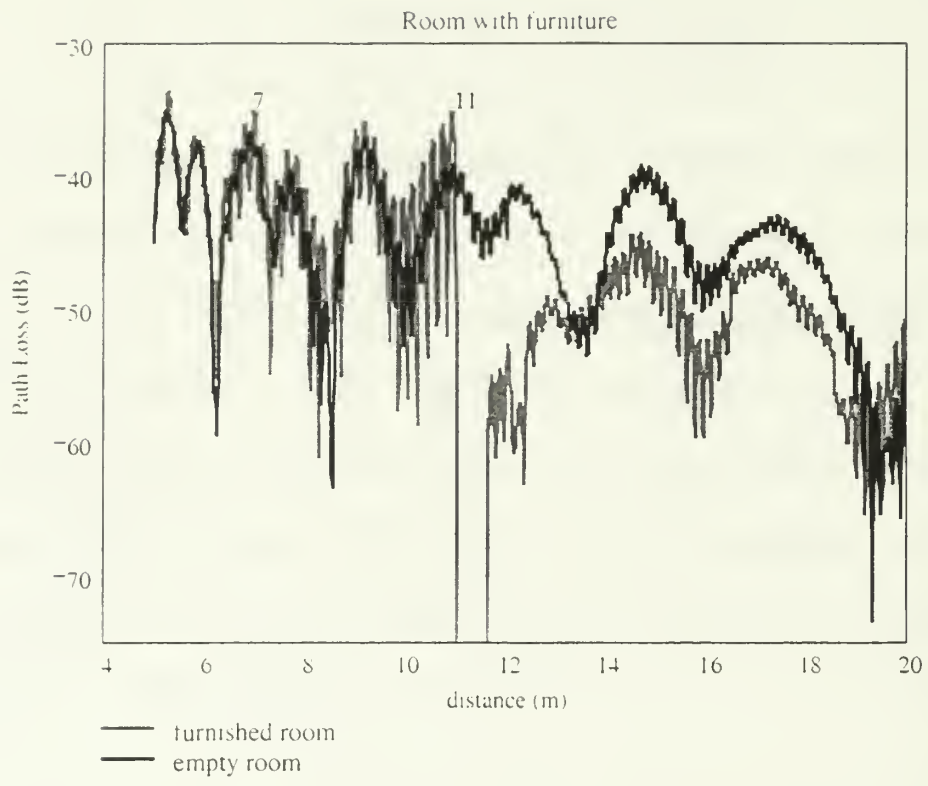


Figure 4.14: NEC-BSC Path Loss Results for the Furnished and Empty Room

V. THE MODEL

No simulation or test is complete without a description of the environment under examination. Equally essential is the inclusion of all indispensable simplifications that had to be made in order to conduct the evaluation of the tool in question. These topics are covered in this chapter.

A. GEOMETRY DEFINITION

The measurements reported in [11] took place on the second floor of Bullard Hall at the Naval Postgraduate School in Monterey, California. This building is rather old, built in 1958. The second floor of this building has enough complexity to create a harsh multipath environment for indoor radio propagation. Its dimensions are 39.8272m x 39.8272m x 3.81m (length x width x height) and it contains a vast diversity of materials like concrete for exterior walls, glass for windows, plasterboard for most partitions, sheetrock with metal studs for some walls, acoustic tiles, wooden tables, concrete reinforced columns and more. Its main function is providing space for laboratory experiments; therefore a large amount of testing equipment is spread around its main hall, which occupies a large part of the total available space. However, it also includes several offices and classrooms (with desks, chairs, wall-shelves etc), which are located at the perimeter leaving the laboratory at the center of the second floor. Hence, both lossy and good reflector objects are present throughout the second floor of Bullard Hall posing a profound problem for all modeling tools. A visual representation of the Bullard's second floor created by NEC-BSC Workbench is shown in figure 5.1.

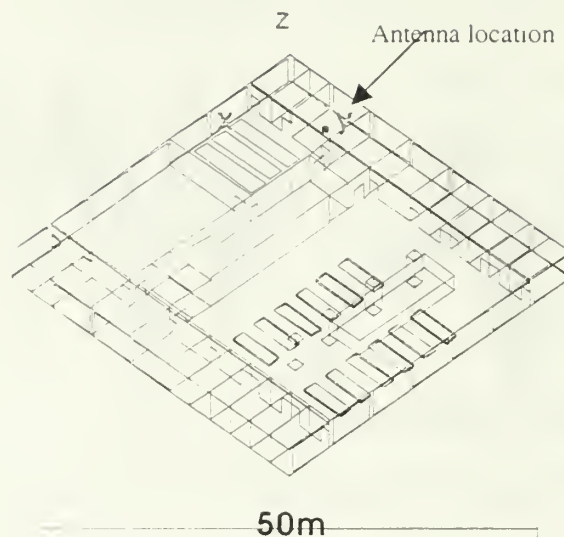


Figure 5.1: Bullard's Second Floor Created with the NEC-BSC

Defining the geometry of the NEC-BSC model in this particular problem was not an easy task. Because of the age of the building CAD data was not available. Instead, the building's blueprints were used to extract all necessary information about dimensions and materials inside Bullard Hall. That data was far from sufficient, and on-site inspection was made in order to ensure the best possible accuracy. Yet it was not possible to model some significant construction details and thus a number of compromises were made, which are described later in this chapter. It should be emphasized that even if data in CAD format were readily available, it would not have been of much help. The current NEC-BSC version is not accompanied by CAD compatible *graphical user interface* (GUI), which would greatly facilitate the ASCII data input. It is assumed that a drawing tool developed particularly for NEC-BSC would minimize the time required for creating the model [46].

Once all dimensions and coordinates were identified, the Bullard's second floor was modeled by employing the single or multiple plates commands. That way, all exterior walls and windows, the floor and ceiling, all office and room partitions, all wooden tables, and most columns and sheetrock walls were included in the model. In writing the input file, special attention was paid to the area near the antenna whereas most details were omitted further away; they were assumed to have an insignificant effect on the radio propagation at close distances from the antenna. Furthermore, in developing the geometry of the simulated floor, one exceedingly favourable fact, which was taken advantage of, was the existing symmetry of many structures. For example, the dimensions of all office/classroom partitions were identical. In such cases, the employment of the RT command expedited the entire work. In short, by virtue of this command, the user has to create only once the plate or structure which repeats itself several times. Once this is done, the object can be duplicated as many times as it is necessary and shifted to the desired location. However, since this capability was not documented in the NEC-BSC manual, several tests had to be performed to confirm its validity. These tests were successful and proved that this "trick" yields correct results. In a different arrangement, for instance, it can be used to create the steps of a staircase faster than using geometry commands repeatedly.

The antenna used in the model was a Hertzian dipole with uniform current distribution and operating frequency 2.45GHz. It was located at the center of the room where the actual access point was during the measurements of [11]. Although the polarization of the antenna is not reported in [11] it is assumed to have been vertical since

it is well known by many experiments that vertical polarization has an advantage of at least 4 dB for same-floor indoor radio propagation [50]. Also, the antenna's height above the ground was assumed to be 1 meter. In fact, in measurements reported in [3], [16], [29], and [31] the antenna's height ranged from 1 up to 3 meters, thereby giving credence to that assumption.

It has been argued countless times in the literature that the correct selection of the constitutive parameters of the walls, floor, ceiling and obstacles plays the most significant role in all physical models. NEC-BSC is no exception to this well-established rule. Unfortunately, the exact values for every single construction material are not available. The immense diversity of both composite and non-composite materials found in all buildings makes it almost impossible to tabulate them all. Hence, it is most of the times the case to approximate these values using various methods. In this model, the standard values for the most common materials used (cement, plaster, glass etc) were taken either from [49] or [29] and they are shown in table 5.1. In all cases the relative permeability and the magnetic loss tangent were assumed to be equal to 1.0 and 0, respectively.

Material	Relative permittivity (ϵ_r)	Dielectric loss tangent ($\tan \delta$)
Concrete	4.0	0.004363
Reinforced concrete	5.84	0.001416
Plaster	2.3	0.001745
Wood	1.5	0.01
Metallic mesh	5.896	0
Artificial composite wall	8.247	0.004363

Table 5.1: Constitutive Parameters Used in the NEC-BSC Input Files

Moreover, in two particular cases a different concept was introduced: in front of the instruments room where a metallic mesh is located, and in one wall of the antenna's room, which consists of approximately 80% plaster and 20% metallic beams. The goal was to calculate the ϵ_r in these cases under the assumption that they be replaced by "artificial walls" with the same EM reflectance and transmittance and proportions of constituent materials. This concept is discussed next.

1. Metallic Mesh

On-site inspection of the metallic mesh in front of the instruments room revealed that if A and a are considered being the total surface of the mesh and the metallic structure, respectively, then a/A equals 0.17355. This conclusion justifies the assumption

that if the actual metallic mesh was to be replaced by an “equivalent” wall having the same material proportions then the latter would consist of 82.6447% air and 17.3553% metal. It can be further assumed then that only the “air-part” of this so-called “equivalent” wall contributes to transmission and only the “metallic-part” reflects back EM energy. Therefore, if P_{in} and P_{tr} are the incident and the transmitted, respectively, power of an EM wave impinging normally on the “equivalent wall,” and if no absorption occurs, then:

$$P_{tr} = \left(1 - \frac{a}{A}\right) * P_{in} * [1 - (|\Gamma_{air}|^2)] \quad (5.1)$$

$$P_{tr} = P_{in} * [1 - (|\Gamma_{mesh}|^2)] \quad (5.2)$$

where Γ_{air} and Γ_{mesh} are the reflection coefficients of air and mesh, respectively. It

is also true that:

$$\Gamma_{mesh} = \frac{1 - \sqrt{\epsilon_{mesh}}}{1 + \sqrt{\epsilon_{mesh}}} \quad (5.3)$$

$$\Gamma_{air} = 0 \quad (5.4)$$

where ϵ_{mesh} is the relative permittivity of the “equivalent wall” replacing the mesh.

From equations (5.1) to (5.4) it follows that:

$$1 - \left(\left| \frac{1 - \sqrt{\epsilon_{mesh}}}{1 + \sqrt{\epsilon_{mesh}}} \right|^2 \right) = 0.826447 \quad (5.5)$$

or

$\epsilon_{mesh} = 5.896$, which is the value that will be used in the input file for the NEC-BSC Bullard Hall model.

2. “Equivalent” Composite Wall

Following the same concept of “replacing” the actual wall by an “equivalent” wall with a supposedly equivalent effect on the transmitted EM energy, the sidewall next to the antenna was assumed to consist of 80% plaster and 20% metallic studs. Consequently, the following equations can be derived:

$$P_{tr} = (1 - 0.2) * P_{in} * [1 - (|\Gamma_{plaster}|^2)] \quad (5.6)$$

$$P_{tr} = P_{in} * [1 - (|\Gamma_{comp}|^2)] \quad (5.7)$$

$$\Gamma_{plaster} = \frac{1 - \sqrt{\epsilon_{plaster}}}{1 + \sqrt{\epsilon_{plaster}}} \quad (5.8)$$

$$\Gamma_{comp} = \frac{1 - \sqrt{\epsilon_{comp}}}{1 + \sqrt{\epsilon_{comp}}} \quad (5.9)$$

where $\Gamma_{plaster}$ and Γ_{comp} are the transmission coefficients of the “plaster-part” of the actual wall and the “equivalent” composite wall, respectively. Also, $\epsilon_{plaster}$ is the relative permittivity of plaster equal to 2.3, and ϵ_{comp} is the relative permittivity of the “equivalent” wall with the same EM properties as the real one. From equations (5.6) to (5.9) it follows that:

$$\epsilon_{comp} = 8.247 \quad (5.10)$$

and that was again the value used in the simulations pertaining to Bullard Hall.

B. MEASUREMENTS

In 1999, laboratory testing was conducted on the 2nd floor of Bullard Hall and the results of the signal strength and throughput measurements were reported in [11]. The goal was to evaluate four commercially available wireless networking components in a typical multipath environment. Therefore four different sets of data were obtained which give a good idea of the actual coverage area.

One access point located in the thesis students' room and two wireless client computers were used for the tests. The transmitted power ranged from 300 to 365mW depending on the type of component. As far as field strength results are concerned, they were measured either in percentage or as signal to noise ratio. The maximum coverage area was determined by detecting the locations at which the client was no longer able to maintain communications with the access point. This fact, of course, limited the extent of measurements as a large portion of the second floor was ruled out and no data were obtained. Furthermore, the signal strength was not measured in the neighbouring to the antenna's location rooms. The best performance was delivered by the Lucent Technologies WaveLAN IEEE components and the pertinent coverage is shown in figure 5.2.

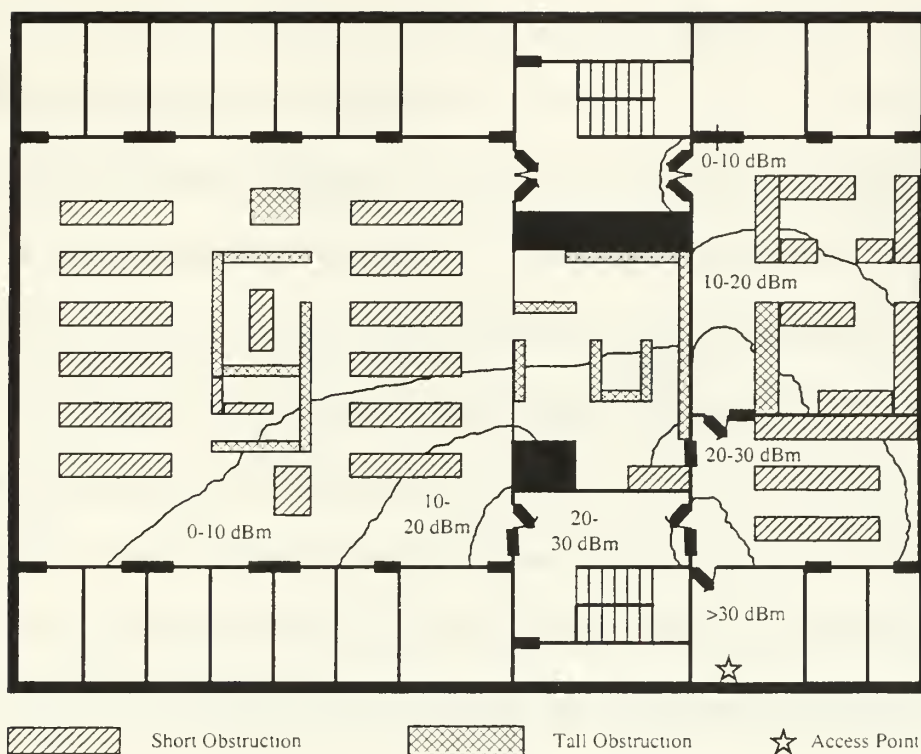


Figure 5.2: Lucent Technologies WaveLAN Coverage (from Ref.[11])

C. SIMPLIFICATIONS

Many practical and code-related difficulties were encountered while developing the NEC-BSC model. Most of them were trivial and a way around was often found. However, some problems were persistent and almost impossible to overcome and a kind of compromise was made. In addition, in other cases for the sake of accelerating the simulations some simplifications were included in the model, which, strictly speaking, are likely to have affected the accuracy of the predicted results. In what follows, all the above actions are identified and described concisely.

1. ZD commands

Whenever an object inserted in the model has different properties (either constitutive parameters or thickness) than the one before, it must be preceded by an appropriate ZD command. Since the current version's configuration allows a maximum number of 25 ZD commands in each input file, the order of alternate geometry and structure definition commands must be meticulously arranged so as to avoid error or warning messages from the code. Furthermore, being restricted for the above reasons, the user will have to limit the overall number of different materials used in the model. For example, if within a particular room there are more than 25 different types of materials, the user will have to devise an "intermediate" set of properties for some of them to account for this limitation of the code.

2. Plates

The model developed in this thesis comprised numerous plates. Various structures and furnishings encountered in Bullard Hall were excluded from the model, nonetheless, and one reason was the maximum allowed number of 200 plates for each input file. Another reason was the difficulty to attach together certain plates. It was found that the suggested plate attachment process described in [39] could not prevent the appearance of problems in some cases. Although all criteria were met in various plate attachments, the code still returned meaningless results sometimes, but not always accompanied by warning messages. This problem could be avoided by either shifting the plate in question slightly away from the originally desired position or by completely removing it from the input file. Despite the above-described difficulties, the second floor NEC-BSC model did

not deviate from the standards of other applications (like the one in [29]) as far as geometrical representation is concerned.

3. Presence of people

It has been shown that the density of people's presence inside a building has a profound effect on the received signal statistics [51]. Even when the transmitter and receiver are fixed the human motion can result in 2-10 dB attenuation of the average signal strength [52]. This fact could not be taken into account.

4. Radiation scattered by neighbouring buildings

EM radiation can leave a building through a window and come back after being scattered by neighbouring buildings [33]. This fact can be crucial for larger distances as these "out-and-in" ray paths can carry substantially more power compared to rays propagating through many walls within the building. The neighbouring buildings were not included in the model, but their actual distance from Bullard Hall is fairly large (ranging from 30 to 60 meters) and therefore it is thought that their effect is negligible.

5. Clear space boundaries

In [32] it is argued that the boundaries of clear space, through which the signal propagates, plays an important role and it should be included in any model. Whereas the lower bound was implicitly taken into consideration by including some furnishings, the same was not true for the upper bound which is formed by pipes, support beams, ventilation ducts, and lighting fixtures that protrude from the ceiling of Bullard Hall's second floor.

THIS PAGE INTENTIONALLY LEFT BLANK

VI. SIMULATION ANALYSIS

A. PLATFORM CONFIGURATION AND TIME PERFORMANCE

All simulations were executed on an IBM-compatible PC using Windows as its operating system. The CPU was an Intel Pentium III at 600 MHz and the RAM memory was 768MB. The NEC-BSC Workbench and the main executable NEC-BSC FORTRAN program versions used were the 4.1.37 and 4.2-06, respectively. These versions were not the most recent ones but, rather, the most stable. In general, the Workbench performed well even when large files (several Mbytes) were analyzed. More specifically, there were only two cases where the Workbench either crashed or displayed erroneous figures. First, when very large rays files (usually a couple Mbytes) were called the Workbench operation stalled and reboot was necessary to resume calculations. Second, sometimes when a relatively big object was placed next to a small one the Workbench responded by showing the former in a clearly shifted position away from the correct one. This problem appeared only in the oblique (default) view option.

As far as time performance is concerned, it was found that it was proportional to the number of observation points, the complexity of the environment and the relative location of the antenna. In particular, the number of observation points varied from 696 points, for the comparison file, to 26,244 points for the statistics files. In the latter files the observation points were taken at a sampling rate twice the wavelength. For all practical purposes, that was the best attainable sampling rate, as anything better would require unreasonable CPU time resources. The total number of plates in the input files

was 181, while the number of materials used was 19. Furthermore, the antenna was placed at five different locations including the room from which all actual measurements were carried out. It was observed that the time required for the calculation of the E-field in the 26,244-points file ranged from 1,536 to 2,293 CPU minutes, whereas only 145 minutes were needed in the 696-points file. The conclusion arising from these findings plainly proves that time performance explicitly depends upon the total number of observation points.

B. COMPARISON WITH MEASUREMENTS

Since the results with regard to signal strength in [11] are presented in the form of range of dBm values for different coverage areas throughout the Bullard's second floor rather than for specific locations, direct comparison between measured and predicted values is not possible. Instead, a qualitative comparison can be accomplished by visually comparing the coverage obtained by the in-site testing and the corresponding predictions of NEC-BSC. Indeed, by contrasting figures 5.2 and 6.1 one can infer that there is a relatively good agreement at least in terms of overall coverage. Figure 6.1 shows the predicted excess gain/loss for the same floor. It is clear that, while the signal is strong inside the antenna room, it rapidly attenuates along the Y-axis where penetration through many walls occurs. On the contrary, across the antenna room (along the X-axis), where only a couple of walls exist, the attenuation is far less and the signal reaches a greater distance before being reduced to low levels.

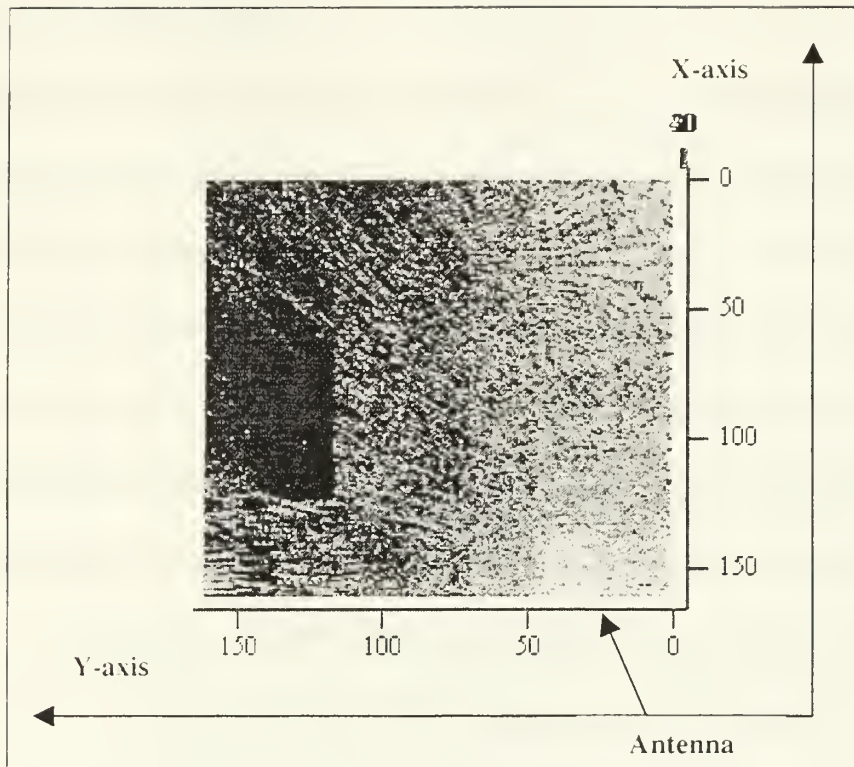


Figure 6.1: Predicted Excess Gain/Loss in Bullard 2nd Floor (open doors)

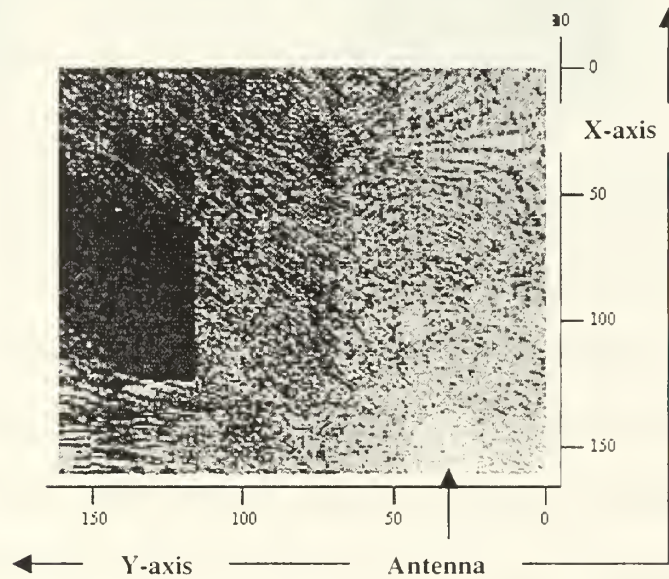


Figure 6.2: Predicted Excess Gain/Loss for Closed Doors

A second comparison approach was also conducted. The figure 5.2 was enlarged and printed out and then the whole floor map was divided into small squares. The side of each of these squares corresponded to 1.32 meters distance. The areas not marked in figure 5.2 were excluded. The antenna room was also ignored because there was not any range of values given for this area. Then, working on the remainder of the floor, a data matrix was extracted whose elements were a function of location and respective signal strength value in dBm. Next, an input file with an equivalent layout of observation points was generated and run and the resulting E-field values were converted to receiving power in dBm. Finally, the two matrices were plotted together in figure 6.3.

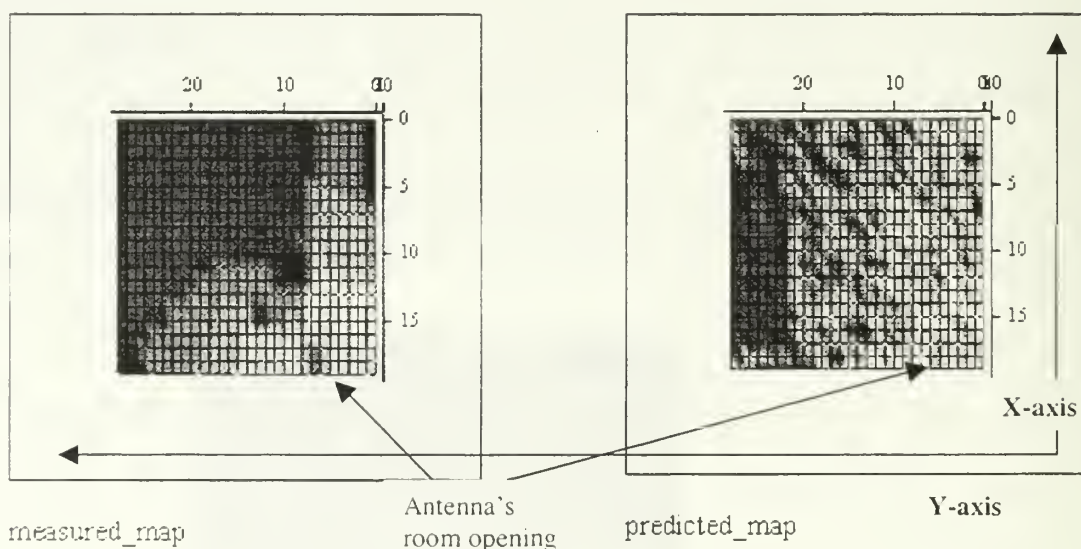


Figure 6.3: Comparison of Measured and Predicted Data Matrices

While comparing the two data matrices, the numerous inherent errors of the afore-discussed procedure have to be taken into account. Large portions of the floor were left out and the measured data matrix was by no means accurate. Rather, “gracious” judgment was often employed in determining the dBm value of certain points. On the other hand,

the observation points of the NEC-BSC input file had be specified so as to approximate the arrangement shown in figure 5.2. That, in turn, is believed to have caused some additional errors. Furthermore, it is well known that due to deep fading in the indoor propagation, the E-field can vary considerably at distances only a fraction of the wavelength in any direction. Thus, if some of the observation points used in the NEC-BSC input file fell into these “deep-fading” regions, the comparison would have been of little merit. Whether this has indeed happened in this particular case cannot be positively verified owing to lack of position-specific measured data. Nevertheless, it can still be seen in figure 6.3 that along the X-axis the coverage area is more or less the same. The difference in the Y-axis could be probably explained by inappropriate modeling of the walls close to the antenna’s site.

C. SIMULATIONS

1. Testing Different Model Approaches

The original input file was slightly modified in two different ways and, consequently, two new files were obtained. The objective was to test the effect of these modifications on the predicted gain/loss map. In particular, in the first test, a couple of walls in the proximity of the antenna were modeled as “double-sided coated” material plates as opposed to transparent slabs [39]. The thickness and constitutive parameters information was retained and only the ZD commands were altered. This was done in order to find the most accurate method of modeling the concrete walls containing metal studs in the antenna’s close neighborhood. This concept failed in bearing meaningful results as it is clearly shown in figure 6.4. No propagation appears to be possible beyond

these walls. Therefore, this result, although expected since there is a PEC in the middle coated on both sides of the wall, does not agree with the measured data.

In the second test, the doors of all rooms in the antenna's side of the floor were assumed to be closed and the input file was modified accordingly. The resulting gain/loss map is shown in figure 6.2. No discernible difference with the original opened-doors file can be seen, which probably implies that this scenario was not accurately modeled, or that the doors have only a modest effect on the signal propagation.

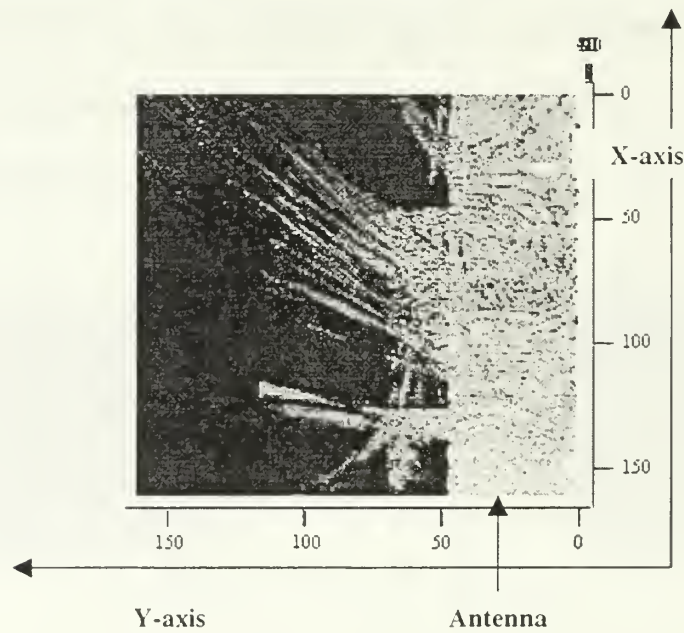


Figure 6.4: Predicted Excess Gain/Loss Using Double-Sided Coated Walls

2. Comparing with Free Space

Apart from the results obtained from the original antenna position input file and shown in figure 6.1, four additional output data files were also computed, each one with the antenna at a different location inside the Bullard 2nd floor. While that was done for the extraction of some interesting statistics described in the following section, some helpful

excess gain/loss maps of the entire floor were also obtained and one of them is shown in figure 6.5. In this figure, resulting from the input file with the antenna in the middle of the floor, it can be seen that the predicted coverage area is significantly larger compared to that of figure 6.1. This fact could most certainly be expected for it has been proved through various measurements reported in the literature that, in the majority of same-floor propagation cases, the best coverage is achieved by placing the antenna in the middle of the floor.

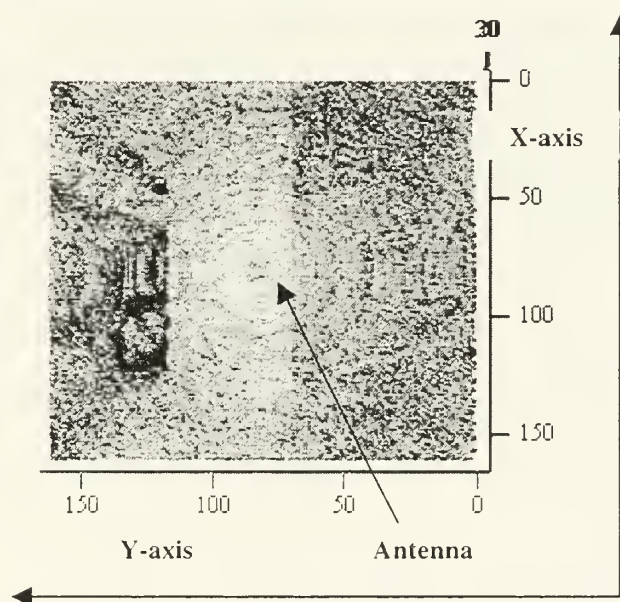


Figure 6.5: Predicted Excess Gain/Loss (antenna in the middle of the floor)

D. STATISTICS

1. Flow of Work

Following the approach already discussed in Chapter IV, the four additional data files for the four different antenna placements were analyzed in the manner described in this section. Once more, the objective was to extract the statistics of the excess gain/loss

of E-field relative to free space in the entire floor for various antenna locations including the initial one. All antenna locations are shown in figure 6.6, which was created by NEC-BSC Workbench. MathCAD was employed in all cases and the flow of work was the following:

- Data input: The program read the two NEC-BSC data files, i.e., the one resulting from the furnished and free space input file, respectively. Two two-column matrices were generated from each data file; the first column contained the distance of the observation point from the antenna while the second one contained the value of the E-field for that specific point.
- Data grouping: The entire observation-points layout was grouped into several circular sectors in steps of 50cm length. Thus, every group comprised those observation points, which fell in its respective sector. Each resulting group had different number of elements, which formed a set of data for every distance increment from the antenna's position.
- Room gain random variable: A random variable was introduced in the following fashion. In every so-called "distance-group" the ratio of the E-field in the room (denoted $|\bar{E}_{room}|$) and the E-field in free space (denoted

$|\bar{E}_{free}|$) was calculated by

$$20 \cdot \log \frac{|\bar{E}_{room_{m,n}}|}{|\bar{E}_{free_{m,n}}|} = R_{m,n} \quad (6.1)$$

where m and n denote the m^{th} distance group and n^{th} particular value for this group, respectively, and $R_{m,n}$ corresponds to the value of the pertinent “room gain” over free space. Consequently, every distance group created one realization (out of m in total) of the so-called E-field room gain random variable.

- Probability density function (pdf): Let us assume R_m to be the random variable describing the variation of the normalized difference for the m^{th} realization. Then the *pdf* for all R_m can be computed and the resulting histogram for all realizations can be drawn. In figure 6.7, the histogram obtained from the output file with the antenna at the center of the room is shown and denoted by L_{pdf} .
- Average pdf: Let us assume r to be the random variable describing the variation of the function resulting from averaging the *pdfs* for all distance groups. The ensemble pdf average of all distance groups was computed and its statistics were investigated. A Gaussian pdf having the same mean and variance as the “average-pdf” was generated. Both pdfs were plotted versus excess gain in dB on the same graph and they are shown in figure 6.8 for the antenna located at the center of the floor. An excellent agreement was observed and it was concluded that the excess room gain random variable r in dB has the lognormal distribution. This deduction is further discussed and explained later in this chapter.

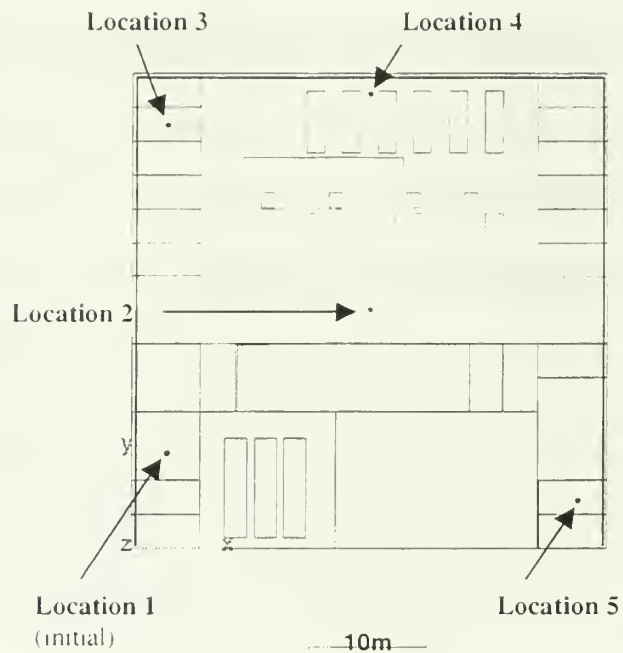


Figure 6.6: Antenna Locations Used in the Statistics Analysis Input Files

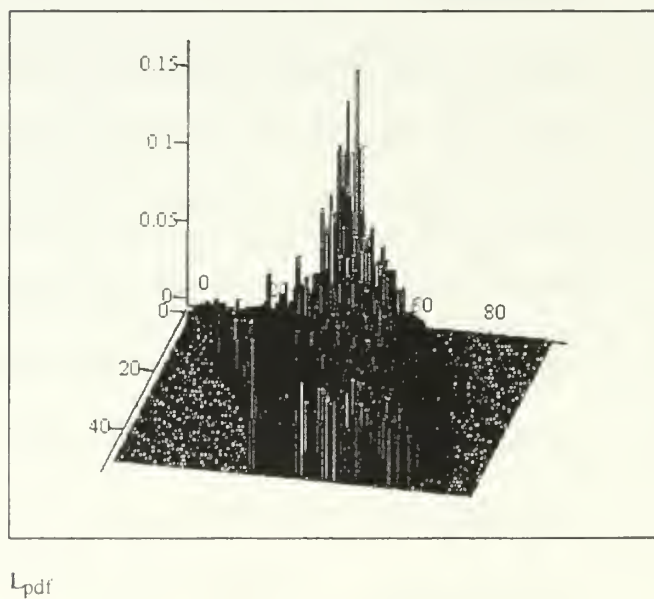


Figure 6.7: Histogram of All Distance-Groups pdfs (Ant. at Location 2)

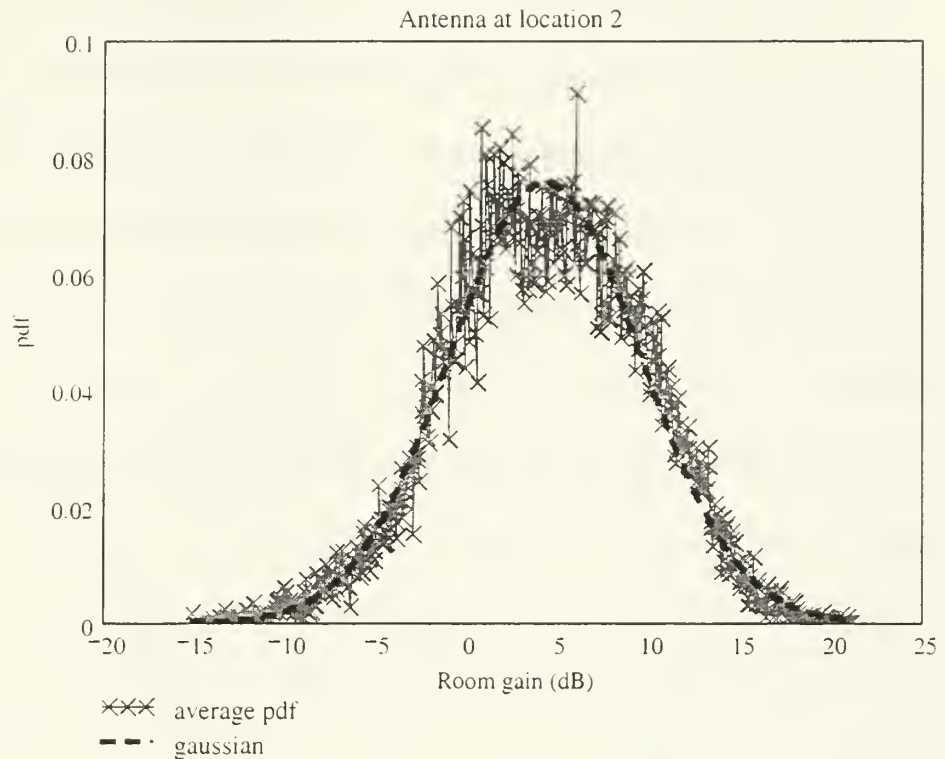


Figure 6.8: Average-pdf of the Room Gain Plotted Against Gaussian pdf

- Cumulative distribution function (cdf): The *cdf* of the random variable r was computed and plotted versus the room gain in dB along with a Gaussian *cdf* again with the same statistical characteristics (mean, variance), and it is shown in figure 6.9 for the antenna at the center of the floor. Once more, the agreement was remarkable yielding another manifestation of the fact that $\log r$ has a normal (Gaussian) distribution. The merits of such graphs as the one shown in figure 6.9 are quite noticeable for the communications engineer for it depicts practical information used for the determination of the link budget expected in the

entire room. In particular, in the example shown in this figure, the points at which the two marked dashed lines of 0.9 and 0.5 intersecting the cdf curve indicate that the estimated probability of encountering less than 11dB and less than 4dB excess gain in the Bullard's second floor is 90% and 50%, respectively.

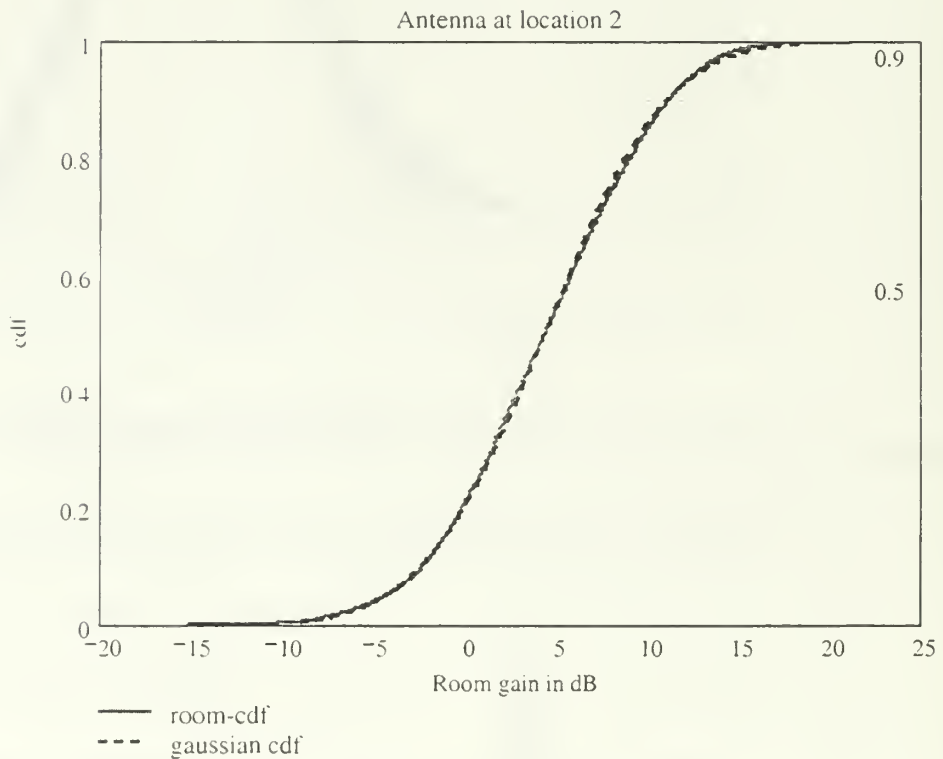


Figure 6.9: Cdf of Random Variable r (antenna at location 2)

2. Results

Reverting to the statistics of the room excess gain random variable r , it should be noted that the lognormal distribution has often been found to describe the amplitude variation of the indoor radio propagation channel, as reported in [14]. However, in our

analysis, yet another testimony to that fact has been given through a different perspective. Contrary to the approach discussed in [14] and elsewhere in literature where the statistics applies to *different* distances, in our case they apply to the *same distance* as defined by the so-called “distance-groups.” More specifically, this concept is employed for arbitrary locations of the transmitter and the “receiver” (i.e., where the observation points are placed), as long as the distance between them is the same and the simulation is conducted on the same floor. A thorough, yet not guaranteed to include everything, research suggests that this “same-distance” approach has not been reported before. In any event, the large number of reflections and the spatial inhomogeneity of the mobile channel seem to be sufficient in explaining this statistical behaviour. More specifically, if each reflection is assumed to contribute by a factor (reflection coefficient) to the total magnitude (a product of any factors) then if the logarithm of the product is taken it will yield a sum of the logarithms of the particular factors. Therefore, by applying the central limit theorem, it can be inferred that for a large number of reflections the resulting signal magnitude will resemble a random variable with normal distribution, which is precisely what it is noted in figures 6.8 and 6.9. As far as the inhomogeneity involvement is concerned in this process, it has been proved to contribute to the transition from Rayleigh and Rician distribution in the outdoor radio channel to lognormal distribution in the indoor radio channel [14]. The values of the “room gain” parameters used for all antenna locations comparison can be found in table 6.1.

Antenna location #	Coordinates	Room gain parameters (dB)	
		Mean	St. Deviation
1	(3,8,1)	7.165	5.164
2	(19.91,19.91,1)	4.276	5.275
3	(3.35,5.1)	7.194	4.624
4	(19.91,38.1)	5.179	4.971
5	(37.5,4,1)	8.322	4.885

Table 6.1: Room Gain Parameters

The resulting average-pdf curves for all, except the initial, antenna placements are shown in figure 6.10. They were plotted against the corresponding Gaussian distribution, i.e., having the same mean and variance. Despite the better accuracy of the results obtained when the antenna is located at the center of the floor, the curves gained from the other locations can still be considered adequate for verifying the Gaussian characteristics of the random variable r . Likewise, the same principle holds for the cdfs of the rest of the antenna placements shown in figure 6.11.

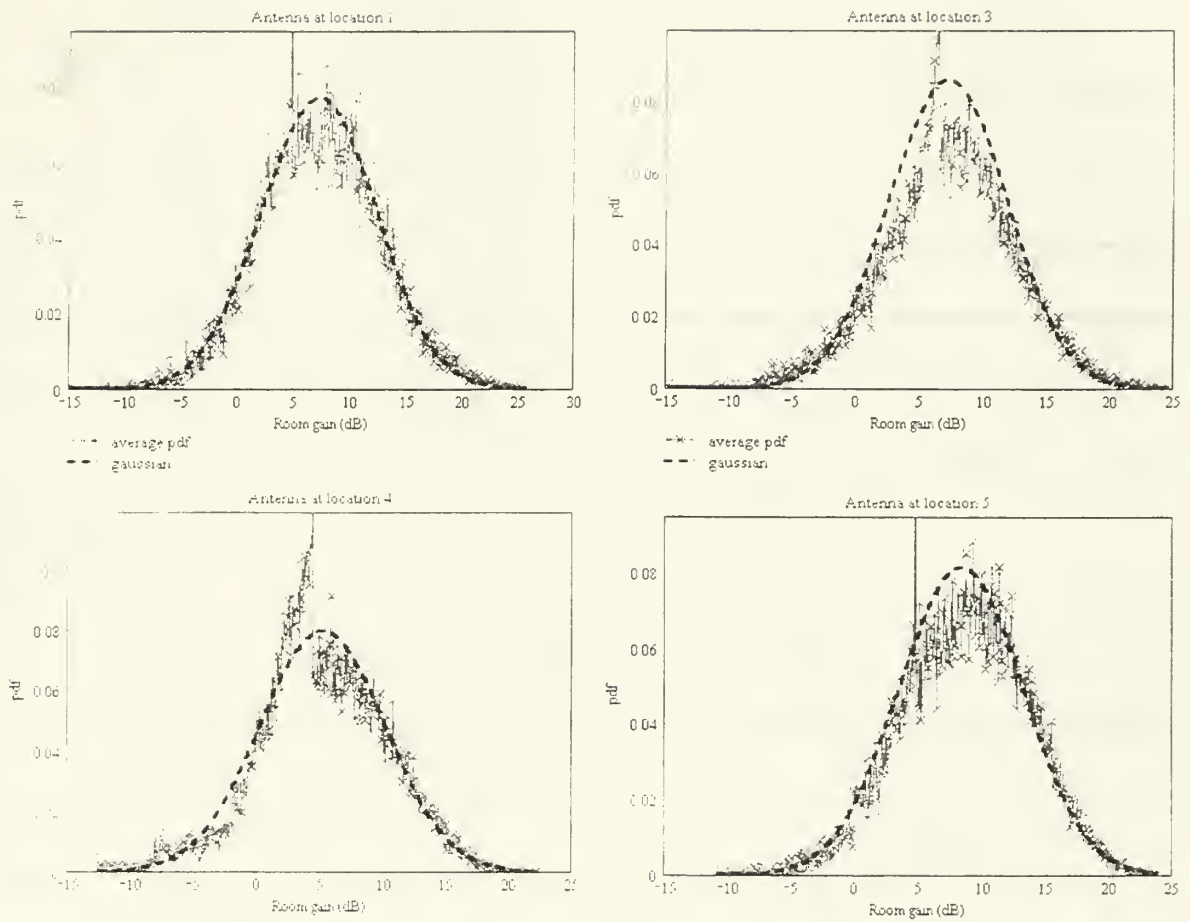


Figure 6.10: Average-pdf Plotted Against Gaussian Distribution

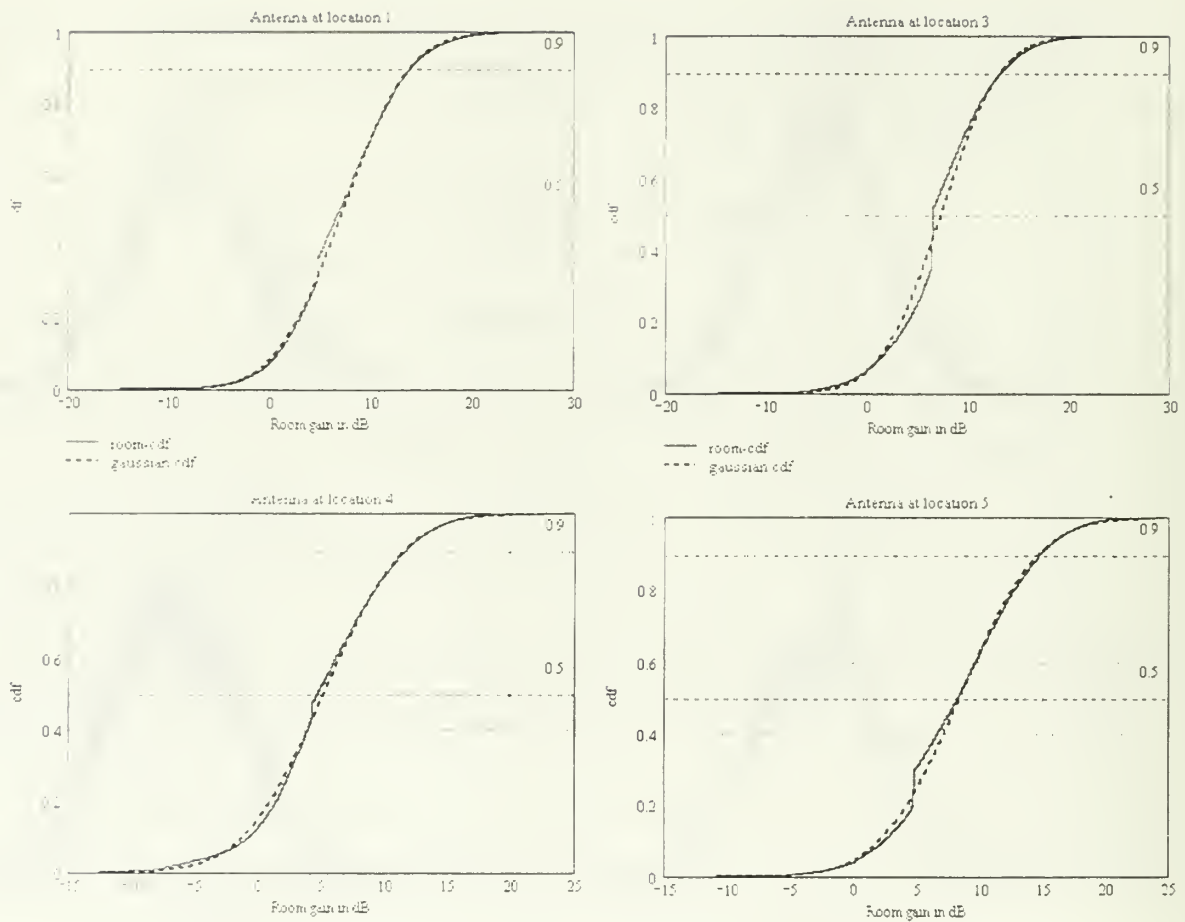


Figure 6.11: Room-Gain cdf Plotted Against Gaussian Distribution

3. Other problems

For the benefit of future work on indoor propagation using NEC-BSC, several problems not directly related to the scope of this thesis will be reported in this section. They were discovered either during the early familiarization stages or during the actual development of the input files. Although many more than those presented here were found, it was reckoned more useful to include only those that have not yet been resolved.

a) Command ZD 11

Even though the command ZD 11, which is used to define absorbing material properties, is described in [39] as being included in the code, it does not cooperate with the NEC-BSC Workbench. Specifically, the window of the ZD command does not list this option and, furthermore, if the user inserts it manually and then double-clicks on it the application crashes. No other cause than a potential bug could be found. It was hoped that this command option could be used to model several absorbing materials in Bullard Hall.

b) Commands not supported by Workbench

It was noticed that the command wizard window of the Workbench did not support the commands BF, FT, LY, PT, TA, TD, TW, TY, VM. Moreover, the Workbench supports the command ZC, but its function remains unknown since it is not included in the Help file.

c) Polar plot command

A minor yet worth reporting problem was detected regarding the command PP that is used to generate either a polar or a rectangular plot. In particular, the problem lies on the logical variable LPPREC. If the user chooses the polar plot option in the PP command window, the Workbench ought to respond by specifying the value “False” to the LPPREC variable according to the Help file. However, this does not occur and the Workbench gives the value “True” automatically, which is the opposite of the desired value. In addition, even if the user persists and corrects manually the LPPREC value back

to "False." the Workbench will again change it to "True" once a double-click is made on the PP command.

VII. CONCLUSIONS AND RECOMMENDATIONS

This thesis dealt with the indoor radio propagation channel and treated the problems caused by the complex characteristics of the latter. Several modeling methods used in this field were discussed and their pros and cons were presented. The major objective, however, was the evaluation of the Numerical Electromagnetic Code- Basic Scattering Code applicability in confined environments. In that respect, the NEC-BSC results were compared to those obtained by other applications as well as actual measurements conducted in the Bullard Hall of NPS in Monterey, California. In general terms the evaluation, although not complete, provided invaluable information regarding the code in question and strong indications of the validity of the code in modeling the indoor radio channel. In what follows, the most significant conclusions are summarized and some recommendations for further study are given.

A. CONCLUSIONS AND UNRESOLVED ISSUES

- Despite the lack of previous work in indoor radio propagation channel modeling based specifically on NEC-BSC, it has been proved that this code agrees to a satisfactory degree with the results reported in [48] for the same arrangement examination. Furthermore, a qualitative comparison between NEC-BSC predicted E-field values and actual measured signal strength for the same building yielded promising results, thus warranting further investigation in other buildings and different indoor radio propagation experiments.

- In simple arrangements, easily meeting the code requirements discussed in Chapter III, NEC-BSC simulation completion was fast. Nevertheless, that was not the case in the Bullard Hall model where the run times were excessively high and proportional to the complexity of the environment, the number of the observation points and the relative placement of the antenna. Because of that, the sampling rate of the observation points had to be reduced below the usually applied “half-wavelength” rule of thumb and this is believed to have affected the accuracy of the results.
- The NEC-BSC user’s manual [39] seems not to have included all plate attachment cases for there were numerous examples encountered during the development of the Bullard Hall model where the suggested process of intersecting/attaching two plates was followed yet the plate attachment clearly failed prompting the code to launch either error or warning messages. Sometimes the relevant code messages were made to vanish by shifting the plate slightly away from the desired position, usually a fraction of the wavelength. Whenever a way around this problem could not be found, the plate under consideration had to be left out of the model degrading that way the accuracy of the actual Bullard Hall representation.
- The E-field amplitude variation in confined environments has been reported to obey the Gaussian distribution statistics [14] when studied in terms of *varying* distance. The approach described in the previous chapter revealed that this is also true for the so-called “room excess gain” random

variable when studied in terms of *same* “distance groups.” This fact, apart from adding credence to the validity of NEC-BSC predicted values, implies that the lognormal distribution may well be applied in both *varying* and *same* distance statistics considerations. However, final conclusions on this matter can be reached only after further study (different rooms, materials etc).

B. RECOMMENDATIONS

- Since the current NEC-BSC graphical user interface (GUI), i.e. the Workbench, does not support any CAD package, it is suggested that a future version of NEC-BSC incorporate AutoCAD interoperability, thereby enhancing the code’s functionality and user-friendliness. Moreover, it is suggested that a database be built containing the constitutive parameters of various frequently encountered walls and materials of the indoor radio channel. This database, if included in a future version of NEC-BSC, could speed-up the geometry development.
- The current NEC-BSC version does not allow insertion of all available commands through the Workbench. It is recommended that this capability be included in one of the future versions of NEC-BSC.
- A *parallel execution* option [37] could also be made available in an improved version of NEC-BSC for it would significantly shorten the run times, especially in cases like the Bullard Hall model where the complexity of the environment is critically high approaching the

limitations of the code illustrated in chapter III. Nevertheless, it should be said that this can be implicitly, but not so efficiently, performed by dividing up the computation “burden” of the observation points into different PCs (e.g. points 0-100 assigned on PC-1, points 100-200 assigned on PC-2, etc).

- Whenever the near-field pattern is computed by NEC-BSC, the results include both the Electric and Magnetic field components along with the Poynting vector components. In case that only the signal strength is desired the computation of the H-field and the Poynting vector could be omitted in order to reduce the simulation time. However, this is not possible in the current version of the code and the user cannot choose the particular data to be calculated.
- As innovative technologies like Bluetooth [5] appear in the forefront of indoor applications and call for transition from *nanocells* to *picocells*, smaller room statistics will become necessary. NEC-BSC could be used in that respect. Furthermore, NEC-BSC could also be employed in surveying the room-to-room propagation and hallway-to-room statistics, which have not been taken into account in this thesis.
- In a future study, NEC-BSC could be utilized for extracting various co-polarization statistics in the same floor or room; these could include but not be limited to horizontal-to-horizontal, vertical-to-vertical and circular-to-circular transmitter-to-receiver polarization. Then their pertinent results

could be contrasted against each other and confirmed through measurements. In the same sense and for the same purpose the resulting cross-polarization (e.g. like vertical-to horizontal, horizontal-to-circular, etc) statistics could be investigated with the help of NEC-BSC.

THIS PAGE INTENTIONALLY LEFT BLANK

APPENDIX A. NEC-BSC INPUT FILES

CE: This is the input file used in the cylinder

CE : room example

CE:A rectangular room with PEC walls

CE: containing a PEC cylinder in the

CE: middle of the room

FR:

2.45000

UN:

1

U'S:

0

ZD: Perfect Electric Conductor

0

GP: Floor

0

PM:

8

0.000000, 0.000000, 0.000000

0.000000, 0.000000, 6.000000

6.000000, 0.000000, 6.000000

6.000000, 0.000000, 0.000000

6.000000, 14.0000, 6.000000

6.000000, 14.0000, 0.000000

0.000000, 14.0000, 6.000000

0.000000, 14.0000, 0.000000

()

1

2

3

4

0

4

3

5

6

0

6

5

7

8

0

8

7
2
1
0
3
5
7
2
0
0

CG: PEC cylinder

3.00000, 7.00000, 3.00000
0.000000, 0.000000, 90.0000, 0.000000
1.00000, 1.00000
-3.00856, 90.0000, 3.00856, 90.0000

SG:

3.00000, 3.00000, 3.00000
0.000000, 0.000000, 90.0000, 0.000000
-1. 0.500000, 0.000000
1.00000, 0.000000

CE: For horizontal polarization

CE: simply comment selection out

CE: the above antenna settings

CE: and uncomment selection out

CE: the settings given below

CM: SG:

CM: 3.00000, 3.00000, 3.00000
CM: 90.0000, 0.000000, 90.0000, 0.000000
CM: -1. 0.500000, 0.000000
CE: 1.00000, 0.000000

PN: Circular pattern around cylinder

3.00000, 7.00000, 3.00000
0.000000, 0.000000, 90.0000, 0.000000

F

2.00000, 90.0000, 0.000000
0.000000, 0.000000, 1.00000

360

CE: For line pattern simply comment selection out

CE: the above PN command and

CE: uncomment selection out the

CE: following PN command

CM: PN: Line pattern running through Cylinder's Center of Mass

CM: 0.000000, 0.000000, 0.000000

CM: 0.000000, 0.000000, 90.0000, 0.000000
CM: T
CM: 3.00000, 0.000000, 3.00000
CM: 0.000000, 0.0612000, 0.000000
CE: 229

PL:
T
LY:
T
XQ:
EN:
CE: End of cylinder room input file
CE:
CE:
CE:
CE:
CE:
CE: This is the input file used in the
CE: typical room example

CE:
FR
0.9
UN
3
RT:
-120.000, 0.000000, 0.000000
0.000000, 0.000000, 90.0000, 0.000000
VN:
0.000000, 0.000000, 0.000000
0.000000, 0.000000, 90.0000, 0.000000
T
6.55715, 6.55715, 48.0000
6.55715, 6.55715, 0.000000
1, 54, 32
RT:
120.000, 0.000000, 0.000000
0.000000, 0.000000, 90.0000, 0.000000
PL:
T
LY
T
CM: TY

CE: 3
CM: PR
CM: 3
CE: 36.514359,36.514359
US
0
SG
60.,72.,48.
0.,0.,90.,0.
-2.0.5.0.0
1.,0.
CM: RG
CM: 0.,0.,0.
CM: 0.,0.,90.,0.
CM: -2.0.5.0.0
CE: 1.,0.
ZD
-3
2.38,0.048,1.,0.
GP FLOOR
0
ZD
1
1
0.5.3.6.0.,1.,0.
PM CEILING
16
0.0, 0.0, 112.0
12.0, 0.0, 112.0
34.0, 0.0, 112.0
120.0, 0.0, 112.0
120.0, 144.0, 112.0
0.0, 144.0, 112.0
44.0, 144.0, 84.0
8.0, 144.0, 84.0
12.0, 0.0, 14.0
44.0, 0.0, 14.0
0.0, 0.0, 0.0
120.0, 0.0, 0.0
120.0, 144.0, 0.0
44.0, 144.0, 0.0
8.0, 144.0, 0.0
0.0, 144.0, 0.0

0
1
6
5
4
3
2
0
0

ZD 6" BRICK

1
3

0.53,3..0.048,1.,0.

5.11.1.5.0.,1.,0.

0.53,3..0.048,1.,0.

PM WALLS

16

0.0, 0.0, 112.0

12.0, 0.0, 112.0

44.0, 0.0, 112.0

120.0, 0.0, 112.0

120.0, 144.0, 112.0

0.0, 144.0, 112.0

44.0, 144.0, 84.0

8.0, 144.0, 84.0

12.0, 0.0, 14.0

44.0, 0.0, 14.0

0.0, 0.0, 0.0

120.0, 0.0, 0.0

120.0, 144.0, 0.0

44.0, 144.0, 0.0

8.0, 144.0, 0.0

0.0, 144.0, 0.0

0

1

2

9

10

3

4

12

11

0

4
5
13
12
0
5
6
16
15
8
7
14
13
0
6
1
11
16
0
0
PM: HALLS
12

120.0, 0.0, 112.0
240.0, 0.0, 112.0
240.0, 216.0, 112.0
-120.0, 216.0, 112.0
-120.0, 0.0, 112.0
0.0, 0.0, 112.0
120.0, 0.0, 0.0
240.0, 0.0, 0.0
240.0, 216.0, 0.0
-120.0, 216.0, 0.0
-120.0, 0.0, 0.0
0.0, 0.0, 0.0

0
1
2
8
7
0
2
3
9

8
0
3
4
10
9
0
4
5
11
10
0
5
6
12
11
0
0

ZD GLASS

1
1
0.125,5.23.0.013,1..0.

PM WINDOW

16
0.0, 0.0, 112.0
12.0, 0.0, 112.0
44.0, 0.0, 112.0
120.0, 0.0, 112.0
120.0, 144.0, 112.0
0.0, 144.0, 112.0
44.0, 144.0, 84.0
8.0, 144.0, 84.0
12.0, 0.0, 14.0
44.0, 0.0, 14.0
0.0, 0.0, 0.0
120.0, 0.0, 0.0
120.0, 144.0, 0.0
44.0, 144.0, 0.0
8.0, 144.0, 0.0
0.0, 144.0, 0.0

0
2
3

10
9
0
0
XT
EN
CE: End of typical room example
CE:
CE:
CE:
CE:
CE:
CE: This is the input file used in the
CE: comparison with the SBR method
CE:
UN:
1
US:
0
FR:
1.00000
ZD:
1
1
0.130000, 4.00000, 0.0900000, 1.00000, 0.000000
GP: floor
0
ZD: walls
1
2
0.149800, 6.00000, 0.0300000, 1.00000, 0.000000
0.100100, 6.00000, 0.0300000, 1.00000, 0.000000
PM:
8
0.000000, 0.000000, 0.000000
10.0000, 0.000000, 0.000000
10.0000, 3.00000, 0.000000
0.000000, 3.00000, 0.000000
0.000000, 3.00000, 21.0000
0.000000, 0.000000, 21.0000
10.0000, 0.000000, 21.0000
10.0000, 3.00000, 21.0000
0

1
2
3
4
0
3
8
7
2
0
7
8
5
6
0
6
1
4
5
0
0
ZD: ceiling
1
1
0.130000, 4.00000, 0.0900000, 1.00000, 0.000000
CM: PG:
CM: 4, 0
CM: 0.000000, 0.000000, 0.000000
CM: 0.000000, 0.000000, 21.0000
CM: 10.0000, 0.000000, 21.0000
CE: 10.0000, 0.000000, 0.000000
PG:
4, 0
0.000000, 3.00000, 0.000000
0.000000, 3.00000, 21.0000
10.0000, 3.00000, 21.0000
10.0000, 3.00000, 0.000000
CE: For the "empty room" solution
CE: simply comment selection out everything
CE: until (but not including) the SG command
ZD: closet
0
RR:

1.50000, 0.000000, 11.0000
0.000000, 0.000000, 90.0000, 0.000000

PM:

8

0.000000, 0.000000, 0.000000

7.00000, 0.000000, 0.000000

7.00000, 2.00000, 0.000000

0.000000, 2.00000, 0.000000

0.000000, 2.00000, 0.600000

0.000000, 0.000000, 0.600000

7.00000, 0.000000, 0.600000

7.00000, 2.00000, 0.600000

0

1

2

3

4

0

4

5

8

3

0

3

8

7

2

0

2

1

6

7

0

7

8

5

6

0

6

1

4

5

0

0
RR:
-1.50000, 0.000000, -11.0000
0.000000, 0.000000, 90.0000, 0.000000
CE: For the PEC backing solution
CE: simply uncomment selection out everything
CE: until (but not including) the SG command
CM: RR:
CM: 0.000000, 0.0020000, 0.000000
CM: 0.000000, 0.000000, 90.0000, 0.000000
CM: PG: ceiling backing
CM: 4, 0
CM: 10.0000, 3.00000, 0.000000
CM: 0.000000, 3.00000, 0.000000
CM: 0.000000, 3.00000, 21.0000
CM: 10.0000, 3.00000, 21.0000
CM: RR:
CM: 0.000000, -0.0040000, 0.000000
CM: 0.000000, 0.000000, 90.0000, 0.000000
CM: PG: floor backing
CM: 4, 0
CM: 10.0000, 0.000000, 0.000000
CM: 0.000000, 0.000000, 0.000000
CM: 0.000000, 0.000000, 21.0000
CM: 10.0000, 0.000000, 21.0000
CM: RR:
CM: 0.000000, 0.002000, 0.000000
CE: 0.000000, 0.000000, 90.0000, 0.000000
CE:
SG:
2.00000, 2.50000, 3.00000
90.0000, 90.0000, 90.0000, 0.000000
-1, 0.500000, 0.000000
1.00000, 0.000000
PN:
0.000000, 0.000000, 0.000000
0.000000, 0.000000, 90.0000, 0.000000
T
8.00000, 1.50000, 5.00000
0.000000, 0.000000, 0.010000
1501
PL:
T

LY:

T

LP:

T

XQ:

EN:

CE: End of SBR comparison

CE: Comparison with measurements

CE: Antenna at original position

CE: containing surrounding walls, floor, ceiling

CE: ALL exterior windows, overhead beam

CE: ALL NORTHERN partition walls (v.1, v.2 and v.3)

CE: with "open" doors (DOUBLE v.3)

CE: ALL SOUTHERN partitions

CE: ALL the rest of INTERIOR PARTITIONS

CE: ALL the wooden tables

CE: including the METALIC BLOCK,

CE: and the interior columns

CE: using volumetric instead of linear pattern

UN: units in meters

1

US: source units in wavelengths

0

FR: frequency of operation

2.45000

ZD: concrete's properties

-4

1

0.061200, 4.00000, 0.00436300, 1.00000, 0.000000

PM: building's exterior structure

8

0.000000, 0.000000, 0.000000

0.000000, 0.000000, 3.81000

0.000000, 39.8272, 3.81000

0.000000, 39.8272, 0.000000

39.8272, 39.8272, 0.000000

39.8272, 39.8272, 3.81000

39.8272, 0.000000, 3.81000

39.8272, 0.000000, 0.000000

0

1

2

3

4
0
3
4
5
6
0
5
6
7
8
0
7
8
1
2
0
2
3
6
7
0
1
4
5
8
0
0

CE: Building exterior windows(NORTHERN part)

CE: Exterior Windows

ZD: glass properties

1
1

0.02000, 4.00000, 0.000600000, 1.00000, 0.000000

PG: exterior window

4, 0

0.000000, 0.444500, 0.177800

0.000000, 5.62610, 0.177800

0.000000, 5.62610, 3.63220

0.000000, 0.444500, 3.63220

RR: translating exterior window

0.000000, 5.68960, 0.000000

0.000000, 0.000000, 90.0000, 0.000000

PG: exterior window
4, 0
0.000000, 0.444500, 0.177800
0.000000, 5.62610, 0.177800
0.000000, 5.62610, 3.63220
0.000000, 0.444500, 3.63220
RR: translating exterior window
0.000000, 5.68960, 0.000000
0.000000, 0.000000, 90.0000, 0.000000
PG: exterior window
4, 0
0.000000, 0.444500, 0.177800
0.000000, 5.62610, 0.177800
0.000000, 5.62610, 3.63220
0.000000, 0.444500, 3.63220
RR: translating exterior window
0.000000, 5.68960, 0.000000
0.000000, 0.000000, 90.0000, 0.000000
PG: exterior window
4, 0
0.000000, 0.444500, 0.177800
0.000000, 5.62610, 0.177800
0.000000, 5.62610, 3.63220
0.000000, 0.444500, 3.63220
RR: translating exterior window
0.000000, 5.68960, 0.000000
0.000000, 0.000000, 90.0000, 0.000000
PG: exterior window
4, 0
0.000000, 0.444500, 0.177800
0.000000, 5.62610, 0.177800
0.000000, 5.62610, 3.63220
0.000000, 0.444500, 3.63220
RR: translating exterior window
0.000000, 5.68960, 0.000000
0.000000, 0.000000, 90.0000, 0.000000
PG: exterior window
4, 0
0.000000, 0.444500, 0.177800
0.000000, 5.62610, 0.177800
0.000000, 5.62610, 3.63220
0.000000, 0.444500, 3.63220
RR: translating exterior window

0.000000, 5.68960, 0.000000
0.000000, 0.000000, 90.0000, 0.000000
PG: exterior window
4, 0
0.000000, 0.444500, 0.177800
0.000000, 5.62610, 0.177800
0.000000, 5.62610, 3.63220
0.000000, 0.444500, 3.63220
RR: reverting to original(GLOBAL)coordinate system
0.000000, -34.1376, 0.000000
0.000000, 0.000000, 90.0000, 0.000000
CE:
CE:END of building NORTHERN windows
CE:
CE:STARTING exterior WESTERN windows
CE:
RR: rotating exterior window
0.000000, 0.000000, 0.000000
0.000000, 0.000000, 90.0000, -90.0000
PG: exterior window
4, 0
0.000000, 0.444500, 0.177800
0.000000, 5.62610, 0.177800
0.000000, 5.62610, 3.63220
0.000000, 0.444500, 3.63220
RR: translating exterior window
0.000000, 5.68960, 0.000000
0.000000, 0.000000, 90.0000, 0.000000
PG: exterior window
4, 0
0.000000, 0.444500, 0.177800
0.000000, 5.62610, 0.177800
0.000000, 5.62610, 3.63220
0.000000, 0.444500, 3.63220
RR: translating exterior window
0.000000, 5.68960, 0.000000
0.000000, 0.000000, 90.0000, 0.000000
PG: exterior window
4, 0
0.000000, 0.444500, 0.177800
0.000000, 5.62610, 0.177800
0.000000, 5.62610, 3.63220
0.000000, 0.444500, 3.63220

RR: translating exterior window
0.000000, 5.68960, 0.000000
0.000000, 0.000000, 90.0000, 0.000000
PG: exterior window
4, 0
0.000000, 0.444500, 0.177800
0.000000, 5.62610, 0.177800
0.000000, 5.62610, 3.63220
0.000000, 0.444500, 3.63220
RR: translating exterior window
0.000000, 5.68960, 0.000000
0.000000, 0.000000, 90.0000, 0.000000
PG: exterior window
4, 0
0.000000, 0.444500, 0.177800
0.000000, 5.62610, 0.177800
0.000000, 5.62610, 3.63220
0.000000, 0.444500, 3.63220
RR: translating exterior window
0.000000, 5.68960, 0.000000
0.000000, 0.000000, 90.0000, 0.000000
PG: exterior window
4, 0
0.000000, 0.444500, 0.177800
0.000000, 5.62610, 0.177800
0.000000, 5.62610, 3.63220
0.000000, 0.444500, 3.63220
CE:
CE:END of building WESTERN exterior windows
CE:
CE:
CE:STARTING SOUTHERN exterior windows
CE:
RR: rotating/translating exterior window

0.000000, 5.68960, 0.000000
0.000000, 0.000000, 90.0000, 90.0000
CM: PG: exterior window
CM: 4, 0
CM: 0.000000, 0.444500, 0.177800
CM: 0.000000, 5.62610, 0.177800
CM: 0.000000, 5.62610, 3.63220
CE: 0.000000, 0.444500, 3.63220
RR: rotating/translating exterior window
0.000000, 5.68960, 0.000000
0.000000, 0.000000, 90.0000, 0.0000
PG: exterior window
4, 0
0.000000, 0.444500, 0.177800
0.000000, 5.62610, 0.177800
0.000000, 5.62610, 3.63220
0.000000, 0.444500, 3.63220
RR: rotating/translating exterior window
0.000000, 5.68960, 0.000000
0.000000, 0.000000, 90.0000, 0.0000
PG: exterior window
4, 0
0.000000, 0.444500, 0.177800
0.000000, 5.62610, 0.177800
0.000000, 5.62610, 3.63220
0.000000, 0.444500, 3.63220
RR: rotating/translating exterior window
0.000000, 5.68960, 0.000000
0.000000, 0.000000, 90.0000, 0.0000
PG: exterior window
4, 0
0.000000, 0.444500, 0.177800
0.000000, 5.62610, 0.177800
0.000000, 5.62610, 3.63220
0.000000, 0.444500, 3.63220
RR: rotating/translating exterior window
0.000000, 5.68960, 0.000000
0.000000, 0.000000, 90.0000, 0.0000
CM: PG: exterior window
CM: 4, 0
CM: 0.000000, 0.444500, 0.177800
CM: 0.000000, 5.62610, 0.177800
CM: 0.000000, 5.62610, 3.63220

CE: 0.000000, 0.444500, 3.63220
RR: rotating/translating exterior window
0.000000, 5.68960, 0.000000
0.000000, 0.000000, 90.0000, 0.0000
CM: PG: exterior window
CM: 4, 0
CM: 0.000000, 0.444500, 0.177800
CM: 0.000000, 5.62610, 0.177800
CM: 0.000000, 5.62610, 3.63220
CE: 0.000000, 0.444500, 3.63220
RR: rotating/translating exterior window
0.000000, 5.68960, 0.000000
0.000000, 0.000000, 90.0000, 0.0000
CM: PG: exterior window
CM: 4, 0
CM: 0.000000, 0.444500, 0.177800
CM: 0.000000, 5.62610, 0.177800
CM: 0.000000, 5.62610, 3.63220
CE: 0.000000, 0.444500, 3.63220
CE:
CE:END of SOUTHERN windows
CE:
CE:
CE:STARTING EASTERN exterior windows
CE:
RR: rotating/translating exterior window
0.000000, 5.68960, 0.000000
0.000000, 0.000000, 90.0000, 90.0000
PG: exterior window
4, 0
0.000000, 0.444500, 0.177800
0.000000, 5.62610, 0.177800
0.000000, 5.62610, 3.63220
0.000000, 0.444500, 3.63220
RR: rotating/translating exterior window
0.000000, 5.68960, 0.000000
0.000000, 0.000000, 90.0000, 0.0000
PG: exterior window
4, 0
0.000000, 0.444500, 0.177800
0.000000, 5.62610, 0.177800
0.000000, 5.62610, 3.63220
0.000000, 0.444500, 3.63220

RR: rotating/translating exterior window
0.000000, 5.68960, 0.000000
0.000000, 0.000000, 90.0000, 0.0000
PG: exterior window
4, 0
0.000000, 0.444500, 0.177800
0.000000, 5.62610, 0.177800
0.000000, 5.62610, 3.63220
0.000000, 0.444500, 3.63220
RR: rotating/translating exterior window
0.000000, 5.68960, 0.000000
0.000000, 0.000000, 90.0000, 0.0000
PG: exterior window
4, 0
0.000000, 0.444500, 0.177800
0.000000, 5.62610, 0.177800
0.000000, 5.62610, 3.63220
0.000000, 0.444500, 3.63220
RR: rotating/translating exterior window
0.000000, 5.68960, 0.000000
0.000000, 0.000000, 90.0000, 0.0000
PG: exterior window
4, 0
0.000000, 0.444500, 0.177800
0.000000, 5.62610, 0.177800
0.000000, 5.62610, 3.63220
0.000000, 0.444500, 3.63220
RR: rotating/translating exterior window
0.000000, 5.68960, 0.000000
0.000000, 0.000000, 90.0000, 0.0000
PG: exterior window
4, 0
0.000000, 0.444500, 0.177800
0.000000, 5.62610, 0.177800

0 000000, 5.62610, 3.63220
0.000000, 0.444500, 3.63220
CE:
CE:END of building EASTERN windows
CE:
CE: reverting to ORIGINAL (GLOBAL)
CE: coordinate system (rotating)
RR:
0.000000, 0.000, 0.000000
0.000000, 0.000000, 90.0000, -90.000000
CE: reverting to ORIGINAL (GLOBAL)
CE: coordinate system (translating)
RR:
-5.68960, -39.8272, 0.000000
0.000000, 0.000000, 90.0000, 0.000000
CE:
CE:END of building ALL exterior windows
CE:
CE: partitions between rooms
ZD: plaster properties
1
2
0.0612000, 2.30000, 0.00174500, 1.00000, 0.000000
0.0100000, 2.30000, 0.00174533, 1.00000, 0.000000
PG:
4. 0
0.000000, 2.84480, 0.000000
0.000000, 2.84480, 3.81000
5.68960, 2.84480, 3.81000
5.68960, 2.84480, 0.000000
RR:
0.000000, 2.84480, 0.000000
0.000000, 0.000000, 90.0000, 0.000000
PG:
4. 0
0 000000, 2.84480, 0.000000
0.000000, 2.84480, 3.81000
5.68960, 2.84480, 3.81000
5.68960, 2.84480, 0.000000
RR:
0.000000, 2.84480, 0.000000
0.000000, 0.000000, 90.0000, 0.000000
CM: PG:

CM: 4.0
 CM: 0.000000, 2.84480, 0.000000
 CM: 0.000000, 2.84480, 3.81000
 CM: 5.68960, 2.84480, 3.81000
 CE: 5.68960, 2.84480, 0.000000
 ZD: concrete wall containing metal beams
 1
 2
 0.0612000, 8.24700, 0.00436300, 1.00000, 0.000000
 0.0612000, 8.24700, 0.00436300, 1.00000, 0.000000
 RR:
 0.000000, 2.84480, 0.000000
 0.000000, 0.000000, 90.0000, 0.000000
 PG:
 4.0
 0.000000, 2.84480, 0.000000
 0.000000, 2.84480, 3.81000
 5.68960, 2.84480, 3.81000
 5.68960, 2.84480, 0.000000
 RR:
 0.000000, 2.84480, 0.000000
 0.000000, 0.000000, 90.0000, 0.000000
 CM: PG:
 CM: 4.0
 CM: 0.000000, 2.84480, 0.000000
 CM: 0.000000, 2.84480, 3.81000
 CM: 5.68960, 2.84480, 3.81000
 CE: 5.68960, 2.84480, 0.000000
 RR:
 0.000000, 2.84480, 0.000000
 0.000000, 0.000000, 90.0000, 0.000000
 PG:
 4.0
 0.000000, 2.84480, 0.000000
 0.000000, 2.84480, 3.81000
 5.68960, 2.84480, 3.81000
 5.68960, 2.84480, 0.000000
 CE: change material properties.
 ZD: plaster properties
 1
 2
 0.0612000, 2.30000, 0.00174500, 1.00000, 0.000000
 0.0100000, 2.30000, 0.00174533, 1.00000, 0.000000

RR:
0.000000, 2.84480, 0.000000
0.000000, 0.000000, 90.0000, 0.000000
CM: PG:
CM: 4, 0
CM: 0.000000, 2.84480, 0.000000
CM: 0.000000, 2.84480, 3.81000
CM: 5.68960, 2.84480, 3.81000
CM: 5.68960, 2.84480, 0.000000
CE:
RR:
0.000000, 2.84480, 0.000000
0.000000, 0.000000, 90.0000, 0.000000
PG:
4, 0
0.000000, 2.84480, 0.000000
0.000000, 2.84480, 3.81000
5.68960, 2.84480, 3.81000
5.68960, 2.84480, 0.000000
RR:
0.000000, 2.84480, 0.000000
0.000000, 0.000000, 90.0000, 0.000000
PG:
4, 0
0.000000, 2.84480, 0.000000
0.000000, 2.84480, 3.81000
5.68960, 2.84480, 3.81000
5.68960, 2.84480, 0.000000
RR:
0.000000, 2.84480, 0.000000
0.000000, 0.000000, 90.0000, 0.000000
PG:
4, 0
0.000000, 2.84480, 0.000000

0.000000, 2.84480, 3.81000
5.68960, 2.84480, 3.81000
5.68960, 2.84480, 0.000000

RR:

0.000000, 2.84480, 0.000000
0.000000, 0.000000, 90.0000, 0.000000

PG:

4, 0

0.000000, 2.84480, 0.000000
0.000000, 2.84480, 3.81000
5.68960, 2.84480, 3.81000
5.68960, 2.84480, 0.000000

RR:

0.000000, 2.84480, 0.000000
0.000000, 0.000000, 90.0000, 0.000000

PG:

4, 0

0.000000, 2.84480, 0.000000
0.000000, 2.84480, 3.81000
5.68960, 2.84480, 3.81000
5.68960, 2.84480, 0.000000

RR: reverting to global axis system

0.000000, -34.1376, 0.000000
0.000000, 0.000000, 90.0000, 0.000000

ZD: concrete wall containing metal beams

1

2

0.0612000, 5.84000, 0.00141600, 1.00000, 0.000000
0.0612000, 5.84000, 0.00141600, 1.00000, 0.000000

CE: exposed concrete containing beams over

CE: the interior partitions

PG:

4, 0

5.68960, 0.000000, 3.81000
5.68960, 0.000000, 3.40360
5.68960, 39.8272, 3.40360
5.68960, 39.8272, 3.81000

RR: moving the fake partition to the right position

5.68960, 0, 0.000000
0.000000, 0.000000, 90.0000, 0.000000

CM:

CM: Building the simplified partition (doors open)

CE:
ZD: plaster properties (prevailing)
1
2
0.0612000, 2.30000, 0.00174500, 1.00000, 0.000000
0.0100000, 2.30000, 0.00174533, 1.00000, 0.000000
PG: simplified partition (doors open)
8, 0
0.000000, 0.000000, 2.13360
0.000000, 1.22240, 2.13360
0.000000, 1.22240, 0.000000
0.000000, 4.46720, 0.000000
0.000000, 4.46720, 2.13360
0.000000, 5.68960, 2.13360
0.000000, 5.68960, 3.40360
0.000000, 0.000000, 3.40360
RR:
0.050000, 0.000000, 0.000000
0.000000, 0.000000, 90.0000, 0.000000
PG: simplified partition (doors open)
8, 0
0.000000, 0.000000, 2.13360
0.000000, 1.22240, 2.13360
0.000000, 1.22240, 0.000000
0.000000, 4.46720, 0.000000
0.000000, 4.46720, 2.13360
0.000000, 5.68960, 2.13360
0.000000, 5.68960, 3.40360
0.000000, 0.000000, 3.40360
RR:
-0.050000, 5.6896, 0.000000
0.000000, 0.000000, 90.0000, 0.000000
CE:
CE: simplified partition v.3
CE:(without door, windows etc)
CE:
CE: we insert a "double-layer" of
CE: plaster wall, each layer with thickness 6cm
CE:
CE:
CE:
ZD: plaster properties (prevailing) double-layer
1

2

0.0612000, 2.30000, 0.00174500, 1.00000, 0.000000

0.0612000, 2.30000, 0.00174500, 1.00000, 0.000000

PG: simplified partition (door open)

6, 0

0.000000, 0.000000, 0.000000

0.000000, 4.46720, 0.000000

0.000000, 4.46720, 2.13360

0.000000, 5.68960, 2.13360

0.000000, 5.68960, 3.40360

0.000000, 0.000000, 3.40360

CE:

CE: we now revert to single-layer

CE:

ZD: plaster properties (prevailing)

1

1

0.061200, 2.30000, 0.00174533, 1.00000, 0.000000

CM: RR:

CM: 0.020000, 0.000000, 0.000000

CM: 0.000000, 0.000000, 90.0000, 0.000000

CM: PG: simplified partition (door open)

CM: 6, 0

CM: 0.000000, 0.000000, 0.000000

CM: 0.000000, 4.46720, 0.000000

CM: 0.000000, 4.46720, 2.13360

CM: 0.000000, 5.68960, 2.13360

CM: 0.000000, 5.68960, 3.40360

CM: 0.000000, 0.000000, 3.40360

CM: RR: reverting to original axis-system

CM: -0.020000, 0.000000, 0.000000

CE: 0.000000, 0.000000, 90.0000, 0.000000

CE:

CE: building the rest of NORTHERN partitions

CE:

RR: moving partition v.1 to the right

0.000000, 5.68960, 0.000000

0.000000, 0.000000, 90.0000, 0.000000

RR: moving partition v.1 to the right

0.000000, 5.68960, 0.000000

0.000000, 0.000000, 90.0000, 0.000000

RR: moving partition v.1 to the right

0.000000, 5.68960, 0.000000

0.000000, 0.000000, 90.0000, 0.000000

PG: simplified partition (doors open)

8, 0

0.000000, 0.000000, 2.13360

0.000000, 1.22240, 2.13360

0.000000, 1.22240, 0.000000

0.000000, 4.46720, 0.000000

0.000000, 4.46720, 2.13360

0.000000, 5.68960, 2.13360

0.000000, 5.68960, 3.40360

0.000000, 0.000000, 3.40360

RR: moving partition v.1 to the right

0.010000, 5.68960, 0.000000

0.000000, 0.000000, 90.0000, 0.000000

PG: simplified partition (doors open)

8, 0

0.000000, 0.000000, 2.13360

0.000000, 1.22240, 2.13360

0.000000, 1.22240, 0.000000

0.000000, 4.46720, 0.000000

0.000000, 4.46720, 2.13360

0.000000, 5.68960, 2.13360

0.000000, 5.68960, 3.40360

0.000000, 0.000000, 3.40360

RR: moving partition v.1 to the right

-0.010000, 5.68960, 0.000000

0.000000, 0.000000, 90.0000, 0.000000

PG: simplified partition (doors open)

8, 0

0.000000, 0.000000, 2.13360

0.000000, 1.22240, 2.13360

0.000000, 1.22240, 0.000000

0.000000, 4.46720, 0.000000

0.000000, 4.46720, 2.13360

0.000000, 5.68960, 2.13360

0.000000, 5.68960, 3.40360

0.000000, 0.000000, 3.40360

CE:

CE: End of building partitions v.1 on NORTHERN side

CE:

CE:

CE: Starting partition v.2

CE:

CE:
RR: moving the axis system to the left
0.000000, -17.0688, 0.000000
0.000000, 0.000000, 90.0000, 0.000000
CE:
CE: simplified partition v.2
CE:(without doors, windows etc)
PG: simplified partition (doors open)
6. 0
0.000000, 0.000000, 2.13360
0.000000, 1.22240, 2.13360
0.000000, 1.22240, 0.000000
0.000000, 5.68960, 0.000000
0.000000, 5.68960, 3.40360
0.000000, 0.000000, 3.40360
CE:
CE:
CE:END of building NORTHERN partitions
CE:
RR: moving back the antenna
0.000000, -11.3792, 0.000000
0.000000, 0.000000, 90.0000, 0.000000
CE:
CE:
CE: Starting the SOUTHERN part
CE:
RR: moving the axis system
28.448, -5.68960, 0.000000
0.000000, 0.000000, 90.0000, 0.000000
CE:
CE:
CE: partitions between rooms
ZD: plaster properties
1
1
0.612000, 2.30000, 0.00174533, 1.00000, 0.000000
PG:
4. 0
0.000000, 2.84480, 0.000000
0.000000, 2.84480, 3.81000
5.68960, 2.84480, 3.81000
5.68960, 2.84480, 0.000000
RR:

0.000000, 2.84480, 0.000000
0.000000, 0.000000, 90.0000, 0.000000
PG:
4, 0
0.000000, 2.84480, 0.000000
0.000000, 2.84480, 3.81000
5.68960, 2.84480, 3.81000
5.68960, 2.84480, 0.000000
RR:
0.000000, 2.84480, 0.000000
0.000000, 0.000000, 90.0000, 0.000000
CM: PG:
CM: 4, 0
CM: 0.000000, 2.84480, 0.000000
CM: 0.000000, 2.84480, 3.81000
CM: 5.68960, 2.84480, 3.81000
CE: 5.68960, 2.84480, 0.000000
ZD: concrete wall containing metal beams
1
2
0.0612000, 5.84000, 0.00141600, 1.00000, 0.000000
0.0612000, 5.84000, 0.00141600, 1.00000, 0.000000
RR:
0.000000, 2.84480, 0.000000
0.000000, 0.000000, 90.0000, 0.000000
CM: PG:
CM: 4, 0
CM: 0.000000, 2.84480, 0.000000
CM: 0.000000, 2.84480, 3.81000
CM: 5.68960, 2.84480, 3.81000
CE: 5.68960, 2.84480, 0.000000
RR:
0.000000, 2.84480, 0.000000
0.000000, 0.000000, 90.0000, 0.000000
PG:
4, 0
0.000000, 2.84480, 0.000000
0.000000, 2.84480, 3.81000
5.68960, 2.84480, 3.81000
5.68960, 2.84480, 0.000000
RR:
0.000000, 2.84480, 0.000000
0.000000, 0.000000, 90.0000, 0.000000

PG:
4, 0
0.000000, 2.84480, 0.000000
0.000000, 2.84480, 3.81000
5.68960, 2.84480, 3.81000
5.68960, 2.84480, 0.000000
CE: change material properties
ZD: plaster properties
1
1
0.612000, 2.30000, 0.00174533, 1.00000, 0.000000
RR:
0.000000, 2.84480, 0.000000
0.000000, 0.000000, 90.0000, 0.000000
CM: PG:
CM: 4, 0
CM: 0.000000, 2.84480, 0.000000
CM: 0.000000, 2.84480, 3.81000
CM: 5.68960, 2.84480, 3.81000
CE: 5.68960, 2.84480, 0.000000
CE:
RR:
0.000000, 2.84480, 0.000000
0.000000, 0.000000, 90.0000, 0.000000
PG:
4, 0
0.000000, 2.84480, 0.000000
0.000000, 2.84480, 3.81000
5.68960, 2.84480, 3.81000
5.68960, 2.84480, 0.000000
RR:
0.000000, 2.84480, 0.000000
0.000000, 0.000000, 90.0000, 0.000000
PG:
4, 0
0.000000, 2.84480, 0.000000
0.000000, 2.84480, 3.81000
5.68960, 2.84480, 3.81000
5.68960, 2.84480, 0.000000
RR:
0.000000, 2.84480, 0.000000
0.000000, 0.000000, 90.0000, 0.000000
PG:

4.0
0.000000, 2.84480, 0.000000
0.000000, 2.84480, 3.81000
5.68960, 2.84480, 3.81000
5.68960, 2.84480, 0.000000
RR:
0.000000, 2.84480, 0.000000
0.000000, 0.000000, 90.0000, 0.000000
PG:
4.0
0.000000, 2.84480, 0.000000
0.000000, 2.84480, 3.81000
5.68960, 2.84480, 3.81000
5.68960, 2.84480, 0.000000
RR:
0.000000, 2.84480, 0.000000
0.000000, 0.000000, 90.0000, 0.000000
PG:
4.0
0.000000, 2.84480, 0.000000
0.000000, 2.84480, 3.81000
5.68960, 2.84480, 3.81000
5.68960, 2.84480, 0.000000
RR:
0.000000, 2.84480, 0.000000
0.000000, 0.000000, 90.0000, 0.000000
PG:
4.0
0.000000, 2.84480, 0.000000
0.000000, 2.84480, 3.81000
5.68960, 2.84480, 3.81000
5.68960, 2.84480, 0.000000
RR: reverting to global axis system
-5.6896, -34.1376, 0.000000
0.000000, 0.000000, 90.0000, 0.000000
CM: PG:
CM: 4.0
CM: 0.000000, 1.5, 0.000000
CM: 0.000000, 1.5, 3.81000
CM: 5.68960, 1.5, 3.81000
CE: 5.68960, 1.5, 0.000000
CE:
CE:

CE:
CE:
CE:
CE: Building the partitions v.1,v.2,v.3
CE: in SOUTHERN side
CE:
CE:
CE:
CE:
CE:
ZD: concrete wall containing metal beams
1
2
0.0612000, 5.84000, 0.00141600, 1.00000, 0.000000
0.0612000, 5.84000, 0.00141600, 1.00000, 0.000000
CE: exposed concrete containing beams over
CE: the interior partitions
PG:
4, 0
5.68960, 0.000000, 3.81000
5.68960, 0.000000, 3.40360
5.68960, 39.8272, 3.40360
5.68960, 39.8272, 3.81000
RR: moving the fake partition to the right position
5.68960, 0, 0.000000
0.000000, 0.000000, 90.0000, 0.000000
CM:
CM: Building the simplified partition (doors open)
CE:
ZD: plaster properties (prevailing)
1
1
0.061200, 2.30000, 0.00174533, 1.00000, 0.000000
PG: simplified partition (doors open)
8, 0
0.000000, 0.000000, 2.13360
0.000000, 1.22240, 2.13360
0.000000, 1.22240, 0.000000
0.000000, 4.46720, 0.000000
0.000000, 4.46720, 2.13360
0.000000, 5.68960, 2.13360
0.000000, 5.68960, 3.40360
0.000000, 0.000000, 3.40360

RR:
 0.050000, 0.000000, 0.000000
 0.000000, 0.000000, 90.0000, 0.000000
 PG: simplified partition (doors open)
 8, 0
 0.000000, 0.000000, 2.13360
 0.000000, 1.22240, 2.13360
 0.000000, 1.22240, 0.000000
 0.000000, 4.46720, 0.000000
 0.000000, 4.46720, 2.13360
 0.000000, 5.68960, 2.13360
 0.000000, 5.68960, 3.40360
 0.000000, 0.000000, 3.40360
 RR:
 -0.050000, 5.6896, 0.000000
 0.000000, 0.000000, 90.0000, 0.000000
 CE:
 CE: simplified partition v.3
 CE:(without door, windows etc)
 PG: simplified partition (door open)
 6, 0
 0.000000, 0.000000, 0.000000
 0.000000, 4.46720, 0.000000
 0.000000, 4.46720, 2.13360
 0.000000, 5.68960, 2.13360
 0.000000, 5.68960, 3.40360
 0.000000, 0.000000, 3.40360
 RR:
 0.020000, 0.000000, 0.000000
 0.000000, 0.000000, 90.0000, 0.000000
 PG: simplified partition (door open)
 6, 0
 0.000000, 0.000000, 0.000000
 0.000000, 4.46720, 0.000000
 0.000000, 4.46720, 2.13360
 0.000000, 5.68960, 2.13360
 0.000000, 5.68960, 3.40360
 0.000000, 0.000000, 3.40360
 RR: reverting to original axis-system
 -0.020000, 0.000000, 0.000000
 0.000000, 0.000000, 90.0000, 0.000000
 CE:

CE: building the rest of NORTHERN partitions
CE:
RR: moving partition v.1 to the right
0.000000, 5.68960, 0.000000
0.000000, 0.000000, 90.0000, 0.000000
RR: moving partition v.1 to the right
0.000000, 5.68960, 0.000000
0.000000, 0.000000, 90.0000, 0.000000
RR: moving partition v.1 to the right
0.000000, 5.68960, 0.000000
0.000000, 0.000000, 90.0000, 0.000000
PG: simplified partition (doors open)
S, 0
0.000000, 0.000000, 2.13360
0.000000, 1.22240, 2.13360
0.000000, 1.22240, 0.000000
0.000000, 4.46720, 0.000000
0.000000, 4.46720, 2.13360
0.000000, 5.68960, 2.13360
0.000000, 5.68960, 3.40360
0.000000, 0.000000, 3.40360
RR: moving partition v.1 to the right
0.000000, 5.68960, 0.000000
0.000000, 0.000000, 90.0000, 0.000000
PG: simplified partition (doors open)
S, 0
0.000000, 0.000000, 2.13360
0.000000, 1.22240, 2.13360
0.000000, 1.22240, 0.000000
0.000000, 4.46720, 0.000000
0.000000, 4.46720, 2.13360
0.000000, 5.68960, 2.13360
0.000000, 5.68960, 3.40360
0.000000, 0.000000, 3.40360
RR: moving partition v.1 to the right
0.000000, 5.68960, 0.000000
0.000000, 0.000000, 90.0000, 0.000000
PG: simplified partition (doors open)
S, 0
0.000000, 0.000000, 2.13360
0.000000, 1.22240, 2.13360
0.000000, 1.22240, 0.000000
0.000000, 4.46720, 0.000000

0.000000, 4.46720, 2.13360
0.000000, 5.68960, 2.13360
0.000000, 5.68960, 3.40360
0.000000, 0.000000, 3.40360
CE:
CE: End of building partitions v.1 on NORTHERN side
CE:
CE:
CE: Starting partition v.2
CE:
CE:
RR: moving the axis system to the left
0.000000, -17.0688, 0.000000
0.000000, 0.000000, 90.0000, 0.000000
CE:
CE: simplified partition v.2
CE:(without doors, windows etc)
PG: simplified partition (doors open)
6. 0
0.000000, 0.000000, 2.13360
0.000000, 1.22240, 2.13360
0.000000, 1.22240, 0.000000
0.000000, 5.68960, 0.000000
0.000000, 5.68960, 3.40360
0.000000, 0.000000, 3.40360
CE:
CE:
CE:
CE:
CE:
RR: reverting to GLOBAL coordinate system
-34.1376, -17.0688, 0.000000
0.000000, 0.000000, 90.0000, 0.000000
CE:
CE:
CE:
CE: Building the rest of interior partitions
CE:
CE:
CE:
CE:
RR: translating the four NORTH-SOUTH partitions
5.68960, 11.3792, 0.000000

0.000000, 0.000000, 90.0000, 0.000000
PG: interior partition (NORTH-SOUTH)
8, 0
0.000000, 0.000000, 0.000000
0.000000, 0.000000, 3.81000
3.04800, 0.000000, 3.81000
3.04800, 0.000000, 0.000000
2.43840, 0.000000, 0.000000
2.43840, 0.000000, 2.13360
0.914400, 0.000000, 2.13360
0.914400, 0.000000, 0.000000
CE: translating the second out of the four
CE: NORTH-SOUTH partitions
RR:
0.000000, 5.68960, 0.000000
0.000000, 0.000000, 90.0000, 0.000000
PG: interior partition (NORTH-SOUTH)
8, 0
0.000000, 0.000000, 0.000000
0.000000, 0.000000, 3.81000
3.04800, 0.000000, 3.81000
3.04800, 0.000000, 0.000000
2.43840, 0.000000, 0.000000
2.43840, 0.000000, 2.13360
0.914400, 0.000000, 2.13360
0.914400, 0.000000, 0.000000
CE: translating the third out of the four
CE: NORTH-SOUTH partitions
RR:
25.39, 0, 0.000000
0.000000, 0.000000, 90.0000, 0.000000
PG: interior partition (NORTH-SOUTH)
8, 0
0.000000, 0.000000, 0.000000
0.000000, 0.000000, 3.81000
3.04800, 0.000000, 3.81000
3.04800, 0.000000, 0.000000
2.43840, 0.000000, 0.000000
2.43840, 0.000000, 2.13360
0.914400, 0.000000, 2.13360
0.914400, 0.000000, 0.000000
CE: translating the fourth out of the four
CE: NORTH-SOUTH partitions

RR:
0. -5.6896, 0.000000
0.000000, 0.000000, 90.0000, 0.000000
PG: interior partition (NORTH-SOUTH)
S. 0
0.000000, 0.000000, 0.000000
0.000000, 0.000000, 3.81000
3.04800, 0.000000, 3.81000
3.04800, 0.000000, 0.000000
2.43840, 0.000000, 0.000000
2.43840, 0.000000, 2.13360
0.914400, 0.000000, 2.13360
0.914400, 0.000000, 0.000000
CE:
CE:
CE:
RR: reverting to GLOBAL coordinates
-31.0796, -11.3792, 0.000000
0.000000, 0.000000, 90.0000, 0.000000
CE:
CE:
CE: Building the WEST-EAST partition
CE:
RR: translating the WEST-EAST partition
17.0688, 0.000000, 0.000000
0.000000, 0.000000, 90.0000, 0.000000
PG: WEST-EAST interior partition
S. 0
0.000000, 0.000000, 0.000000
0.000000, 0.000000, 3.81000
0.000000, 11.3792, 3.81000
0.000000, 11.3792, 0.000000
0.000000, 10.6172, 0.000000
0.000000, 10.6172, 2.13360
0.000000, 9.09320, 2.13360
0.000000, 9.09320, 0.000000
RR: reverting to GLOBAL coordinates
-17.0688, 0, 0.000000
0.000000, 0.000000, 90.0000, 0.000000
CE:
CE:
CE:
CE: Building central room's light long

CE: NORTH-SOUTH partition
CE:
RR: translating the LONG central partition
11.3792, 11.3792, 0.000000
0.000000, 0.000000, 90.0000, 0.000000
PG: central room's long partition
12, 0
0.000000, 0.000000, 0.000000
0.000000, 0.000000, 3.81000
17.0688, 0.000000, 3.81000
17.0688, 0.000000, 0.000000
14.2240, 0.000000, 0.000000
14.2240, 0.000000, 2.13360
11.3792, 0.000000, 2.13360
11.3792, 0.000000, 0.000000
5.68960, 0.000000, 0.000000
5.68960, 0.000000, 2.13360
4.77520, 0.000000, 2.13360
4.77520, 0.000000, 0.000000
CE:
CE:
CE:
RR: reverting to GLOBAL coordinates
-11.3792, -11.3792, 0.000000
0.000000, 0.000000, 90.0000, 0.000000
CE:
CE:
CE:
CE: Building the concrete wall in front of
CE: the stairs; using "artificial"
CE: constitutive parameters
ZD: concrete wall containing metal beams
1
2
0.0612000, 8.247, 0.00141600, 1.00000, 0.000000
0.0612000, 8.247, 0.00141600, 1.00000, 0.000000
RR: translating the concrete wall
8.73760, 11.3792, 0.000000
0.000000, 0.000000, 90.0000, 0.000000
CE: concrete wall in front of the stairs
PM:
16
0.00500000, 0.00500000, 0.000000

0.00500000, 0.00500000, 3.81000
0.00500000, 5.68960, 3.81000
0.00500000, 5.68960, 0.000000
2.64160, 5.68960, 0.000000
2.64160, 5.68960, 3.81000
2.64160, 5.65960, 3.81000
2.64160, 5.65960, 0.000000
0.0300000, 5.65960, 0.000000
0.0300000, 5.65960, 3.81000
0.0300000, 0.0300000, 3.81000
0.0300000, 0.0300000, 0.000000
2.64160, 0.0300000, 0.000000
2.64160, 0.0300000, 3.81000
2.64160, 0.00500000, 3.81000
2.64160, 0.00500000, 0.000000

0
1
2
3
4
0
4
3
6
5
0
6
5
8
7
0
7
8
9
10
0
10
9
12
11
0
11
12

13
14
0
14
13
16
15
0
15
16
1
2
0
0
CE:
CE:
CE:
RR: reverting to GLOBAL coordinates
-8.73760, -11.3792, 0.000000
0.000000, 0.000000, 90.0000, 0.000000
CE:
CE:
CE:
RR: translating the MESH
11.4792, 17.0688, 0.000000
0.000000, 0.000000, 90.0000, 0.000000
CE:
CE:
CE: MESH of the instrument room
CE:
CE:
ZD: using made-up properties for MESH
1
1
0.0100000, 5.896, 0, 1.00000, 0.000000
PG: metallic MESH substitute
4, 0
0.000000, 0.000000, 0.000000
0.000000, 0.000000, 3.81000
16.9088, 0.000000, 3.81000
16.9088, 0.000000, 0.000000
RR: reverting to GLOBAL coordinates
-11.4792, -17.0688, 0.000000

0.000000, 0.000000, 90.0000, 0.000000

CE:

CE:

CE:

CE: changing properties again

CE:

CE:

ZD: concrete wall containing metal beams

1

2

0.0612000, 8.247, 0.00141600, 1.00000, 0.000000

0.0612000, 8.247, 0.00141600, 1.00000, 0.000000

RR: translating the second and last concrete wall

28.4480, 11.3792, 0.000000

0.000000, 0.000000, 90.0000, 0.000000

CE: second and last concrete wall

CE:

CE:

PM:

8

0.00500000, 0.00500000, 0.000000

0.00500000, 0.00500000, 3.81000

0.00500000, 5.68960, 3.81000

0.00500000, 5.68960, 0.000000

2.64160, 5.68960, 0.000000

2.64160, 5.68960, 3.81000

2.64060, 0.00500000, 3.81000

2.64060, 0.00500000, 0.000000

0

1

2

3

4

0

4

3

6

5

0

5

6

7

8

0
7
8
1
2
0
0
RR: reverting to GLOBAL coordinates
-28.4480, -11.3792, 0.000000
0.000000, 0.000000, 90.0000, 0.000000
CE:
CE:
CE:
CE:
CE:
CE: Building the wooden tables
CE:
CE:
CE:
ZD: wood properties
1
1
0.0612000, 1.50000, 0.0100000, 1.00000, 0.000000
CE:
CE:
RR: translating the tables v.1
7.82320, 0.914400, 0.000000
0.000000, 0.000000, 90.0000, 0.000000
PG: wooden table v.1
4, 0
0.000000, 0.000000, 0.914400
0.000000, 8.22960, 0.914400
1.82880, 8.22960, 0.914400
1.82880, 0.000000, 0.914400
RR: translating the second table v.1
2.5, 0, 0.000000
0.000000, 0.000000, 90.0000, 0.000000
PG: wooden table v.1
4, 0
0.000000, 0.000000, 0.914400
0.000000, 8.22960, 0.914400
1.82880, 8.22960, 0.914400
1.82880, 0.000000, 0.914400

RR: translating the third table v.1
2.5. 0. 0.000000
0.000000, 0.000000, 90.0000, 0.000000
PG: wooden table v.1
4, 0
0.000000, 0.000000, 0.914400
0.000000, 8.22960, 0.914400
1.82880, 8.22960, 0.914400
1.82880, 0.000000, 0.914400
CE:
CE:
RR: reverting to GLOBAL
-12.82320, -0.914400, 0.000000
0.000000, 0.000000, 90.0000, 0.000000
CE:
CE:
CE:
CE: Building the wooden tables v.2
CE:
CE:
CE:
RR: translating the wooden tables v.2
29.6164, 22.7584, 0.000000
0.000000, 0.000000, 90.0000, 0.000000
PM: wooden tables v.2 (1st of 1st row)
8
0.000000, 0.000000, 0.990600
0.000000, 5.28320, 0.990600
1.47320, 5.28320, 0.990600
1.47320, 0.000000, 0.990600
1.47320, 0.000000, 1.16840
0.000000, 0.000000, 1.16840
0.000000, 5.28320, 1.16840
1.47320, 5.28320, 1.16840
0
1
2
3
4
0
5
4
1

6
0
1
2
7
6
0
2
3
8
7
0
3
4
5
8
0
6
7
8
5
0
0

CE:

RR: translating tables v.2

-3, 0.000000, 0.000000

0.000000, 0.000000, 90.0000, 0.000000

PM: wooden tables v.2 (2nd of 1st row)

8

0.000000, 0.000000, 0.990600

0.000000, 5.28320, 0.990600

1.47320, 5.28320, 0.990600

1.47320, 0.000000, 0.990600

1.47320, 0.000000, 1.16840

0.000000, 0.000000, 1.16840

0.000000, 5.28320, 1.16840

1.47320, 5.28320, 1.16840

0

1

2

3

4

0

5
4
1
6
0
1
2
7
6
0
2
3
8
7
0
3
4
5
8
0
6
7
8
5
0
0

RR: translating tables v.2

-3, 0.000000, 0.000000

0.000000, 0.000000, 90.0000, 0.000000

PM: wooden tables v.2 (3rd of 1st row)

8

0.000000, 0.000000, 0.990600

0.000000, 5.28320, 0.990600

1.47320, 5.28320, 0.990600

1.47320, 0.000000, 0.990600

1.47320, 0.000000, 1.16840

0.000000, 0.000000, 1.16840

0.000000, 5.28320, 1.16840

1.47320, 5.28320, 1.16840

0

1

2

3

4
0
5
4
1
6
0
1
2
7
6
0
2
3
8
7
0
3
4
5
8
0
6
7
8
5
0
0

RR: translating tables v.2

-3, 0.000000, 0.000000

0.000000, 0.000000, 90.0000, 0.000000

PM: wooden tables v.2 (4th of 1st row)

8

0.000000, 0.000000, 0.990600

0.000000, 5.28320, 0.990600

1.47320, 5.28320, 0.990600

1.47320, 0.000000, 0.990600

1.47320, 0.000000, 1.16840

0.000000, 0.000000, 1.16840

0.000000, 5.28320, 1.16840

1.47320, 5.28320, 1.16840

0

1

2
3
4
0
5
4
1
6
0
1
2
7
6
0
2
3
8
7
0
3
4
5
8
0
6
7
8
5
0
0

RR: translating tables v.2
-3, 0.000000, 0.000000
0.000000, 0.000000, 90.0000, 0.000000
PM: wooden tables v.2 (5th of 1st row)
8
0.000000, 0.000000, 0.990600
0.000000, 5.28320, 0.990600
1.47320, 5.28320, 0.990600
1.47320, 0.000000, 0.990600
1.47320, 0.000000, 1.16840
0.000000, 0.000000, 1.16840
0.000000, 5.28320, 1.16840
1.47320, 5.28320, 1.16840

0
1
2
3
4
0
5
4
1
6
0
1
2
7
6
0
2
3
8
7
0
3
4
5
8
0
6
7
8
5
0
0

RR: translating tables v.2

-3, 0.000000, 0.000000

0.000000, 0.000000, 90.0000, 0.000000

PM: wooden tables v.2 (6th of 1st row)

8

0.000000, 0.000000, 0.990600

0.000000, 5.28320, 0.990600

1.47320, 5.28320, 0.990600

1.47320, 0.000000, 0.990600

1.47320, 0.000000, 1.16840

0.000000, 0.000000, 1.16840

0.000000, 5.28320, 1.16840

1.47320, 5.28320, 1.16840

0

1

2

3

4

0

5

4

1

6

0

1

2

7

6

0

2

3

8

7

0

3

4

5

8

0

6

7

8

5

0

0

CE:

CE: End of FIRST ROW of tables v.2

CE:

RR: translating the SECOND ROW of the tables v.2

15.0000, 10.3124, 0.000000

0.000000, 0.000000, 90.0000, 0.000000

PM: wooden tables v.2 (1st of 2nd row)

8

0.000000, 0.000000, 0.990600

0.000000, 5.28320, 0.990600
1.47320, 5.28320, 0.990600
1.47320, 0.000000, 0.990600
1.47320, 0.000000, 1.16840
0.000000, 0.000000, 1.16840
0.000000, 5.28320, 1.16840
1.47320, 5.28320, 1.16840

0
1
2
3
4
0
5
4
1
6
0
1
2
7
6
0
2
3
8
7
0
3
4
5
8
0
6
7
8
5
0
0

CE:

RR: translating tables v.2
-3, 0.000000, 0.000000
0.000000, 0.000000, 90.0000, 0.000000

PM: wooden tables v.2 (2nd of 2nd row)

8
0.000000, 0.000000, 0.990600
0.000000, 5.28320, 0.990600
1.47320, 5.28320, 0.990600
1.47320, 0.000000, 0.990600
1.47320, 0.000000, 1.16840
0.000000, 0.000000, 1.16840
0.000000, 5.28320, 1.16840
1.47320, 5.28320, 1.16840

0
1
2
3
4
0
5
4
1
6
0
1
2
7
6
0
2
3
8
7
0
3
4
5
8
0
6
7
8
5
0
0

RR: translating tables v.2

-3, 0.000000, 0.000000
0.000000, 0.000000, 90.0000, 0.000000
PM: wooden tables v.2 (3rd of 2nd row)

8
0.000000, 0.000000, 0.990600
0.000000, 5.28320, 0.990600
1.47320, 5.28320, 0.990600
1.47320, 0.000000, 0.990600
1.47320, 0.000000, 1.16840
0.000000, 0.000000, 1.16840
0.000000, 5.28320, 1.16840
1.47320, 5.28320, 1.16840

0
1
2
3
4
0
5
4
1
6
0
1
2
7
6
0
2
3
8
7
0
3
4
5
8
0
6
7
8
5
0

0
RR: translating tables v.2
-3, 0.000000, 0.000000
0.000000, 0.000000, 90.0000, 0.000000
PM: wooden tables v.2 (4th of 2nd row)
S
0.000000, 0.000000, 0.990600
0.000000, 5.28320, 0.990600
1.47320, 5.28320, 0.990600
1.47320, 0.000000, 0.990600
1.47320, 0.000000, 1.16840
0.000000, 0.000000, 1.16840
0.000000, 5.28320, 1.16840
1.47320, 5.28320, 1.16840
0
1
2
3
4
0
5
4
1
6
0
1
2
7
6
0
2
3
8
7
0
3
4
5
8
0
6
7
8

5
0
0
RR: translating tables v.2
-3, 0.000000, 0.000000
0.000000, 0.000000, 90.0000, 0.000000
PM: wooden tables v.2 (5th of 2nd row)
8
0.000000, 0.000000, 0.990600
0.000000, 5.28320, 0.990600
1.47320, 5.28320, 0.990600
1.47320, 0.000000, 0.990600
1.47320, 0.000000, 1.16840
0.000000, 0.000000, 1.16840
0.000000, 5.28320, 1.16840
1.47320, 5.28320, 1.16840
0
1
2
3
4
0
5
4
1
6
0
1
2
7
6
0
2
3
8
7
0
3
4
5
8
0
6

7
8
5
0
0
8
8
4
1
6
0
1
2
7
6
0
2
3
8
7
0
3
4
5
8

RR: translating tables v.2
-3. 0.000000, 0.000000
0.000000, 0.000000, 90.0000, 0.000000
PM: wooden tables v.2 (6th of 2nd row)
8
0.000000, 0.000000, 0.990600
0.000000, 5.28320, 0.990600
1.47320, 5.28320, 0.990600
1.47320, 0.000000, 0.990600
1.47320, 0.000000, 1.16840
0.000000, 0.000000, 1.16840
0.000000, 5.28320, 1.16840
1.47320, 5.28320, 1.16840

0
6
7
8
5
0
0
CE:
CE:END OF SECOND ROW
CE:
RR: reverting to GLOBAL coordinates
-14.6164, -33.0708, 0.000000
0.000000, 0.000000, 90.0000, 0.000000
CE:
CE:
CE:END OF ALL WOODEN TABLES
CE:
CE:
CE:
CE:
CE: Building the metallic block
CE:
CE:
RR: translating the metallic block
22.7584, 28.4480, 0.000000
0.000000, 0.000000, 90.0000, 0.000000
ZD: metallic properties (PEC)
0
PM: Metallic Block
8
-13.4112, 4.26720, 0.000000
0.000000, 4.26720, 0.000000
0.000000, 0.000000, 0.000000
-13.4112, 0.000000, 0.000000
-13.4112, 4.26720, 1.98120
0.000000, 4.26720, 1.98120
0.000000, 0.000000, 1.98120
-13.4112, 0.000000, 1.98120
0
1
5
8
4

0
1
2
6
5
0
3
4
8
7
0
2
3
7
6
0
0
CE:
CE:
CE:
RR: reverting to GLOBAL
-22.7584, -28.4480, 0.000000
0.000000, 0.000000, 90.0000, 0.000000
CE:
CE:
CE:
CE:
CE:
ZD: concrete columns containing metal beams
-2
1
0.0612000, 4.00000, 0.00436300, 1.00000, 0.000000
CE: Building the columns
CE:
CE:
RR: translating the columns
11.3792, 29.1, 0.000000
0.000000, 0.000000, 90.0000, 0.000000
CE:
CE: columns
CE:
PM: first column
8

0.600000, 0.600000, 0.000000
-0.600000, 0.600000, 0.000000
-0.600000, -0.600000, 0.000000
0.600000, -0.600000, 0.000000
0.600000, 0.600000, 3.81000
-0.600000, 0.600000, 3.81000
-0.600000, -0.600000, 3.81000
0.600000, -0.600000, 3.81000

0

1

5

8

4

0

1

2

6

5

0

2

3

7

6

0

3

7

8

4

0

0

RR: translating the 2nd column

5.68960, 0.000000, 0.000000

0.000000, 0.000000, 90.0000, 0.000000

PM: second column

8

0.600000, 0.600000, 0.000000

-0.600000, 0.600000, 0.000000

-0.600000, -0.600000, 0.000000

0.600000, -0.600000, 0.000000

0.600000, 0.600000, 3.81000

-0.600000, 0.600000, 3.81000

-0.600000, -0.600000, 3.81000

0.600000, -0.600000, 3.81000

0
1
5
8
4
0
1
2
6
5
0
2
3
7
6
0
3
7
8
4
0
0

RR: translating the 3rd column

6.5. 0.000000, 0.000000
0.000000, 0.000000, 90.0000, 0.000000

PM: third column

8
0.600000, 0.600000, 0.000000
-0.600000, 0.600000, 0.000000
-0.600000, -0.600000, 0.000000
0.600000, -0.600000, 0.000000
0.600000, 0.600000, 3.81000
-0.600000, 0.600000, 3.81000
-0.600000, -0.600000, 3.81000
0.600000, -0.600000, 3.81000

0
1
5
8
4
0
1
2

6
5
0
2
3
7
6
0
3
7
8
4
0
0

RR: translating the 4th column

4.8792, 0.000000, 0.000000

0.000000, 0.000000, 90.0000, 0.000000

PM: fourth column

8

0.600000, 0.600000, 0.000000

-0.600000, 0.600000, 0.000000

-0.600000, -0.600000, 0.000000

0.600000, -0.600000, 0.000000

0.600000, 0.600000, 3.81000

-0.600000, 0.600000, 3.81000

-0.600000, -0.600000, 3.81000

0.600000, -0.600000, 3.81000

0

1

5

8

4

0

1

2

6

5

0

2

3

7

6

0

3
7
8
4
0
0
RR: reverting to GLOBAL coordinates again
-28.448, -29.1, 0.000000
0.000000, 0.000000, 90.0000, 0.000000
CE:
CE:
CE:END of building the columns
CE:
CE:
CE:
CE:END OF BUILDING THE WHOLE FLOOR
CE:
CE:
CE:
SG:
3.00000, 8.00000, 1.00000
0.000000, 0.000000, 90.0000, 0.000000
-1, 0.500000, 0.000000
1.00000, 0.000000
CE: For location #2
CE: uncomment selection out the
CE: SG command below and
CE: comment selection out the above
CE: SG command
CM: SG:
CM: 19.9136, 19.9136, 1.00000
CM: 0.000000, 0.000000, 90.0000, 0.000000
CM: -1, 0.500000, 0.000000
CE: 1.00000, 0.000000
CE: For location #3
CE: uncomment selection out the
CE: SG command below and
CE: comment selection out the above
CM: SG:
CM: 3.00000, 35.5000, 1.00000
CM: 0.000000, 0.000000, 90.0000, 0.000000
CM: -1, 0.500000, 0.000000
CE: 1.00000, 0.000000

CE: For location #4
CE: uncomment selection out the
CE: SG command below and
CE: comment selection out the above
CM: SG:
CM: 19.9136, 38.0000, 1.00000
CM: 0.000000, 0.000000, 90.0000, 0.000000
CM: -1, 0.500000, 0.000000
CE: 1.00000, 0.000000
CE: For location #5
CE: uncomment selection out the
CE: SG command below and
CE: comment selection out the above
CM: SG:
CM: 37.5000, 4.00000, 1.00000
CM: 0.000000, 0.000000, 90.0000, 0.000000
CM: -1, 0.500000, 0.000000
CE: 1.00000, 0.000000
CE:
VN: volumetric pattern
0.000000, 0.000000, 0.000000
0.000000, 0.000000, 90.0000, 0.000000
T
0.244800, 0.244800, 1.50000
0.244800, 0.244800, 0.000000
1, 162, 162
CE: The following commented-out
CE: volumetric pattern was used in the
CE: comparison input file and the
CE: rest of the input file remained the same
CM: VN: volumetric pattern
CM: 0.000000, 0.000000, 0.000000
CM: 0.000000, 0.000000, 90.0000, 0.000000
CM: T
CM: 1.32500, 1.32000, 1.50000
CM: 1.39000, 1.24000, 0.000000
CE: 1, 24, 29
CM: LY:
CE: T
PL:
T
LP:
T

XQ.

EN:

CE: End of input file used in the comparison with measurements

APPENDIX B. MATHCAD FILES

In what follows, all MathCAD files used in the thesis calculations and plots generation are given in the order they were presented in the main body.

MathCAD file used in the cylinder room example.

Reading the data:

EE:= READPRN("Cylinder_Room2_E.txt")

Calculating the total E-field:

$$E_{x\text{dB}} := EE^{(3)}$$

$$E_{y\text{dB}} := EE^{(5)}$$

$$E_{z\text{dB}} := EE^{(7)}$$

$$E_x := 10^{\frac{E_{x\text{dB}}}{20}}$$

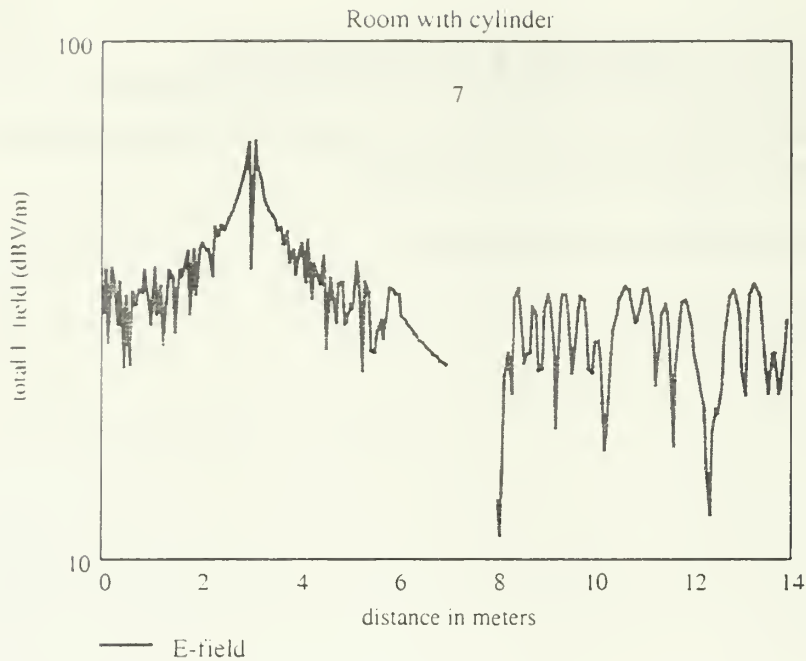
$$E_y := 10^{\frac{E_{y\text{dB}}}{20}}$$

$$E_z := 10^{\frac{E_{z\text{dB}}}{20}}$$

$$E_{\text{tot}} := \sqrt{E_x^2 + E_y^2 + E_z^2}$$

$$n := 0.228$$

The Cylinder's center of mass is at distance 7 meters.



End of cylinder room example

MathCAD file used in the typical room example (comparison)

Read the Data

```
room_data := READPRN("Marhefka_room2_E.txt")
```

```
free_data := READPRN("Marhefka_room2_free_E.txt")
```

```
M := rows(room_data)
```

```
M = 1.728 × 103
```

```
N := cols(room_data)
```

```
N = 9
```

$$E_r := \left(\frac{\text{room_data}^{(3)}}{20} \right)$$

$$E_\theta := 10 \frac{\text{room_data}^{(5)}}{20}$$

$$E_\phi := 10 \frac{\text{room_data}^{(7)}}{20}$$

$$e_r := \left(\frac{\text{free_data}^{(3)}}{10 \quad 20} \right)$$

$$e_\theta := 10 \frac{\text{free_data}^{(5)}}{20}$$

$$e_\phi := 10 \frac{\text{free_data}^{(7)}}{20}$$

Calculating the total E-field in the room and in free space

$$E_{\text{tot}} := \sqrt{(E_r)^2 + (E_\theta)^2 + (E_\phi)^2}$$

$$e_{\text{tot}} := \sqrt{(e_r)^2 + (e_\theta)^2 + (e_\phi)^2}$$

$$n := 0..M - 1$$

Each step is 6.55715 inches (16.6551cm) long

N_x is the # points in the outer loop

$$\text{rows}(E_{\text{tot}}) = 1.728 \times 10^3$$

$$N_x := 54$$

$$N_y := \frac{\text{rows}(E_{\text{tot}})}{N_x}$$

$$N_y = 32$$

$$q := 0..N_y - 1$$

$$\text{start}_q := q \cdot N_x$$

$$\text{stop}_q := \text{start}_q + N_x - 1$$

$$\text{room}^{(q)} := \text{submatrix}(E_{\text{tot}}, \text{start}_q, \text{stop}_q, 0, 0)$$

$$E_{\text{tot_dB}} := 20 \cdot \log(E_{\text{tot}})$$

$$\text{room_dB}^{(q)} := \text{submatrix}(E_{\text{tot_dB}}, \text{start}_q, \text{stop}_q, 0, 0)$$

$$\text{max}(\text{room_dB}) = 58.13$$

$$\text{min}(\text{room_dB}) = 0.797$$

$$\text{max_field_dB} = \text{max}(\text{room_dB})$$

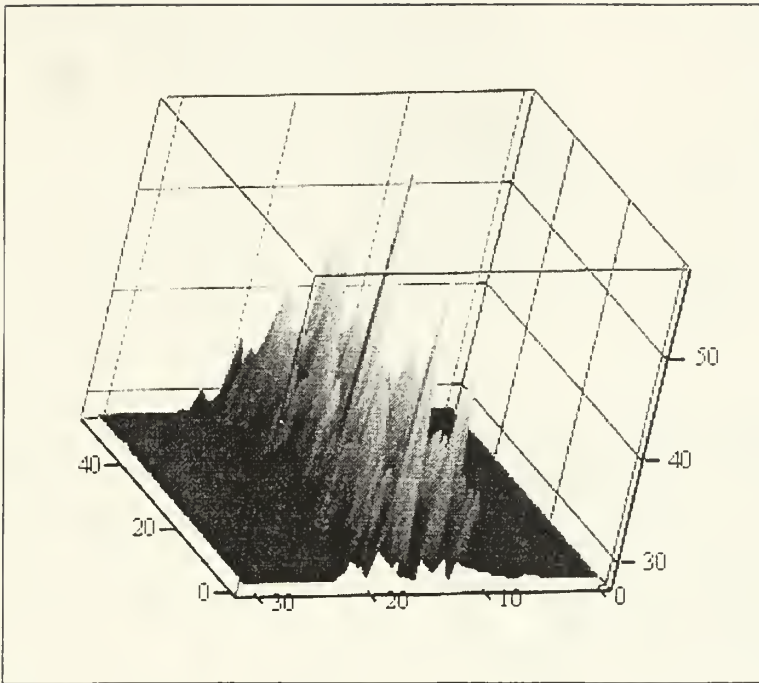
Accounting for the 30dB dynamic range of NEC-BSC

$$\text{dyn_range} := 30$$

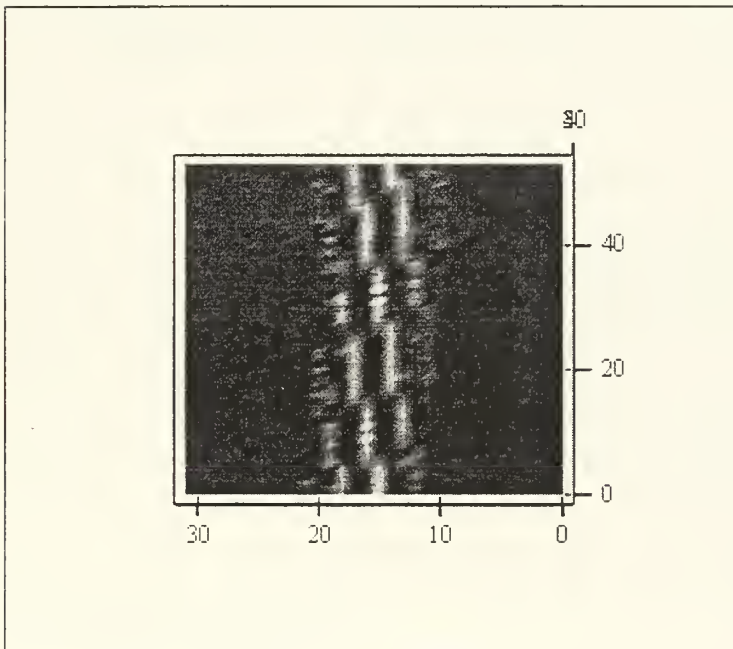
```

field_limit= max_field_dB- dyn_range
p := 0.. rows(room_dB) - 1
room_fieldp,q := if(room_dBp,q > field_limitroom_dBp,q, field_lim)t
room_lin(q) := submatrix(Etot, startq, stopq, 0, 0)
free(q) := submatrix(etot, startq, stopq, 0, 0)
etot_dB := 20 · log( $\overrightarrow{e_{tot}}$ )
free_dB(q) := submatrix(etot_dB, startq, stopq, 0, 0)
max(free_dB) = 58.04
min(free_dB) = 20.53
max_field_dB:= max(free_dB)
dyn_range:= 30
field_limit= max_field_dB- dyn_range
field_limit= 28.04
p := 0.. rows(free_dB) - 1
free_fieldp,q := if(free_dBp,q > field_limitfree_dBp,q, field_lim)t
free_lin(q) := submatrix(etot, startq, stopq, 0, 0)
diff_free_room= free_lin- room_lin
diff_free_room_dBp,q := if(diff_free_roomp,q > 0, 20 · log(diff_free_roomp,q), 0)
min_val:= min diff_free_room_dB
min_val= -27.444
diff_fr_dBp,q := if(diff_free_room_dBp,q = 0, min_val|diff_free_room_dBp,q)

```



room_field



room_field

End of typical room example (comparison)

MathCAD file used in the typical room example (random variable calculation)

Calculating the normalized difference random variable in the typical room example

In this program we are aiming at calculating all the random variables of the normalized difference between the room's and the free space field strength (E_{tot} and E_{tot_free} respectively).

We start by reading the associated data files generated by NEC_BSC.

NEC_BSC_data := READPRN "Marhefka_room2_E.txt")

M := rows(NEC_BSC_data)

M = 1.728 × 10³

N := cols(NEC_BSC_data)

N = 9

x_{coord} = NEC_BSC_data⁽⁰⁾

y_{coord} := NEC_BSC_data⁽¹⁾

z_{coord} := NEC_BSC_data⁽²⁾

$$\rho := \sqrt{(x_{\text{coord}} - 4.572)^2 + (y_{\text{coord}} - 5.486)^2 + (z_{\text{coord}} - 1.219)^2}$$

free_space_data := READPRN "Marhefka_room2_free_E.txt")

MM := rows(free_space_data)

MM = 1.728 × 10³

NN := cols(free_space_data)

NN = 9

$$E_x := \left(\frac{\text{NEC_BSC_data}^{(3)}}{10 \quad 20} \right)$$

$$E_y := 10 \quad \frac{\text{NEC_BSC_data}^{(5)}}{20}$$

$$E_z := 10 \quad \frac{\text{NEC_BSC_data}^{(7)}}{20}$$

$$E_{\text{tot}} = \sqrt{(E_x)^2 + (E_y)^2 + (E_z)^2}$$

rows(E_{tot}) = 1.728 × 10³

$$E_{x_free} := \left(\frac{\text{free_space_data}^{(3)}}{10 \quad 20} \right)$$

$$E_{y_free} := 10 \quad \frac{\text{free_space_data}^{(5)}}{20}$$

$$\text{free_space_data} := \begin{matrix} \xrightarrow{7} \\ \hline 20 \end{matrix}$$

$$E_{z_free} := 10$$

$$E_{tot_free} := \sqrt{(E_{x_free})^2 + (E_{y_free})^2 + (E_{z_free})^2}$$

Let us now create the two datamatrices, namely the "datamatrix" which consists of the room's field strength values for every observed point and the "freespacedata01" which includes the corresponding data for the free space case.

$$\text{datamatrix} := \text{augment}(\rho, E_{tot})$$

$$\text{freespacedata01} := \text{augment}(\rho, E_{tot_free})$$

At this point, owing to the non-uniform layout of the distance (from the antenna) points in the array, we will have to distinguish them into several different groups using the following approach:

$$\text{lower} := \text{floor}(\min(\rho))$$

$$\text{upper} := \text{ceil}(\max(\rho))$$

$$\text{lower} = 0$$

$$\text{upper} = 7$$

$$\text{bins} := \text{upper} - \text{lower}$$

$$\text{bins} = 14$$

$$h := \frac{\text{upper} - \text{lower}}{\text{bins}}$$

$$h = 0.5$$

$$n := 0.. \text{bins}$$

$$k_n := \text{lower} + n \cdot h$$

It should be noted that the number of bins may be chosen in a fashion which best suits our desirable "distance steps". For instance, should we choose to have groups points separated by 50cm, where the maximum distance from the antenna is 49m, our intuitive selection should be 98.

We next introduce a new function, which shall be utilized, several times in our subsequent calculations. As input, it expects a two-column matrix and an array. It looks for those values of the first column (i.e., in our problem, the distance array ρ) which fall within our made-up groups and then creates a new matrix that contains all those second column's values whose respective first column value satisfy our requirement. It finally returns this new matrix which, it should be underlined, normally has a **different number of elements in each row**.

```

build(M, binvector) :=
  A ← M(0)
  B ← M(1)
  k ← binvector
  for l ∈ 0..rows(k) - 2
    Dl ← 0
  for i ∈ 0..rows(k) - 2
    for j ∈ 0..rows(M) - 1
      Dl ← augment(Bj, Dl) if ki < Aj ≤ ki+1
  for i ∈ 0..rows(D) - 1
    Di ← submatrix(Di, 0, rows(Di) - 1, 0, cols(Di) - 2) if Di ≠ 0
  D

```

It is high time we used this helping function.

```
datamatrix02 := build(datamatrix, k)
```

```
freespacedata02 := build(freespacedata01, k)
```

The following new function is, seemingly, of high importance since it is the one which calculates the "normalized difference" random variables. It receives two matrices of the same dimensions and returns a new matrix, which in each row contains the values of the random variable pertinent to that row's "distance group."

```

difference(X, Y) :=
  for k ∈ 0..rows(X) - 1
    Ck ← 0
    for j ∈ 0..rows(X) - 1
      n ← cols(Xj)
      A ← Xj
      B ← Yj
      i ← 0
      for i ∈ 0..n - 1
        diffi ←  $\frac{A_{0,i} - B_{0,i}}{B_{0,i}}$ 
      n ← cols(Xj)
      Cj ← stack(Cj, diff)
      Cj ← (Cj)T
      k ← rows(Cj)
      l ← cols(Cj)
      Cj ← submatrix(Cj, 0, k - 1, 1, l - 1)
    C

```

We now get rid of the redundant first row zeros and then calculate the normalized difference variables.

```

new_datamatrix02 := submatrix(datamatrix02, 1, rows(datamatrix02) - 2, 0, cols(datamatrix02) - 1)
new_freespacedata02 := submatrix(freespacedata02, 1, rows(freespacedata02) - 2, 0, cols(freespacedata02) - 1)
norm_diff := difference(new_datamatrix02, new_freespacedata02)

```

Surprisingly and unexpectedly the Mathcad appears to suffer from a bug for it returns an erroneous matrix. The cause of this weird occurrence remains unknown, however we shall attempt to effectively overcome this mishap by applying an easy trick.

```

i := 0..rows(new_datamatrix02) - 1
ri := cols(new_datamatrix02i)
corr_norm_diffi := submatrix(norm_diff, 0, rows(norm_diffi) - 1, 0, ri - 1)

```

This last matrix named "corr_norm_diff" is the one we intended to find. In each row of unequal element number, it contains a different random variable as function of our "devised" groups. Let us take a closer look in one of them, say the 5th.

```

test_0 = (corr_norm_diffT)(0)
mean(test_00) = -0.156

```

$$\text{test}_1 := (\text{corr_norm_diff}^T)^{(1)}$$

$$\text{mean}(\text{test}_1) = -0.059$$

Defining the number of the bins:

$$N_{\text{points}} = 30$$

$$i := 0..N_{\text{points}} - 1$$

$$j := 0.. \text{rows}(\text{corr_norm_diff}) - 1$$

$$\text{upper}_j := \max(\text{corr_norm_diff}_j)$$

$$\text{lower}_j := \min(\text{corr_norm_diff}_j)$$

$$\text{upper_max} := \max(\text{upper}_j)$$

$$\text{lower_min} := \min(\text{lower}_j)$$

$$\text{step} = \frac{\text{upper_max} - \text{lower_min}}{N_{\text{points}}}$$

$$\text{gen_intervals}_{ij} := \text{lower_min} + \text{step} \cdot i$$

$$L_j := \frac{\text{hist}(N_{\text{points}}, \text{corr_norm_diff}_j)}{\text{cols}(\text{corr_norm_diff}_j)}$$

$$\text{step} = 0.071$$

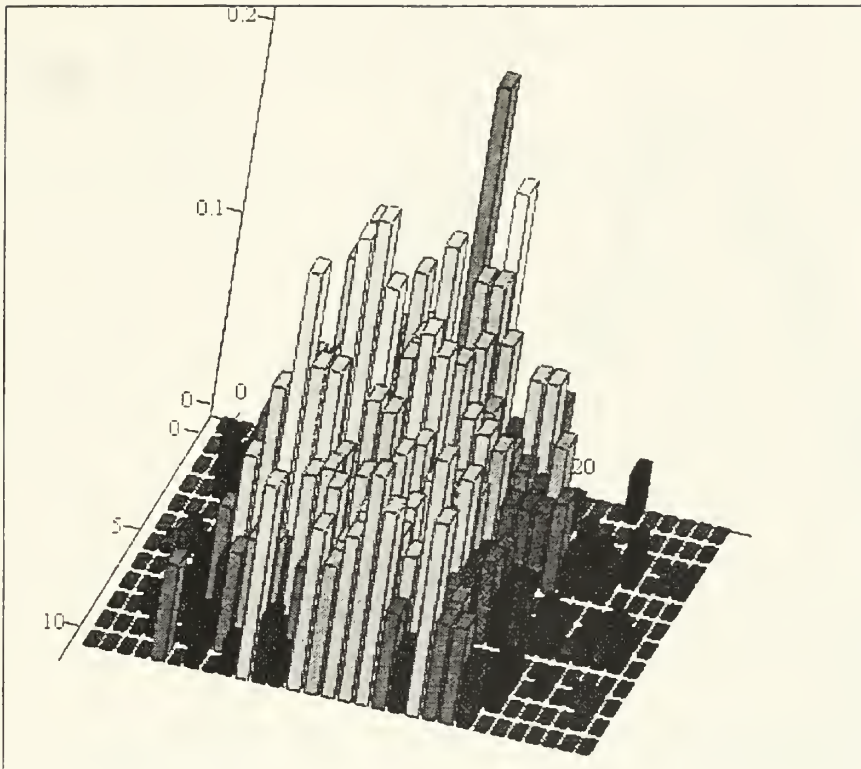
$$\text{buildL}(L) := \left| \begin{array}{l} L_{\text{new}} \leftarrow L_0^T \\ \text{für } q \in 1.. \text{rows}(L) - 1 \\ \left| \begin{array}{l} A \leftarrow L_q^T \\ L_{\text{new}} \leftarrow \text{stack}(L_{\text{new}}, A) \end{array} \right. \end{array} \right.$$

$$L_{\text{pdf}} := \text{buildL}(L)$$

$$\text{rows}(L_{\text{pdf}}) = 12$$

$$\text{cols}(L_{\text{pdf}}) = 30$$

$$\sum_{r=0}^{29} l_{\text{pdf}}_{r,1} = 1$$



L_{pdf}

$avg_pdf_{ii} := \text{mean}(L_{pdf}^{(ii)})$

$\sum avg_pdf = 1$

$\text{mean}(avg_pdf) = 0.033$

Defining the Gaussian pdf:

$\text{mean_pdf} := \text{mean}(avg_pdf)$

$\text{mean_gauss} := 0 - \text{mean_pdf}$

$\text{var_pdf} := \text{var}\left(\frac{avg_pdf}{\text{step}}\right)$

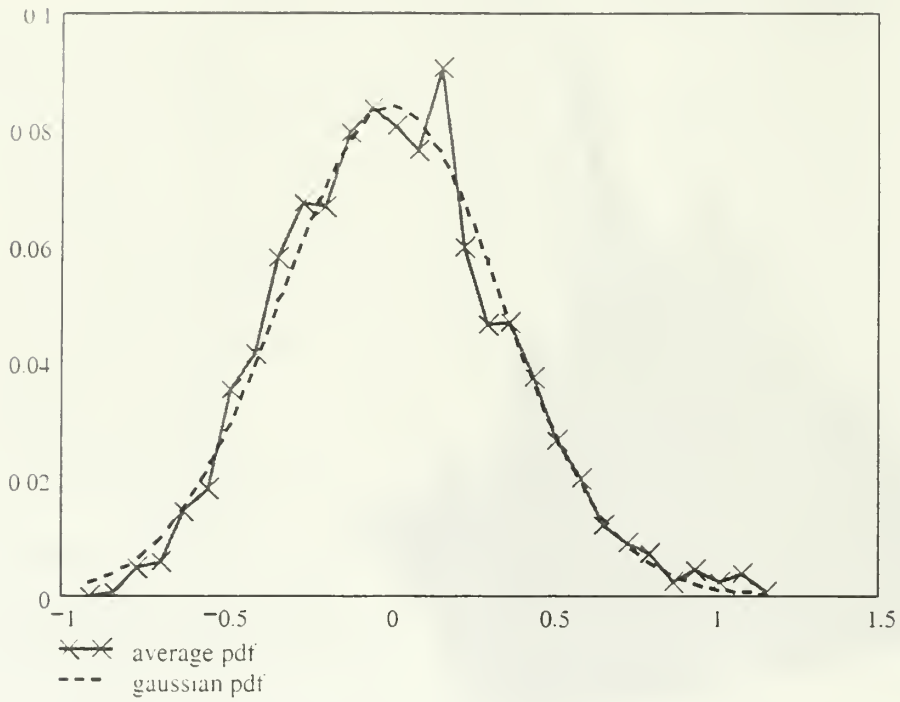
$\text{var_gauss} := 0.65 \text{var_pdf}$

$\text{stdev_pdf} := \sqrt{\text{var_pdf}}$

$\text{stdev_pdf} = 0.42$

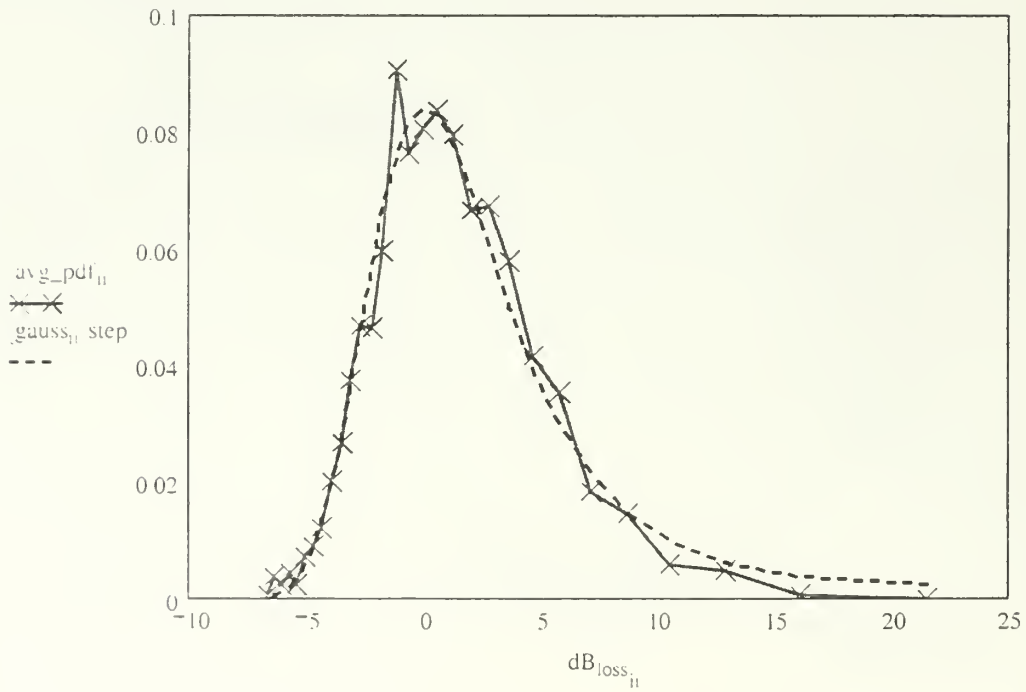
$\text{var_gauss} = 0.115$

$$gauss_{ii} := \frac{1}{\sqrt{2 \cdot \pi \cdot \text{var_gauss}}} \cdot e^{-\frac{(\text{gen_intervals}_i - \text{mean_gauss})^2}{2 \cdot \text{var_gauss}}}$$



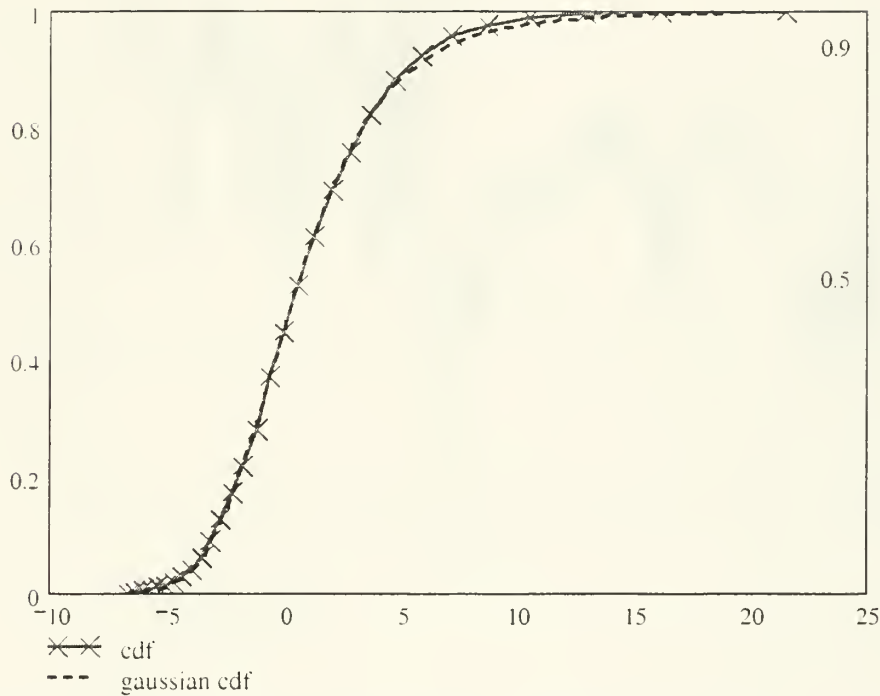
$$dB_{gain_{11}} := 20 \cdot \log(1 + gen_intervals_{11})$$

$$dB_{loss_{11}} := -dB_{gain_{11}}$$



$$cdf_{11} := 1 - \sum_{m=0}^{11} avg_pdf_m$$

$$\text{cdf}_{\text{gauss}_i} := 1 - \text{step} \cdot \sum_{m=0}^i \text{gauss}_m$$



End of typical room example (random variable calculation)

MathCAD file used in the room with furniture example (No PEC backing)

Reading the setting the data:

$$c := 2.99 \cdot 10^8$$

$$f := 1.00 \cdot 10^9$$

$$\lambda := \frac{c}{f}$$

$$\lambda = 0.299$$

For the PEC backing case we simply change the data files.

EE := READPRN("BSC_results08.txt")

SBR := READPRN("SBR_results.txt")

EE_{free} := READPRN("BSC_results_free02_1.txt")

PL_{SBR_dB} := SBR⁽ⁱ⁾

m := 0..rows(PL_{SBR_dB}) - 1

zz := SBR⁽⁰⁾

E_{λdB} := EE⁽³⁾

E_{ydB} := EE⁽⁵⁾

$$E_{zdB} := EE^{(7)}$$

$$E_x = 10^{20 \frac{E_{vdB}}{10}}$$

$$E_y = 10^{20 \frac{E_{vdB}}{10}}$$

$$E_z := 10^{20 \frac{E_{zdB}}{10}}$$

$$E_{xfreeB} := EE_{free}^{(3)}$$

$$E_{yfreeB} := EE_{free}^{(5)}$$

$$E_{zfreeB} := EE_{free}^{(7)}$$

$$E_{xfree} := 10^{20 \frac{E_{xfreeB}}{10}}$$

$$E_{yfree} := 10^{20 \frac{E_{yfreeB}}{10}}$$

$$E_{zfree} := 10^{20 \frac{E_{zfreeB}}{10}}$$

$$E_{tot_free} := \sqrt{E_{xfree}^2 + E_{yfree}^2 + E_{zfree}^2}$$

$$E_{tot} := \sqrt{E_x^2 + E_y^2 + E_z^2}$$

$$z := EE^{(2)}$$

$$n := 0..rows(z) - 1$$

$$PL_{free_n} = 10 \cdot \log \left[\frac{\lambda^2 \cdot 1.64^2}{(4\pi)^2 \cdot (z_n)^2} \right]$$

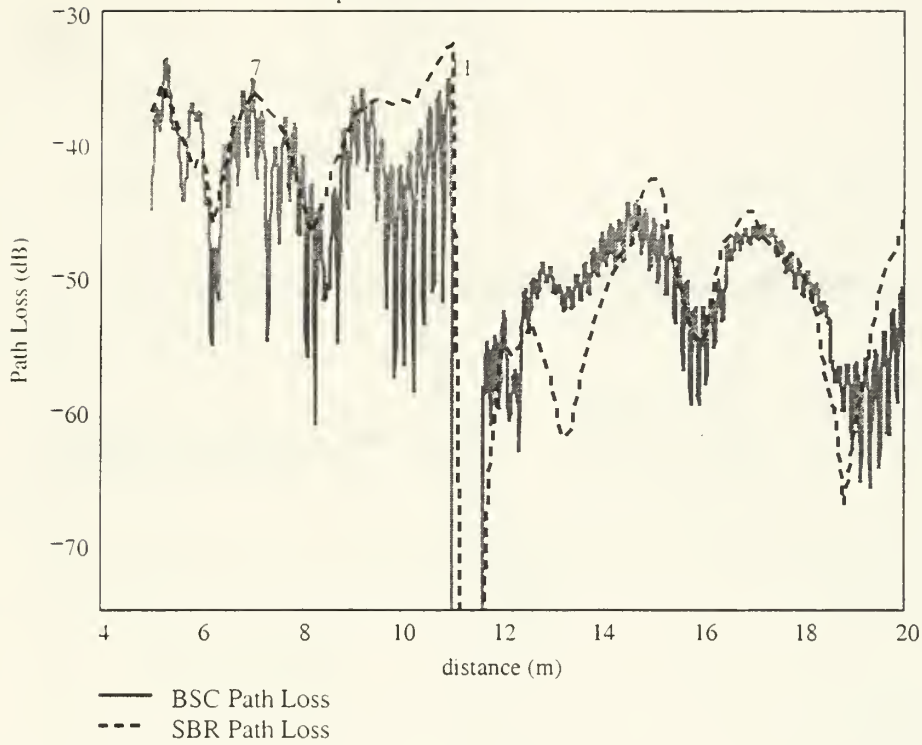
Calculating the excess path loss and the NEC-BSC predicted path loss

$$Excess_{dB} := 20 \cdot \log \left(\frac{E_{tot}}{E_{tot_free}} \right)$$

$$PL_{BSC} := PL_{free} + Excess_{dB}$$

$$rows(z) = 1.501 \times 10^3$$

Comparison: SBR and NEC-BSC w/o PEC



$$p_{\text{new}_n} := 10^{\frac{PL_{\text{BSC}_n}}{10}}$$

$$p_{\text{SBR}_m} := 10^{\frac{PL_{\text{SBR_dB}_m}}{10}}$$

$$\text{mean_square_BSC} := \text{mean}\left(\overrightarrow{p_{\text{new}}^2}\right)$$

$$\text{mean_square_BSC} = 6.003 \times 10^{-9}$$

$$\text{mean_square_SBR} := \text{mean}\left(\overrightarrow{p_{\text{SBR}}^2}\right)$$

$$\text{mean_square_SBR} = 1.866 \times 10^{-8}$$

$$\text{mean_BSC} := \text{mean}(p_{\text{new}})$$

$$\text{mean_BSC} = 4.26 \times 10^{-5}$$

$$\text{mean_SBR} := \text{mean}(p_{\text{SBR}})$$

$$\text{mean_SBR} = 7.737 \times 10^{-5}$$

$$\text{SBR_power} := \text{mean_square_SBR}$$

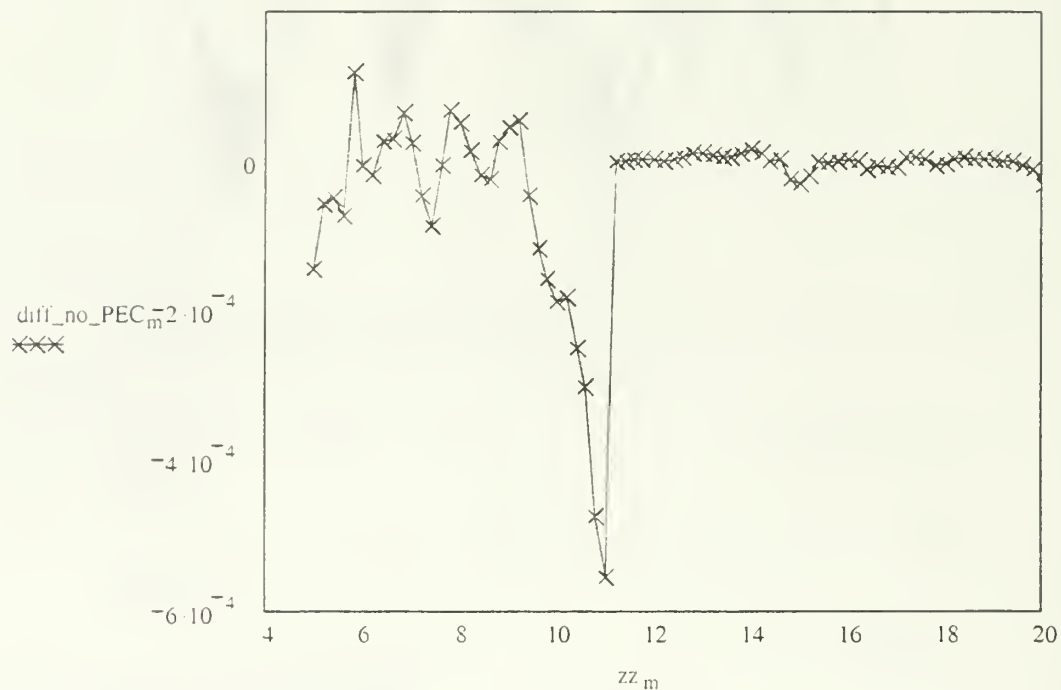
$$\text{SBR_power} = 1.866 \times 10^{-8}$$

$$\text{BSC_power} := \text{mean_square_BSC}$$

```

BSC_power = 6.003 × 10-9
sel_m := m:20
BSC_comp_m := plnew(sel_m)
rows(BSC_comp) = 76
diff_no_PEC_m := BSC_comp_m - plSBR_m
WRITEPRN("no_PEC.dat") := diff_no_PEC

```



End of room with furniture example (no PEC backing)

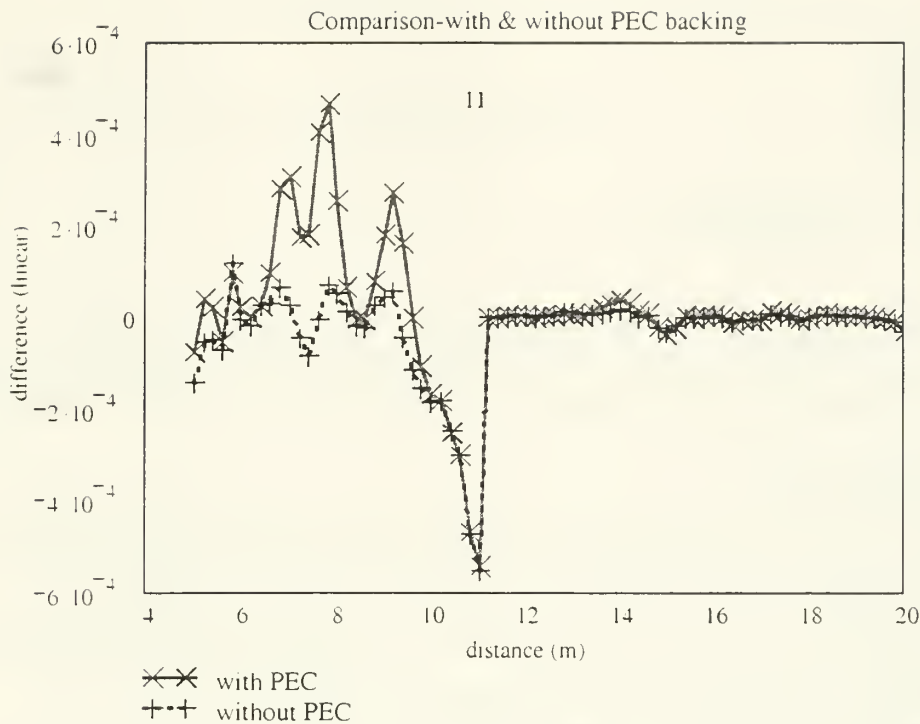
MathCAD file used in the room with furniture example (comparison)

Comparing the no-PEC and PEC results

```

with_PEC = READPRN("with_PEC.dat")
without_PEC := READPRN("no_PEC.dat")
m := 0..rows(with_PEC) - 1
z_m := 5 + 0.2 · m

```



$$\text{var}(\text{with_PEC}) = 2.103 \times 10^{-8}$$

$$\text{mean}(\text{with_PEC}) = 1.239 \times 10^{-5}$$

$$\text{var}(\text{without_PEC}) = 1.055 \times 10^{-8}$$

$$\text{mean}(\text{without_PEC}) = -3.149 \times 10^{-5}$$

$$\text{mean}\left(\overrightarrow{\text{with_PEC}^2}\right) = 2.119 \times 10^{-8}$$

$$\text{mean}\left(\overrightarrow{\text{without_PEC}^2}\right) = 1.154 \times 10^{-8}$$

$$10 \log \left(\frac{\text{mean}\left(\overrightarrow{\text{with_PEC}^2}\right)}{\text{mean}\left(\overrightarrow{\text{without_PEC}^2}\right)} \right) = 2.638$$

End of room with furniture example (comparison)

MathCAD file used for the calculation of the composite walls constitutive parameters

Computing the relative permittivity for composite walls

In the input NEC-BSC file we come across basically two composite walls being located close to antenna's room. The first one is not a real wall but simply a metal mesh which we model as an "imaginary wall." The second one consists of approximately 80% plaster and 20% metallic studs.

The formula derived last time for the mesh was the following:

$$\Gamma = \frac{1 - \sqrt{\epsilon_r}}{1 + \sqrt{\epsilon_r}}$$

$$\left(\frac{1 - \sqrt{\epsilon_r}}{1 + \sqrt{\epsilon_r}} \right)^2 = \frac{\text{metal_area}}{\text{wall_area}} = \frac{a}{A}$$

(equation 1)

where "epsilon subscript r" is the relative permittivity of the "imaginary material" composing the mesh. Bear in mind that if A is the total surface of the mesh and a the total surface of the metal structure then a/A equals 0.17355. The above equation 1 **does** have a real solution.

Composite material case 1

We consider the following approach. An EM wave with power P_{in} impinges on a wall consisting of plaster and metallic studs in proportion 80 and 20% respectively. The transmission coefficient of this wall is T_{comp} . We then let $T_{plaster}$ being the transmission coefficient of a plaster wall with surface 0.80 times the wall's surface. It must be true that:

$$P_{transmitted} = (1 - 0.2) \cdot P_{in} \cdot \left[1 - (|\Gamma_{plaster}|)^2 \right]$$

(equation 2)

$$P_{transmitted} = P_{in} \cdot \left[1 - (|\Gamma_{comp}|)^2 \right]$$

(equation 3)

REFLECTED POWER IS PROPORTIONAL TO THE MAGNITUDE SQUARED OF THE REFLECTION COEFFICIENT!

assuming the transmission due to the metallic portion of the composite wall being negligible and therefore contributing negatively to the resulting transmitted power.

For normal incidence, we have:

$$\Gamma_{plaster} = \frac{1 - \sqrt{\epsilon_{r_plaster}}}{1 + \sqrt{\epsilon_{r_plaster}}}$$

$$\Gamma_{comp} = \frac{1 - \sqrt{\epsilon_{r_comp}}}{1 + \sqrt{\epsilon_{r_comp}}}$$

$$\epsilon_{r_plaster} := 2.3$$

(equations 4)

Thus, from equations 2,3, and 4 we obtain:

$$\left[1 - \left(\left| \frac{1 - \sqrt{\epsilon_{r_comp}}}{1 + \sqrt{\epsilon_{r_comp}}} \right| \right)^2 \right] = 0.8 \cdot \left[1 - \left(\left| \frac{1 - \sqrt{\epsilon_{r_plaster}}}{1 + \sqrt{\epsilon_{r_plaster}}} \right| \right)^2 \right]$$

(equation 5)

from which it follows that:

$$x^2 - 3.22 \cdot x + 1 = 0$$

(equation 6)

where x equals $(\epsilon_{r_comp})^{1/2}$. Therefore:

$$x_1 := 2.8717$$

or

$$x_2 := 0.3483$$

(equation 7)

And finally:

$$\epsilon_{r_comp1} := x_1^2$$

or

$$\epsilon_{r_comp2} := x_2^2$$

$$\epsilon_{r_comp1} = 8.247$$

$$\epsilon_{r_comp2} = 0.121$$

(equations 8)

Composite material case II

In this case we consider the metallic mesh being "replaced" by an imaginary wall consisting of air and metal in proportions 82.6447 and 17.3553%, respectively. We assume that only the "air-part" of this imaginary wall contributes to transmission and only the "metallic-part" reflects back EM energy. Therefore, if T_{wall} and R_{wall} are the transmission and reflection coefficients, respectively, of the "imaginary wall" then (no absorption occurring):

$$P_{transmitted} = (1 - 0.173553) \cdot P_{in} \cdot [1 - (|\Gamma_{air}|)^2]$$

(equation 9)

$$P_{transmitted} = P_{in} \cdot [1 - (|\Gamma_{mesh}|)^2]$$

(equation 10)

where Γ_{mesh} equals:

$$\Gamma_{mesh} = \frac{1 - \sqrt{\epsilon_{r_mesh}}}{1 + \sqrt{\epsilon_{r_mesh}}}$$

and

$$\Gamma_{air} = 0$$

(equation 11)

From equations 9,10 and 11 it follows that:

$$0.826447 = \left[1 - \left(\left| \frac{1 - \sqrt{\epsilon_{r_mesh}}}{1 + \sqrt{\epsilon_{r_mesh}}} \right| \right)^2 \right]$$

(equation 12)

From which we obtain:

$$x^2 - 2.84 \cdot x + 1 = 0$$

(equation 13)

Therefore:

$$x_1 := 2.4281$$

$$x_2 := 0.4118$$

(equation 14)

And finally:

$$\varepsilon_{r_mesh1} := x_1^2$$

$$\varepsilon_{r_mesh2} := x_2^2$$

$$\varepsilon_{r_mesh1} = 5.896$$

or

$$\varepsilon_{r_mesh2} = 0.17$$

(equation 15)

End of MathCAD file used for the calculation of the composite walls constitutive parameters

MathCAD file used in the comparison with measurements in Bullard 2nd floor

Comparison between measured and predicted results in Bullard

Reading the measured data

hall := READPRN("bullard.txt")

rows(hall) = 29

cols(hall) = 24

Cropping in order to rule out the "ambiguous" regions.

cropped_hall := submatrix(hall, 0, 28, 4, 23)

rows(cropped_hall) = 29

cols(cropped_hall) = 20

Reading the NEC-BSC predicted data

predicted := READPRN("predicted.txt")

rows(predicted) = 696

cols(predicted) = 9

$$E_x := \left(\begin{array}{c} \xrightarrow{\text{predicted}^{(3)}} \\ \hline 10 \quad 20 \\ \hline \end{array} \right)$$

$$E_y := \begin{array}{c} \xrightarrow{\text{predicted}^{(5)}} \\ \hline 10 \quad 20 \end{array}$$

$$\overrightarrow{\text{predicted}}^{(7)}$$

$$E_z := 10 \cdot 20$$

$$E_{\text{tot}} := \sqrt{(E_x)^2 + (E_y)^2 + (E_z)^2}$$

$$\text{rows}(E_{\text{tot}}) = 696$$

Converting the values to dBm

$$G_{\text{dipole}} := 1.64$$

$$G_{\text{monopole}} := G_{\text{dipole}}$$

$$G_{\text{monopole}} = 1.64$$

$$\lambda := 0.122364$$

$$A_{\text{effective}} := \frac{\lambda^2 \cdot G_{\text{monopole}}}{4 \cdot \pi}$$

$$A_{\text{effective}} = 1.954 \times 10^{-3}$$

$$P_{\text{density}} := \frac{(|E_{\text{tot}}|)^2}{2 \cdot 377}$$

$$P_{\text{received}} := P_{\text{density}} \cdot A_{\text{effective}}$$

Creating the NEC-BSC data matrix in the same fashion with the measured data matrix.

N.x is the # points in the inner loop

N.y is the # points in the outer loop

$$N_x = 29$$

$$N_y := \frac{\text{rows}(P_{\text{received}})}{N_x}$$

$$N_y = 24$$

$$q := 0.. N_y - 1$$

$$\text{start}_q := q \cdot N_x$$

$$\text{stop}_q := \text{start}_q + N_x - 1$$

$$\text{room}^{(q)} := \text{submatrix}(P_{\text{received}}, \text{start}_q, \text{stop}_q, 0, 0)$$

$$P_{\text{received_dBW}} := 10 \cdot \log(P_{\text{received}})$$

$$\text{room_dBW}^{(q)} := \text{submatrix}(P_{\text{received_dBW}}, \text{start}_q, \text{stop}_q, 0, 0)$$

$$\text{rows}(P_{\text{received_dBW}}) = 696$$

$$\text{rows}(\text{room_dBW}) = 29$$

$$\text{cols}(\text{room_dBW}) = 24$$

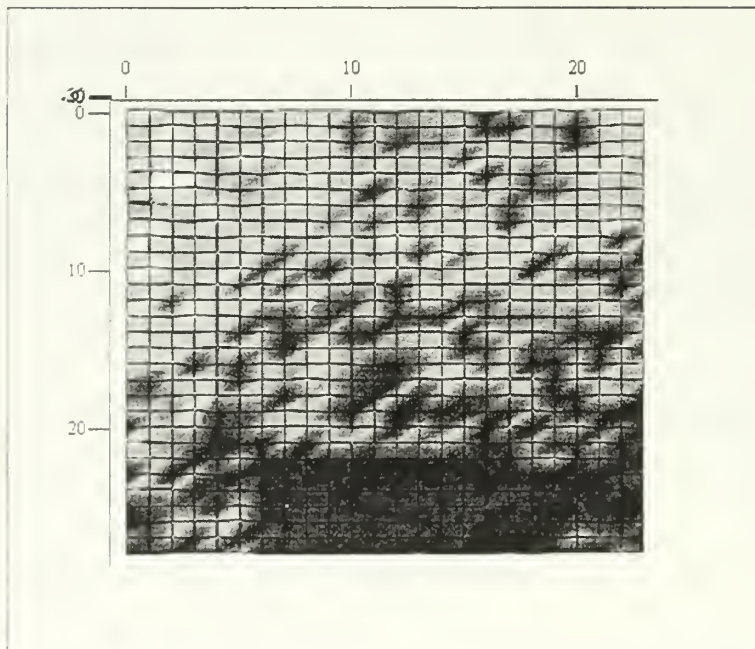
$$\text{max}(\text{room_dBW}) = -14.51$$

$$\text{min}(\text{room_dBW}) = -251.093$$

```

max_power_dB := max(room_dBW)
dyn_range := 30
power_limit := max_power_dB - dyn_range
power_limit = -44.51
p := 0.. rows (room_dBW) - 1
room_power_dBW_p,q := if(room_dBW_p,q > power_limit, room_dBW_p,q, power_limit)
room_lin(q) := submatrix(P_received, start_q, stop_q, 0, 0)
rows (room_lin) = 29
cols (room_lin) = 24

```



room_power_dBW

Converting to dBm and "cropping" appropriately.

$P_{transpose_dBm} := \text{room_power_dBW} + 30$

$P_{received_dBm} := P_{transpose_dBm}^T$

$\min(P_{transpose_dBm}) = -14.51$

$\max(P_{transpose_dBm}) = 15.49$

$\text{rows}(P_{received_dBm}) = 24$

$\text{cols}(P_{received_dBm}) = 29$


```

rows (Ptranspose_dBm) = 29
cols (Ptranspose_dBm) = 24
cropped_Prec_dBm := submatrix (Preceived_dBm, 0, rows (Preceived_dBm) - 1, 4, cols (Preceived_dBm) - 1)
cropped_Ptrans_dBm := submatrix (Ptranspose_dBm, 0, rows (Ptranspose_dBm) - 1, 4, cols (Ptranspose_dBm) - 1)
rows (cropped_Prec_dBm) = 24
cols (cropped_Prec_dBm) = 25
rows (cropped_hall) = 29
cols (cropped_hall) = 20
rows (cropped_Ptrans_dBm) = 29
cols (cropped_Ptrans_dBm) = 20

```

Converting to linear in mWatts

```

      ┌───────────┐
      │cropped_hall│
      └───────────┘
linear_hall := 1010
max_linear_hall := max (linear_hall)
max_linear_hall = 3.162 × 103
      ┌───────────┐
      │cropped_Ptrans_dBm│
      └───────────┘

```

```

linear_Prec := 1010
max_linear_Prec := max (linear_Prec)
max_linear_Prec = 9.451

```

Scaling accordingly

```

linear_Prec10,14 = 0.072
scaled_BSC :=  $\frac{\max\_linear\_hall}{\max\_linear\_Prec} \cdot linear\_Prec$ 
scaled_BSC10,14 = 24.251

```

Converting the scaled BSC values to dBm again

```

BSC_dBm := (10 · log (scaled_BSC))

```

Calculating the difference between BSC and measured values

```

      ┌───────────┐
      │cropped_hall - BSC_dBm│
      └───────────┘
difference_dB := (cropped_hall - BSC_dBm)
      ┌───────────┐
      │|linear_hall - scaled_BSC|│
      └───────────┘
difference := (|linear_hall - scaled_BSC|)
mean_diff_linear := mean (difference)
mean_diff_linear = 245.294

```

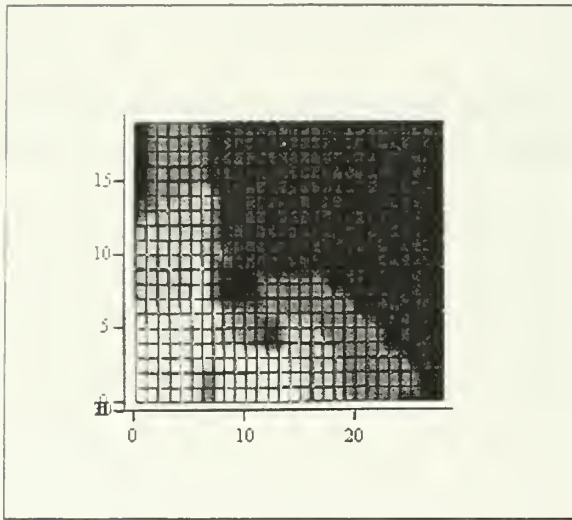
in mWatts

Reversing the matrices to improve visualization

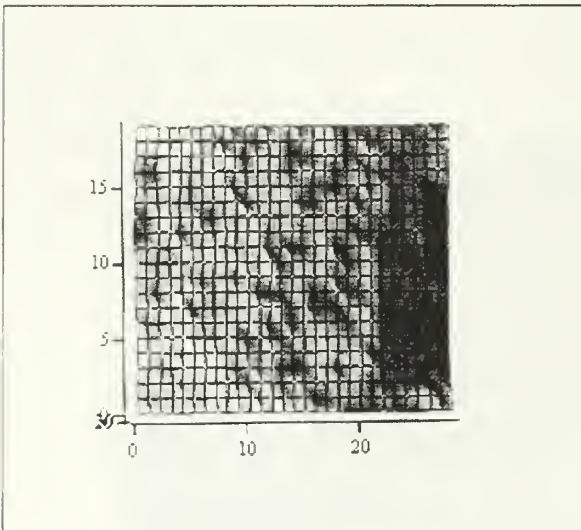
```

qq := 0.. cols (cropped_hall) - 1
measured_map⟨qq⟩ := cropped_hall⟨cols (cropped_hall) - 1 - qq⟩
predicted_map⟨qq⟩ := BSC_dBm⟨cols (BSC_dBm) - 1 - qq⟩

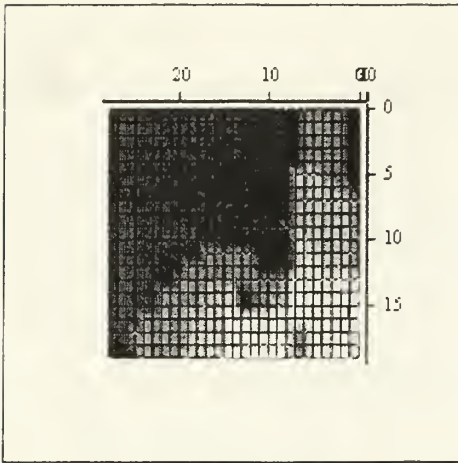
```



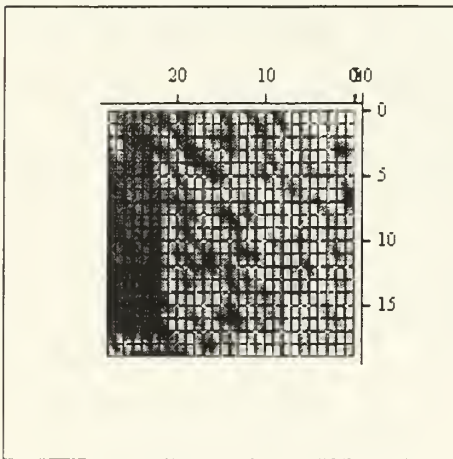
cropped_hall



BSC_dBm



measured_map



predicted_map

End of MathCAD file used in the comparison with measurements in Bullard 2nd floor

MathCAD file used in the comparison with free space (Bullard 2nd floor)

Plot of the BSC Results

Read the Data for antenna at location 1. For the rest of locations we simply change the data files

```
room_data := READPRN("CH6_original_position.txt")
```

```
free_data := READPRN("BSC_Bullard_free_space.txt")
```

```
M := rows(room_data)
```

```
M =  $2.624 \times 10^4$ 
```

```
N := cols(room_data)
```

$$N = 9$$

$$\text{phi}_1 := \text{room_data}^{\langle 2 \rangle}$$

$$E_r := \left(\frac{\text{room_data}^{\langle 3 \rangle}}{20} \right)$$

$$E_\theta := 10 \frac{\text{room_data}^{\langle 5 \rangle}}{20}$$

$$E_\phi := 10 \frac{\text{room_data}^{\langle 7 \rangle}}{20}$$

$$e_r := \left(\frac{\text{free_data}^{\langle 3 \rangle}}{20} \right)$$

$$e_\theta := 10 \frac{\text{free_data}^{\langle 5 \rangle}}{20}$$

$$e_\phi := 10 \frac{\text{free_data}^{\langle 7 \rangle}}{20}$$

$$E_{\text{tot}} := \sqrt{(E_r)^2 + (E_\theta)^2 + (E_\phi)^2}$$

$$e_{\text{tot}} := \sqrt{(e_r)^2 + (e_\theta)^2 + (e_\phi)^2}$$

$$n := 0..M - 1$$

N_x is the # points in the outer loop

$$\text{rows}(E_{\text{tot}}) = 2.624 \times 10^4$$

$$N_x := 162$$

$$N_y := \frac{\text{rows}(E_{\text{tot}})}{N_x}$$

$$N_y = 162$$

$$q := 0..N_y - 1$$

$$\text{start}_q := q \cdot N_x$$

```

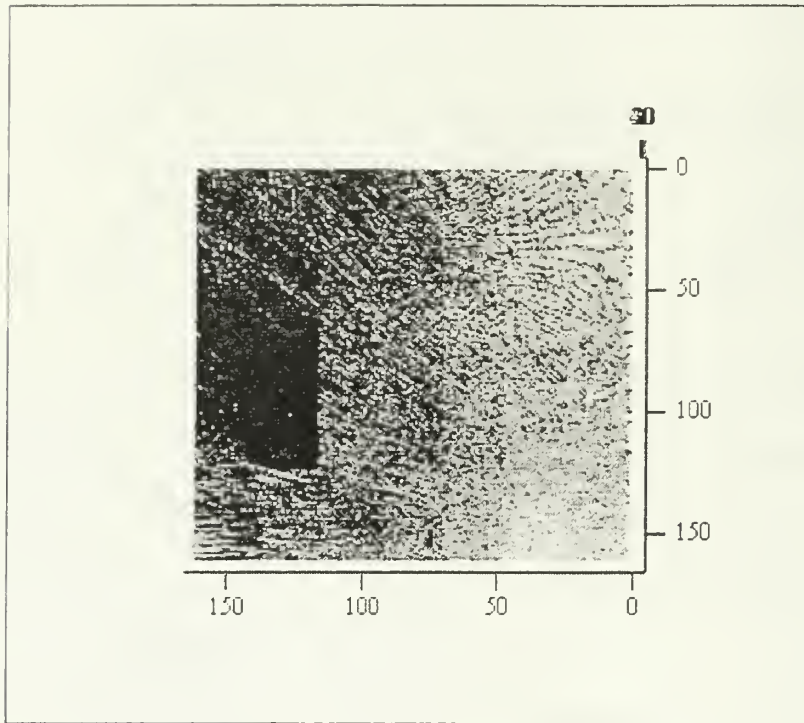
stopq := startq + Nx - 1
room(q) := submatrix(Etot, startq, stopq, 0, 0)
Etot_dB := 20·log(Etot)
room_dB(q) := submatrix(Etot_dB, startq, stopq, 0, 0)
max(room_dB) = 42.59
min(room_dB) = -195.229
max_field_dB = max(room_dB)
dyn_range := 30
field_limit = max_field_dB - dyn_range
p := 0..rows(room_dB) - 1
room_fieldp,q := if(room_dBp,q > field_limit, room_dBp,q, field_limit)
room_lin(q) := submatrix(Etot, startq, stopq, 0, 0)
free(q) := submatrix(etot, startq, stopq, 0, 0)
etot_dB := 20·log(etot)
free_dB(q) := submatrix(etot_dB, startq, stopq, 0, 0)
max(free_dB) = 37.821
min(free_dB) = 5.77
max_field_dB = max(free_dB)
dyn_range := 30
field_limit = max_field_dB - dyn_range
field_limit = 7.821
p := 0..rows(free_dB) - 1
free_fieldp,q := if(free_dBp,q > field_limit, free_dBp,q, field_limit)
free_lin(q) := submatrix(etot, startq, stopq, 0, 0)
diff_free_room = free_lin - room_lin
diff_free_room_dBp,q := if(diff_free_roomp,q > 0, 20·log(diff_free_roomp,q), 0)
min_val := min(diff_free_room_dB)
min_val = -92.194
diff_fr_dBp,q := if(diff_free_room_dBp,q = 0, min_val, diff_free_room_dBp,q)
rows(room_field) = 162
cols(room_field) = 162

```

```

rr := 0..rows(room_field) - 1
inversed_room_field<rr> := room_field<(rows(room_field))-1-rr>

```



inversed_room_field

End of MathCAD file used in the comparison with free space (Bullard 2nd floor)

MathCAD file used in calculating the excess gain/loss random variables

In this program we are aiming at calculating all the random variables of the excess gain/loss of the room over free space field strength (Etot and Etoi_free respectively). We start by reading the associated data files generated by NEC_BSC.

```

NEC_BSC_data := READPRN "CH6_original_position.txt" )

```

```

M := rows( NEC_BSC_data)

```

```

M = 2.624 × 104

```

```

N := cols( NEC_BSC_data)

```

```

N = 9

```

```

x_coord := NEC_BSC_data<0>

```

```

y_coord := NEC_BSC_data<1>

```

```

z_coord := NEC_BSC_data<2>

```

Antenna coordinates for Location 1. For the rest of locations we simply change the coordinates:

$x_{\text{ant}} := 3.0$

$y_{\text{ant}} := 8.0$

$z_{\text{ant}} := 1$

Distance from the antenna:

$$\rho := \sqrt{(x_{\text{coord}} - x_{\text{ant}})^2 + (y_{\text{coord}} - y_{\text{ant}})^2 + (z_{\text{coord}} - z_{\text{ant}})^2}$$

free_space_data := READPRN("BSC_Bullard_free_space.txt")

MM := rows(free_space_data)

MM = 2.624×10^4

NN := cols(free_space_data)

NN = 9

$$E_x := \left(\frac{\text{NEC_BSC_data}^{(3)}}{10} \right)$$

$$E_y := 10 \frac{\text{NEC_BSC_data}^{(5)}}{20}$$

$$E_z := 10 \frac{\text{NEC_BSC_data}^{(7)}}{20}$$

$$E_{\text{tot}} := \sqrt{(E_x)^2 + (E_y)^2 + (E_z)^2}$$

rows(E_{tot}) = 2.624×10^4

$$E_{x_free} := \left(\frac{\text{free_space_data}^{(3)}}{10} \right)$$

$$E_{y_free} := 10 \frac{\text{free_space_data}^{(5)}}{20}$$

$$E_{z_free} := 10 \frac{\text{free_space_data}^{(7)}}{20}$$

$$E_{\text{tot_free}} := \sqrt{(E_{x_free})^2 + (E_{y_free})^2 + (E_{z_free})^2}$$

Since the **NEC-BSC dynamic range** is only 30dB, we will have to account for this fact by "filtering" out all values which are out of that range. This is done in the following fashion:

$$E_{\text{tot_dB}} := \left(20 \cdot \log(E_{\text{tot}}) \right)$$

```

dyn_range := 30
M = 0; rows(E_tot_dB) = 1
lowest_allowed_Etot_value := max(E_tot_dB) = dyn_range
lowest_allowed_Etot_value = 12.59
E_tot_free_dB := (20*log(E_tot_free))
lowest_allowed_Etot_fr_val := max(E_tot_free_dB) - dyn_range
lowest_allowed_Etot_fr_val = 7.821
E_total_dB_ij := if[(E_tot_dB_ij) < lowest_allowed_Etot_value , lowest_allowed_Etot_value , E_tot_dB_ij]
E_total_free_dB_ij := if(E_tot_free_dB_ij < lowest_allowed_Etot_fr_val , lowest_allowed_Etot_fr_val , E_tot_free_dB_ij)

```

Converting to linear:

$$E_{total} := 10^{\frac{E_{total_dB}}{20}}$$

$$E_{total_free} := 10^{\frac{E_{total_free_dB}}{20}}$$

Let us now create the two datamatrices, namely the "datamatrix" which consists of the room's field strength values for every observed point and the "freespacedata01" which includes the corresponding data for the free space case.

```

datamatrix := augment(ρ, E_total)
freespacedata01 := augment(ρ, E_total_free)

```

At this point, owing to the non-uniform layout of the distance (from the antenna) points in the ρ array, we will have to distinguish them into several different groups using the following approach:

```

lower := floor(min(ρ))
upper := ceil(max(ρ))

```

Maximum and minimum distance for this antenna location:

```

upper = 49
lower = 0

```

Groups separation for this calculation (in cm):

```

separation := 50

```

"Step factor" for this calculation:

```

factor = ceil( (100 / separation) )
factor = 2

```

Number of distance bins for this calculation:

```

bins := upper / factor
bins = 98

```


$$h := \frac{\text{upper} - \text{lower}}{\text{bins}}$$

$$h = 0.5$$

$$n := 0.. \text{bins}$$

$$k_n := \text{lower} + n \cdot h$$

It should be noted that the number of bins may be chosen in a fashion which best suits our desirable "distance steps". For instance, **should we choose to have groups points separated by 50cm**, where the maximum distance from the antenna is 49m, our intuitive selection should be 98. Unfortunately, for reasons that could not be explained at the time of thesis write-up, the "build" function does not yield correct results for some values (e.g. for separation equal to 25cm).

We next introduce a new function, which shall be utilized, several times in our subsequent calculations. As input, it expects a two-column matrix and an array. It looks for those values of the first column (i.e., in our problem, the distance array $\square\square\square$ which fall within our made-up groups and then creates a new matrix that contains all those second column's values whose respective first column value satisfy our requirement. It finally returns this new matrix, which, it should be underlined, normally has a **different number of elements in each row**.

```

build(M, binvector) :=
  A ← M<0>
  B ← M<1>
  k ← binvector
  for l ∈ 0..rows(k) - 2
    Dl ← 0
  for i ∈ 0..rows(k) - 2
    for j ∈ 0..rows(M) - 1
      Dl ← augment(Bj, Dl) if kl < Aj ≤ kl+1
  for i ∈ 0..rows(D) - 1
    Di ← submatrix(Di, 0, rows(Di) - 1, 0, cols(Di) - 2) if Di ≠ 0
  D

```

It is high time we used this helping function.

```
datamatrix02 := build(datamatrix, k)
```

```
freespacedata02 := build(freespacedata01, k)
```

The following new function is, seemingly, of high importance since it is the one which calculates the "normalized difference" random variables. It receives two matrices of the same dimensions and returns a new matrix, which in each row contains the values of the random variable pertinent to that row's "distance group."

```

difference(X, Y) :=
  for k ∈ 0..rows(X) - 1
    Ck ← 0
    (
      for j ∈ 0..rows(X) - 1
        n ← cols(Xj)
        A ← Xj
        B ← Yj
        i ← 0
        for i ∈ 0..n - 1
          diffi ← 20·log( $\frac{A_{0,i}}{B_{0,i}}$ )
        n ← cols(Xj)
        Cj ← stack(Cj, diff)
        Cj ← (Cj)T
        k ← rows(Cj)
        l ← cols(Cj)
        Cj ← submatrix(Cj, 0, k - 1, l - 1)
    )
  C

```

The "room gain" is defined here in dB

We now get rid of the redundant first row zeros and then calculate the normalized difference variables.

```

new_datamatrix02 := submatrix(datamatrix02, 1, rows(datamatrix02) - 2, 0, cols(datamatrix02) - 1)
new_treespacedata02 := submatrix(freespacedata02, 1, rows(freespacedata02) - 2, 0, cols(freespacedata02) - 1)
norm_diff := difference(new_datamatrix02, new_freespacedata02)

```

Surprisingly and unexpectedly Mathcad appears to suffer from a bug for it returns an erroneous matrix. The cause of this weird occurrence remains unknown, however we shall attempt to effectively overcome this mishap by applying an easy trick.

```

r := 0..rows(new_datamatrix02) - 1
r1 := cols(new_datamatrix02)
corr_norm_diff1 := submatrix(norm_diff1, 0, rows(norm_diff1) - 1, 0, r1 - 1)

```

This last matrix named "corr_norm_diff" is the one we intended to find. In each row of unequal element number, it contains a different random variable as function of our "devised" groups. Let us take a closer look in one of them, say the 5th.

```

test_0 := (corr_norm_diffT)(0)

```

$$\text{mean}(\text{test}_0) = 0.484$$

$$\text{test}_1 := (\text{corr_norm_diff}^T)^{(1)}$$

$$\text{mean}(\text{test}_1) = 1.006$$

Defining the number of the bins:

$$N_{\text{points}} := 500$$

$$ii := 0..N_{\text{points}} - 1$$

$$j := 0.. \text{rows}(\text{corr_norm_diff}) - 1$$

$$\text{upper}_j := \max(\text{corr_norm_diff}_j)$$

$$\text{lower}_j := \min(\text{corr_norm_diff}_j)$$

$$\text{upper_max} := \max(\text{upper})$$

$$\text{lower_min} := \min(\text{lower})$$

$$\text{step} := \frac{\text{upper_max} - \text{lower_min}}{N_{\text{points}}}$$

$$\text{upper_max} = 25.861$$

$$\text{lower_min} = -14.794$$

$$\text{step} = 0.081$$

$$\text{gen_intervals}_{ii} := \text{lower_min} + \text{step} \cdot ii$$

$$L_j := \frac{\text{hist}(\text{gen_intervals}, \text{corr_norm_diff}_j)}{\text{cols}(\text{corr_norm_diff}_j)}$$

$$\text{buildL}(L) := \begin{array}{|l} L_{\text{new}} \leftarrow L_0^T \\ \text{for } q \in 1.. \text{rows}(L) - 1 \\ \quad \left| \begin{array}{l} A \leftarrow L_q^T \\ L_{\text{new}} \leftarrow \text{stack}(L_{\text{new}}, A) \end{array} \right. \end{array}$$

$$L_{\text{pdf}} := \text{buildL}(L)$$

$$\text{rows}(L_{\text{pdf}}) = 96$$

$$\text{cols}(L_{\text{pdf}}) = 499$$

$$N_{\text{pdfs}} := \text{cols}(L_{\text{pdf}}) - 1$$

$$qq := 0..N_{\text{pdfs}} - 1$$

$$\text{avg_pdf}_{qq} := \text{mean}(L_{\text{pdf}}^{(qq)})$$

$$\sum \text{avg_pdf} = 1$$

$$\text{mean_rv} := \sum_{qq=0}^{N_{\text{pdfs}}-1} \text{gen_intervals}_{qq} \cdot \text{avg_pdf}_{qq}$$

$$\text{mean_rv} = 7.165$$

step = 0.081

$$\text{mean_sq_rv} := \sum_{qq=0}^{\sqrt{pd_{rv}}-1} (\text{gen_intervals}_{qq})^2 \cdot \text{avg_pdf}_{qq}$$

mean_sq_rv = 78.007

$$\text{var_rv} := \text{mean_sq_rv} - \text{mean_rv}^2$$

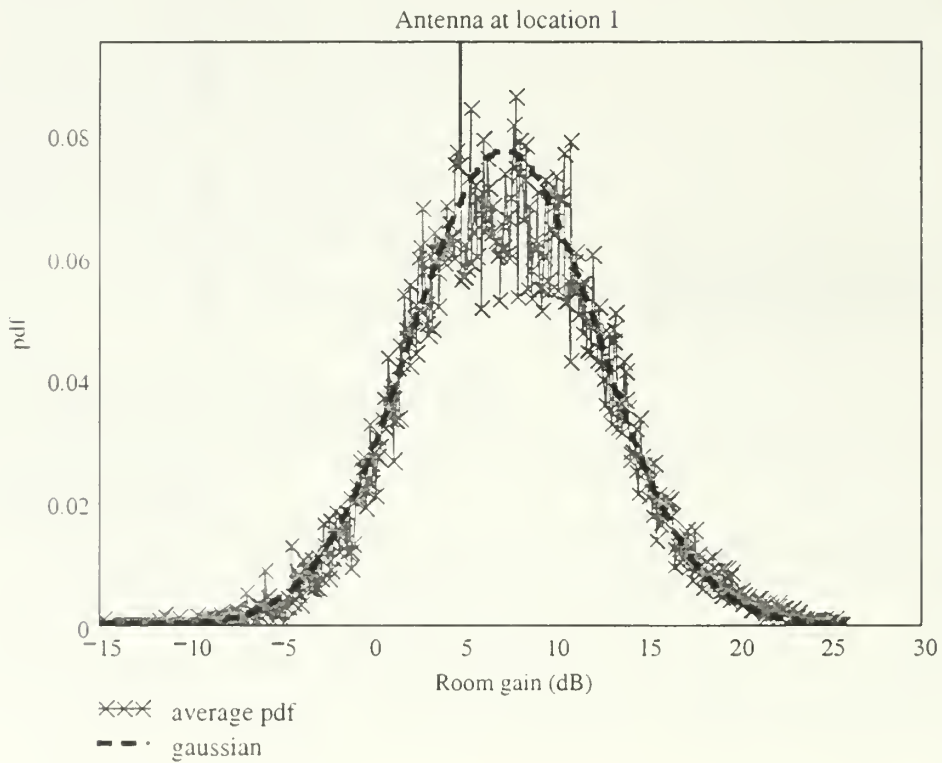
var_rv = 26.671

mean_rv = 7.165

Defining **Gaussian** pdf:

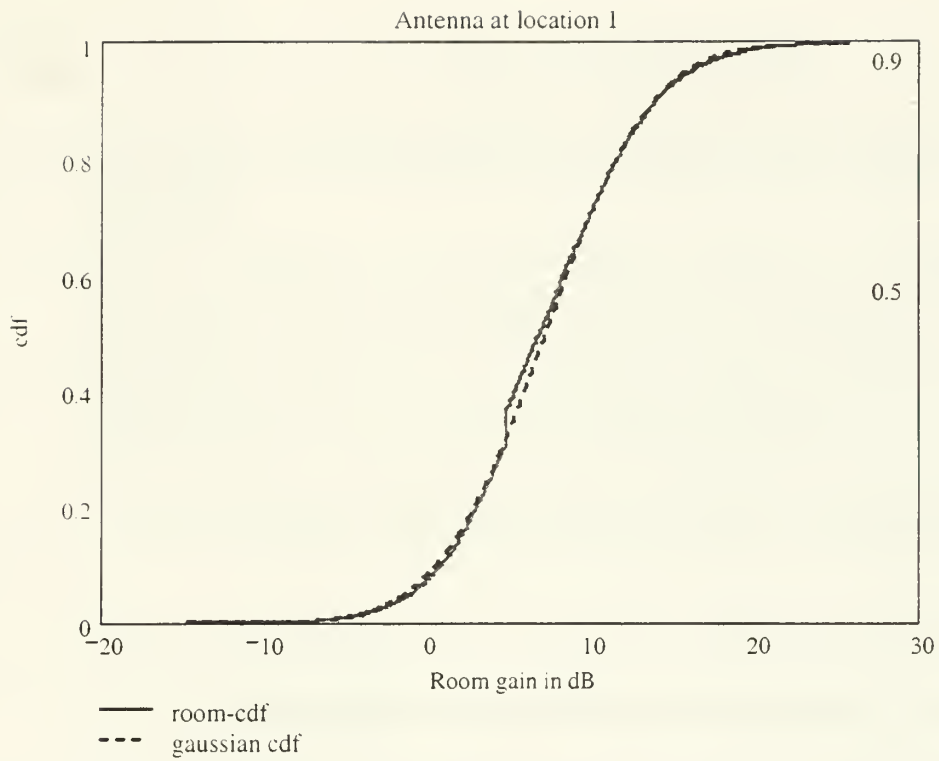
$$\text{gauss}_{ii} := \frac{1}{\sqrt{2 \cdot \pi \cdot \text{var_rv}}} \cdot e^{-\frac{(\text{gen_intervals}_{ii} - \text{mean_rv})^2}{2 \cdot \text{var_rv}}}$$

room_gain_dB := gen_intervals



$$\text{cdf}_{qq} := \sum_{m=0}^{qq} \text{avg_pdf}_m$$

$$\text{cdf}_{\text{gauss}_{ii}} = \text{step} \cdot \left(\sum_{m=0}^{ii} \text{gauss}_m \right)$$



End of MathCAD file used in calculating the excess gain/loss random variables

End of all MathCAD files

THIS PAGE INTENTIONALLY LEFT BLANK

LIST OF REFERENCES

1. R. Grosskopf, "GTD-Based indoor propagation prediction method," *Millennium Conference on Antennas and Propagation AP2000*, Davos, Switzerland, 9-14 April 2000.
2. B.P. Crow, I. Widjaja, J.G. Kim and P.T. Sakai, "IEEE 802.11 Wireless Local Area Networks," *IEEE Communications Magazine*, September 1997, pp. 116-126.
3. J. Khun-Jush, G. Malmgren, P. Schramm and J. Torsner, "Overview and Performance of HIPERLAN Type 2- A Standard for Broadband Wireless Communications," *Proceedings of VTC 2000*, pp.112-117.
4. K.J. Negus, A.P. Stephens and Jim Lansford, "HomeRF: Wireless Networking for the Connected Home," *IEEE Personal Communications*, February 2000, pp. 20-27.
5. J.C. Haartsen, "The Bluetooth Radio System," *IEEE Personal Communications*, February 2000, pp. 28-36.
6. T.S. Rappaport, *Wireless Communications*, Prentice Hall, Upper Saddle River, New Jersey, Inc., 1999.
7. NOKIA White Paper, *Nokia Rooftop Wireless Routing*, August 2000.
8. P.K. Das, UC San Diego, "Characterization of Signal Propagation Loss of Radio WLAN in a Shipboard Environment," [<http://uc-core.UCSD.EDU/program/COR-99-10052.html>]. September 2000.
9. Naval Research Laboratory, *Initial Bistatic Measurements of Electromagnetic Propagation in an Enclosed Ship Environment*, by E.L. Mokole, M. Parent, J. Valenzi, E. Thomas, B.T. Gold, T.T. Street, February 1998.
10. Steven M. Debus, *Feasibility Analysis for a Submarine Wireless Computer Network Using Commercial-off-the-Shelf Components*. Master's Thesis, Naval Postgraduate School, Monterey, CA, September 1998.
11. Mark M. Matthews, *Analysis of Radio Frequency Components for Shipboard Wireless Networks*. Master's Thesis, Naval Postgraduate School, Monterey, CA, December 1999.
12. G.L. Miller, "Shipboard Wireless Communications Program." [<http://www.spawar.navy.mil>]. December 1998.
13. J. Lebaric R. Adler, C. Deyannis and D. Xifaras, *Effects of Fire and Fire Extinguishing on Wireless Communications in the 2.4 GHz ISM Band*, Naval Postgraduate School, Monterey, CA, June 6, 2000.
14. H. Hashemi, "The Indoor Propagation Channel," *Proceedings of the IEEE*, Vol.81, No.7, July 1993, pp.943-968.

15. P. Pechac, M. Klepal and M. Mazanek, "Indoor Propagation Modelling in Multi-Storey Buildings in Prague," *Millennium Conference on Antennas and Propagation AP2000*, Davos, Switzerland, 9-14 April 2000.
16. U. Dersch, R. Ruegg, H. Kaufmann and R. Rufener, "Modelling and Simulation of Indoor Radio Channels," *IEEE International Conference on Communications*, Geneva, 1993, vol.3, pp.1970-1974.
17. S.R. Saunders, *Antennas and Propagation for Wireless Communication Systems*, John Wiley & Sons, New York, NY, Inc, 1999.
18. G.J.M. Janssen and R. Prasad, "Propagation Measurements in an Indoor Radio Environment at 2.4 GHz, 4.75 GHz and 11.5 GHz," *Vehicular Technology Conference*, 1992, vol.2, pp.617-620.
19. D.I. Laurenson, A U.H. Sheikh and S. McLaughlin, "Characterisation of the Indoor Mobile Radio Channel Using a Ray Tracing Technique," *IEEE International Conference on Selected Topics in Wireless Communications*, 1992, pp.65-68.
20. A.M.D. Turkmani and A.F. de Toledo, "Modelling of Radio Transmissions into and within Multistorey Buildings at 900, 1800 and 2300 MHz," *IEEE Proceedings*, Vol.140, No6, December 1993, pp. 462-470.
21. W. Honcharenko, H.L. Bertoni, J.L. Dailing, J. Qian and H.D. Yee, "Mechanisms Governing UHF Propagation on Single Floors in Modern Office Buildings," *IEEE Transactions on Vehicular Technology*, Vol.41, No.4, November 1992, pp.496-504.
22. Interview between Dr. Jovan Lebaric and the author, 11 October 2000.
23. A.F. de Toledo and AM.D. Turkmani, "Propagation into and Within Buildings at 900, 1800 and 2300 MHz," *Proceedings of Vehicular Technology Conference*, 1992, vol.2, pp.633-636.
24. A.F. de Toledo, A.M.D. Turkmani and J.D. Parsons, "Estimating Coverage of Radio Transmission into and within Buildings at 900, 1800, and 2300 MHz," *IEEE Personal Communications*, April 1998, pp. 40-47.
25. E.H. Newman and R.J. Marhefka, "Overview of MM and UTD Methods at the Ohio State University," *Proceedings of the IEEE*, Vol.77, No.5, pp.700-708.
26. P. Selormey and Y. Miyazaki, "Propagation and Interference Characteristics by Group of Buildings in Mobile Communication Channels," *Proceedings of ISAP 2000*, Fukuoka, Japan, August 2000.
27. R.A. Valenzuela, "A Ray Tracing Approach to Predicting Indoor Wireless Transmission," *Proceedings of Vehicular Technology Conference*, 1993, pp.214-218.

28. L.C. Lawton and J.P. McGeehan, "The Application of GTD and Ray Launching Techniques to Channel Modelling for Cordless Radio Systems," *Proceedings of Vehicular Technology Conference*, 1992, vol.1, pp.125-130.
29. Juan Calle, *Indoor Propagation Simulation Software*, Master's Thesis, Naval Postgraduate School, Monterey, CA, September 2000.
30. M.F. Catedra, J. Perez, F. Saez de Adana and O. Gutierrez, "Efficient Ray-Tracing Techniques for Three-Dimensional Analyses of Propagation in Mobile Communications: Application to Picocell and Microcell Scenarios," *IEEE Antennas and Propagation Magazine*, Vol.40, No.2, April 1998, pp.15-28.
31. R.P.Torres, L.Valle, M.Domingo, S.Loredo and M.C. Diez, "CINDOOR: An Engineering tool for planning & Design of Wireless Systems in Enclosed Spaces," *IEEE Antennas & Propagation Magazine*, Vol.41, No.4, August 1999, pp.11-22.
32. W. Honcharenko, H.L. Bertoni and J. Dailing, "Theoretical Prediction of UHF Propagation within Office Buildings," *1st International Conference on Universal Personal Communications Proceedings*, 1992, pp.04.04/1-04.04/4.
33. S.Y. Seidel and T.S. Rappaport, "A Ray Tracing Technique to Predict Path Loss and Delay Spread Inside Buildings," *IEEE Global Communications Conference Proceedings*, 1992, vol.2, pp.649-653.
34. T. Fruhwirth and P. Brisset, "Placing Base Stations in Wireless Indoor Communication Networks," *IEEE Intelligent Systems*, vol.15, issue 1, February 1996, pp.50-55.
35. K.W. Cheung, J.H.M. Sau and R.D. Murch, "A New Empirical Model for Indoor Propagation Prediction," *IEEE Transactions on Vehicular Technology*, Vol.47, No.3, August 1998, pp.996-1001.
36. A. Neskovic, Natasa Neskovic and Dodre Paunovic, "Indoor Electric Field Level Prediction Model Based on the Artificial Neural Networks," *IEEE Communications Letters*, Vol.4, No.6, June 2000, pp.190-192.
37. Andre Fourie and Derek Nitch, "SuperNEC: Antenna & Indoor Propagation Simulation Program," *IEEE Antennas & Propagation Magazine*, Vol.42, No.3, June 2000, pp.31-48.
38. R.J. Marhefka, "Numerical Electromagnetic Code-Basic Scattering Code, NEC-BSC (Version 4.2), User's Manual," Installation Package, Joint Preliminary Report, December 1998, The Ohio State University Electroscience Laboratory, Department of Electrical Engineering, prepared under Contract No. N66001-97-C-6013.
39. R.J. Marhefka, "Numerical Electromagnetic Code-Basic Scattering Code, NEC-BSC (Version 3), User's Manual," Technical Report 718422-3, 1989, The Ohio State University Electroscience Laboratory, Department of Electrical Engineering, prepared under Contract No. N60530-85-C-0249 for Naval Weapons Center.

40. A.M. Bucceri, J.C. Herper and E. Mertz, "Computer Simulation for a High Gain Antenna Including Interactions with Local Scatterers," *Antennas and Propagation Society International Symposium*, 1991, vol.2, pp.922-925.
41. R.J. Marhefka, "Navy develops new antennas."
[<http://www.aerotechnews.com/starc/030998/031398d.html>]. September 1998.
42. G. Toso, A. Bruno, G. Manetti, G.B. Gentili and G. Pelosi, "On-Glass Cellular Telephone Patch-Antennas for Vehicular Applications," *Proceedings of ISAP 2000*, Fukuoka, Japan, August 2000.
43. J.M. Harris and M.L. Wheeler, "H-60 Helicopter Antenna Placement Evaluation: Experimental and NEC-BSC Results," *Proceedings of the 1994 Applied Computational Electromagnetics Society (ACES) Conference*, March 21-26, 1994.
44. Y. Kim and E.K. Walton, "Ground Bounce Reduction Using a Tapered Resistive Sheet Fence," The Ohio State University Electroscience Laboratory, Department of Electrical Engineering.
[<http://www.amta.org/amta2000/schedule/Abstract/A00-031.htm>]. September 2000.
45. R.J. Marhefka, e-mail message, Subject: NEC-BSC Questions, May 24, 2000.
46. A.P. Tsitsopoulos and M.J. Packer, "EAM: BSC An Electromagnetic Scattering Analysis Tool for Windows, *Proceeding of the 1994 ACES Conference*, March 21-26, 1994.
47. R.J. Marhefka, e-mail message, Subject: NEC-BSC Questions, June 07, 2000.
48. S.H. Chen and S.K.Jeng, "An SBR/Image approach for Radio Wave Propagation in indoor environments with metallic furniture," *IEEE Transactions on Antennas & Propagation*, Vol.45, No.1, Jan. 1997, pp. 98-106.
49. C.E. Balanis, *Advanced Engineering Electromagnetics*, John Wiley, New York, NY, Inc., 1989.
50. J.F. Lafortune and M. Lecours, "Measurement and Modeling of Propagation Losses in a Building at 900 MHz," *IEEE transactions on Vehicular Technology*, Vol.39, No.2, May 1990, pp.101-108.
51. D. Molkdar, "Review on Radio Propagation into and within Buildings," *IEEE Proceedings-H*, Vol.138, No.1, February 1991, pp.61-73.
52. D. Ndzi, J. Austin and E. Vilar, "Indoor Channel Characterisation Using Hyper-Resolution Impulse Response," *Millennium Conference on Antennas and Propagation AP2000*, Davos, Switzerland, 9-14 April 2000.

INITIAL DISTRIBUTION LIST

1. Defense Technical Information Center 2
8725 John J. Kingman Rd., STE 0944
Ft. Belvoir, Virginia 22060-6218
2. Dudley Knox Library 2
Naval Postgraduate School
411 Dyer Road
Monterey, California 93943-5101
3. Engineering and Technology Curriculum Code 34 2
Naval Postgraduate School
700 Dyer Road, Room 115
Monterey, CA 93943-5107
4. Chairman, Code EC 1
Electrical and Computer Engineering Department
Naval Postgraduate School
Monterey, CA 93943-5121
5. Dr. Jovan Lebaric, Code EC/Lb..... 2
Electrical and Computer Engineering Department
Naval Postgraduate School
Monterey, CA 93943-5121
6. Dr. Richard Adler, Code EC/Ab..... 1
Electrical and Computer Engineering Department
Naval Postgraduate School
Monterey, CA 93943-5121
7. Dr. James Luscombe, Code PH/Lj..... 1
Physics Department
Naval Postgraduate School
Monterey, CA 93943-5117
8. Dr. Ronald J. Marhefka..... 1
The Ohio State University Electroscience Laboratory
1320 Kinnear Rd
Columbus, OH 43212-1191
9. LT Ilias Bolanis H.N..... 3
Zanni 107-109, Piraeus, TK 18536,
Greece

72 290NP6 3083
TH
6/02 22527-200 NLE



DUDLEY KNOX LIBRARY



3 2768 00403070 0